5-2015

DEVELOPMENTAL ORIGINS OF RENAL CONNECTING TUBULE AND COLLECTING DUCT: ROLE OF AQP2+ PROGENITOR CELLS

Lihe Chen

DEVELOPMENTAL ORIGINS OF RENAL CONNECTING TUBULE AND COLLECTING DUCT: ROLE OF AQP2^{+} PROGENITOR CELLS

By

Lihe Chen, B.S.

APPROVED:

_____
Advisor, Wenzheng Zhang, Ph.D.

_____
Rodney E. Kellems, Ph.D.

_____
Cheng Chi Lee, Ph.D.

_____
Pierre D. McCrea, Ph.D.

_____
Jianping Jin, Ph.D.

_____
Rachel K. Miller, Ph.D.

APPROVED:

_____
Dean, The University of Texas
Graduate School of Biomedical Sciences at Houston

DEVELOPMENTAL ORIGINS OF RENAL CONNECTING TUBULE AND COLLECTING DUCT: ROLE OF AQP2^{+} PROGENITOR CELLS

A

DISSERTATION

Presented to the Faculty of
The University of Texas
Health Science Center at Houston
and
The University of Texas
MD Anderson Cancer Center
Graduate School of Biomedical Sciences
in Partial Fulfillment

of the Requirements

for the Degree of

DOCTOR OF PHILOSOPHY

by

Lihe Chen, B.S.

Houston, Texas

May 2015

Dedication

I dedicate this work to my family for their love, encouragement, and guidance. My parents, Mr. Jizhang Chen and Mrs. Jinlian Zhang, have given caring and everything they have to my growth throughout my life. My sister, Xiang Chen, has always been the one sharing thoughts with me. I also dedicate this work to my wife, Mrs. Tianjiao Dai, for always being in love with me since we first met in 2012.

Acknowledgements

My most sincere thanks go to my advisor, Dr. Wenzheng Zhang for his dedication, guidance, and support throughout my research over the past few years. Dr. Zhang has shaped my thoughts and the way that I think about science by his patience, inspiration, encouragement, and experience. Not only a great scientific mentor, Dr. Zhang has also been a good friend in my life. He always believes in me and provides me an environment of freedom to pursue my goals. I really enjoyed the time in his lab and I wish I could work with him continuously.

I would like to thank those who have served as my past and current committee members. Many thanks to Dr. Yi Li, Dr. Mingyao Liu, Dr. Eric J. Wagner, Dr. Vasanthi Jayaraman, Dr. Jianping Jin, Dr. Rodney E. Kellems, Dr. Cheng Chi Lee, Dr. Pierre D. McCrea, and Dr. Rachel K. Miller. Their guidance has greatly helped my growth towards becoming an independent investigator in the future.

I would also like to thank my past lab members, Dr. Jiong Bi, Dr. Wo Li, Dr. Hongyu Wu, and Mrs. Zhou Xiao for their help and support. I cherished every minute with them.

As a member of the Graduate Program in Biochemistry and Molecular Biology, I would like to especially thank the faculty, postdoctoral fellows, and graduate students associated with this program for their persistent support. I especially express my thanks to Dr. Michael Blackburn for allowing me to use his epifluorescence microscope, Dr. Yang Xia for offering access to her tissue culture facility, and Dr. Jianping Jin for sharing many reagents.

Finally, I would like to acknowledge the support of the Graduate School of Biomedical Sciences, American Physiology Society, and the Department of Biochemistry and Molecular Biology for travel awards.

DEVELOPMENTAL ORIGINS OF RENAL CONNECTING TUBULE AND COLLECTING DUCT: ROLE OF AQP2^{+} PROGENITOR CELLS

Lihe Chen, B.S.

Advisor: Wenzheng Zhang, Ph.D.

The connecting tubule interconnects the nephron and collecting duct, which arise from kidney mesenchyme and the ureteric bud, respectively, to generate the functional tubular networks. The collecting duct is comprised of principal cells and intercalated cells, which bear different molecular signatures and regulate sodium/water and acid/base balance, respectively. The progenitor cells of the connecting tubule and the collecting duct remain virtually unknown.

We generated two Aqp2 lineage tracing mouse models. In these models, *Aqp2Cre* transgene drives Cre expression by the *Aqp2* promoter to exclusively either inactivate histone H3 K79 methyltransferase *Dot1l* (*Dot1l*$^{f/f}$ *Aqp2Cre*) or activate RFP in Aqp2 lineage cells during development (*Aqp2Cre RFP*). H3 K79 methylation and RFP were used as the tracing markers. Kidney sections were examined by immunofluorescence staining combined with epifluorescence and confocal microscopy.

Analyses of *Dot1l*$^{f/f}$ *Aqp2Cre* revealed that *Dot1l* ablation abolished H3 K79 methylation, which occurs in both principal and intercalated cells. These results suggest that Aqp2^{+} progenitor cells give rise to principal cells and intercalated

cells in the absence of Dot1l function. With *Aqp2Cre RFP* mice, we not only confirmed that derivation of intercalated cells from $Aqp2^+$ progenitor cells is not an artifact of *Dot1l* deletion, but also identified the origin and molecular identities of connecting tubules. $Aqp2^+$ progenitors contribute to renal tubular interconnection by differentiating into various types of transitional cells in the connecting tubule to form three molecularly distinct segments: $RFP^+Aqp2^+NCC^-$, $RFP^+Aqp2^-NCC^-$, and $RFP^+Aqp2^-NCC^+$. RFP^+ indicates progenitors of $Aqp2^+$ origin. $Aqp2^-$ represents the loss of the original $Aqp2^+$ progenitors. NCC^+ is the signature of distal convoluted tubule, the last segment of nephron linking to the connecting tubule.

In summary, our study 1) highlights the molecular identity and the origin of novel and distinct connecting tubule segments; and 2) reveals $Aqp2^+$ progenitors as the origin of various cell types of connecting tubule as well as collecting duct. Therefore, our study demonstrates novel functions of $Aqp2^+$ progenitors in the origin of collecting duct and connecting tubule formation. The discovery of the Aqp2+ progenitor cells may facilitate their further molecular and functional characterization, which is critical for regenerative medicine.

Table of contents

List of illustrations

List of tables

Chapter 1

Introduction

1.1 Kidney overall structure and function.

The adult kidney is a complex epithelial filtration network that maintains whole-body homeostasis, including elimination of nitrogenous waste metabolites, and regulation of the body volume and blood pressure. Structurally, the kidney is comprised of cortex, medulla, and papilla. The basic filtration units are termed nephrons. Nephrons are highly differentiated epithelial structures, from proximal to distal, consisting of the glomerulus, proximal tubule, loop of Henle, and distal convoluted tubule. The urine formation process starts from the glomerulus, after filtration and processing, the wastes exit the kidney via collecting duct system and ureters.

1.2 Three distinct developmental stages of mammalian kidney.

The mammalian kidney derives from the intermediate mesoderm through a series of successive stages: pronephros, mesonephros, and metanephros (1, 2). These structures appear in sequence and develop in a cranial-to-caudal direction within the embryo. At the E18 of human and E7.5 of mouse, epithelial cells within the intermediate mesoderm arrange themselves to form a few pairs of tubules at the same level and join with the pronephric duct. The pronephric duct continues to migrate caudally and induces the formation of the mesonephric tubules at E24 in humans and E9.5 in mice. At these stages, the mesonephric tubules form the glomerulus-like structure and begin to filtrate blood. The filtrate passes through mesonephric tubules and is collected by the mesonephric duct now called the wolffian duct. The pronephros and mesonephros gradually degenerate during the

course of gestation. At the fifth week of gestation of human and E11 of mouse, a group of special intermediate mesoderm cells called metanephric mesenchyme cells form and induce the formation of the ureteric bud at the very end of the wolffian duct. Metanephros persists as the definitive adult kidney, which is formed via reciprocal interaction between the ureteric bud and its surrounding metanephric mesenchyme.

1.3 Different origins of collecting duct and nephron during development.

In mammals, pronephros and mesonephros exist transiently (1-3). Mouse nephrogensis, which starts at E11, is characterized by an outgrowth of the ureteric bud from the wolffian duct and an extensive invasion of the ureteric bud into the surrounding metanephric mesenchyme (1-4) (Figure 1). At this stage, the ureteric bud is evident as a T-shape structure and subsequently undergoes a series of branching morphogenesis. The ureteric bud is able to undergo multiple rounds of branching and creates the whole collecting duct system. Signals secreted from the ureteric bud tip induce the surrounding mesenchymal cells to produce cap mesenchyme, and initiate the mesenchyme-to-epithelial transition of the cap mesenchyme to generate the early nephron structures. The induced cap mesenchyme cells around the ureteric bud tip form the renal vesicles with a small lumen. The comma shaped body develops subsequently with the appearance of a cleft in the renal vesicles. The s-shaped body is evident when a second cleft appears in the comma shaped body. The distal end of the s-shaped body attaches to the ureteric bud and forms the continuous tubule through a yet

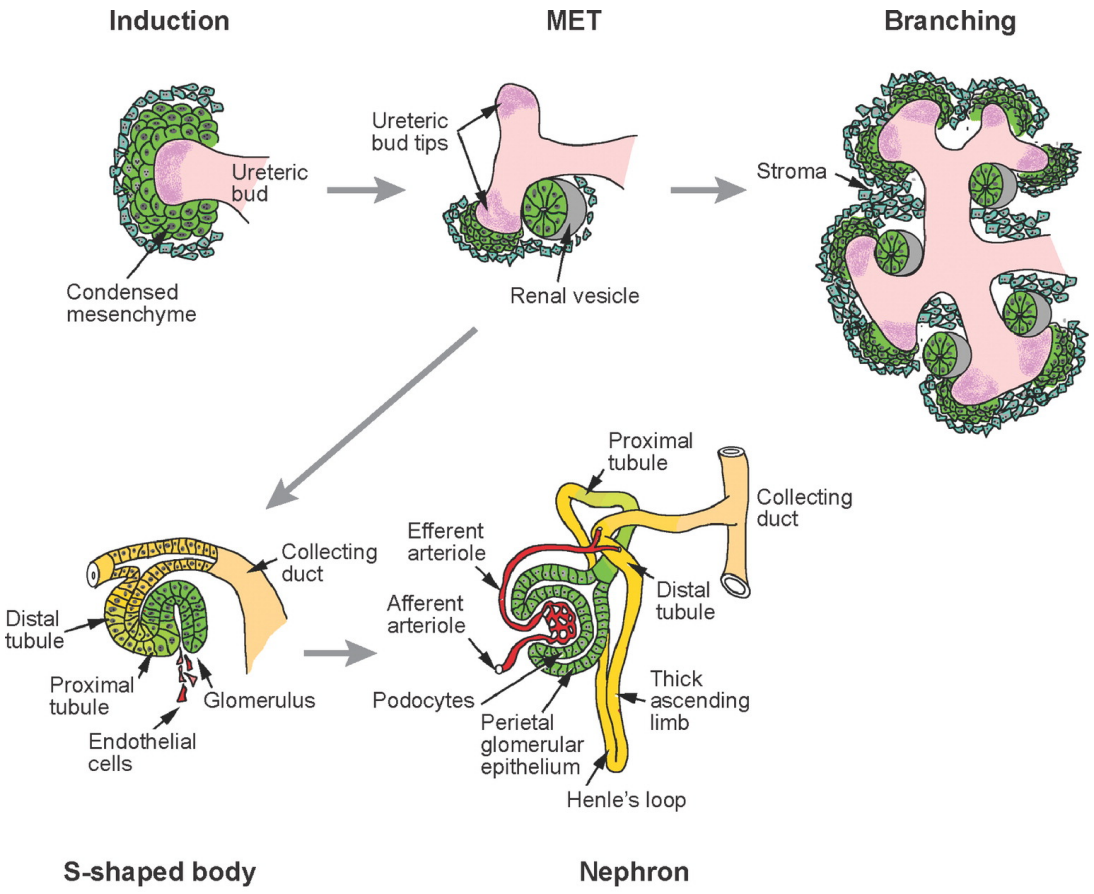

Dressler GR. 2006.
Annu. Rev. Cell Dev. Biol. 22:509–29

Figure 1. Overview of nephrogenesis.

Signals secreted from the ureteric bud tip induce the surrounding mesenchymal cells to form condensed mesenchyme or cap mesenchyme (CM), and initiate the mesenchyme-to-epithelial transition of the CM to generate the early nephron structures (i.e. RV, S-shaped body). CM contains progenitors to give rise to whole nephron segments, from distal to proximal, including proximal tubule, Henle's loop, thick ascending limb, and distal tubule. Ureteric bud is able to undergo multiple rounds of branching and creates the whole collecting duct system. This figure is cited from reference (1) Dressler, G. R. (2006) The cellular basis of kidney development. *Annual review of cell and developmental biology* 22, 509-529 with permission.

undefined mechanism, while the proximal part of the s-shaped body interacts with the endothelial cells to begin the glomerulogenesis.

The metanephric mesenchyme is a pool for the stem and progenitor cells. In addition to giving rise to the whole body of nephrons, the stem cells or progenitors within the metanephric mesenchyme also give rise to either vascular progenitors to create the blood vessels (5), or stromal progenitors to generate the stromal tissues (3, 6). With the continuation of ureteric bud branching, new ureteric bud tips form and repeat the same process. Connection of the nephrons with the ureteric bud allows the urine to flow continuously out of the body via the ureters.

Although recent advances have led to a better understanding of the morphological changes of the metanephric kidney development, the signal pathways that orchestrate these events remain elusive.

The principal molecular pathway that is responsible for the outgrowth and branching of the ureteric bud involves glial cell-derived neurotrophic factor (Gdnf) and its tyrosine kinase receptor (RTK) (2, 3). Gdnf secreted by the metanephric mesenchyme acts as a chemotactic cue for the outgrowth of the ureteric bud toward the metanephric mesenchyme. In turn, Wnts, especially Wnt9b and Wnt11, which are released by ureteric bud, have been shown to induce the metanephric mesenchyme to form cap mesenchyme, and promote mesenchyme-to-epithelial transition to generate the renal vesicles. Wnt4, which is secreted by cap mesenchyme, acts in an autocrine manner to maintain the induced metanephric mesenchyme. In this pattern, with the interplay and integration of

multiple signal pathways, cap mesenchyme gives rise to diverse nephron epithelial segments while ureteric bud differentiates into collecting duct system.

1.4 Function and cellular composition of the collecting duct system.

The collecting duct system serves as the final part of the renal filtration system to maintain water and electrolyte homeostasis. It consists of connecting tubules and collecting ducts.

As the initial part of the collecting duct system, the connecting tubule interconnects nephron and collecting duct, which emerge from mesenchyme and ureteric epithelia, respectively. The embryological origin of connecting tubule is controversial. Connecting tubule is thought to be a derivative of nephrogenic blastema (7). Consistently, it expresses calcium-regulating proteins NaCa and calbindin (8), which are not produced in collecting duct. Distal tubular cells break into the lumen of collecting duct. Such active cell invasion is thought to contribute to the connecting tubule (9, 10). $Lgr5^+$ progenitors have been proposed to produce the thick ascending limb, distal convoluted tubule, and connecting tubule (11). In contrast, Howie et al proposed that connecting tubule originates from the ureteric bud (12). Supporting this idea, the connecting tubule has some collecting duct features, including possessing intercalated cells and expressing 11β-hydroxysteroid dehydrogenase and epithelial Na^+ channel (ENaC) (13). To reconcile these observations, connecting tubule has been proposed as a hybrid epithelia generated by mutual induction from adjoining segments (14). However,

the identity of the ureteric contributor remains virtually unknown because a collecting duct-specific lineage-tracing marker is still unavailable.

In the collecting duct, two functionally and morphologically distinct cells are present: principal cells and interacted cells (15) (Figure 2). The homeostasis of water and electrolyte is fine-tuned by the expression of many transporters in principal cells and intercalated cells (16). Principal cells express apical sodium channel ENaC and water channel Aqp2, and basolateral Aqp3 and Aqp4. They mediate the water and sodium balance. Aqp2-positive cells are present in the connecting tubule, cortical collecting duct, outer medullary collecting duct, and inner medullary collecting duct (17). Consistent with their primary role in regulating the acid-base balance, intercalated cells express V-ATPase and carbonic anhydrase II (CAII). Intercalated cells can be further divided into two types according to their immunological differences: α-intercalated cells and β-intercalated cells. α-Intercalated cells display V-ATPase at the apical membrane and anion exchanger 1 (AE1) at the basolateral membrane, which is responsible for secreting protons into the urine and reabsorbing bicarbonates, respectively (16). While β-intercalated cells mirror the polarity and function of α-intercalated cells, they are characterized by the apical expression of pendrin, that secretes bicarbonates, and the basolateral expression of V-ATPase that reabsorbs protons (16). In addition, Non-A, Non-B intercalated cells express both pendrin and V-ATPase at the apical side and likely secrete bicarbonates and protons (16).

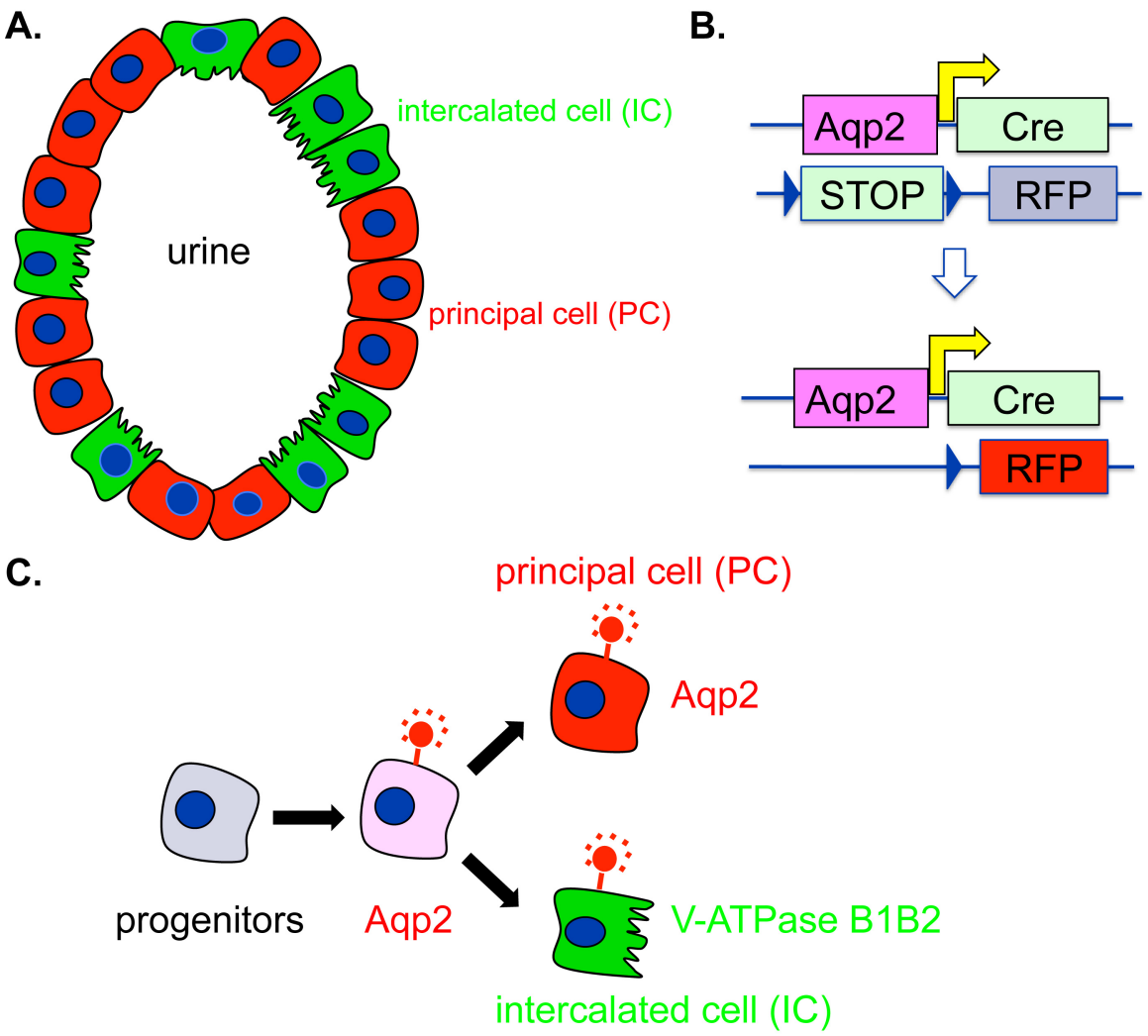

Figure 2. Aqp2^{+} progenitors give rise to both principal cells and intercalated cells.

(*A*) Collecting ducts contain principal cells (red) and intercalated cells (green). **(*B*)** Ai14 mice harbor a construct with a *loxP* site flanked a "STOP" cassette, which prevents the transcription of red fluorescence protein (RFP). Ai14 mice were bred with *Aqp2Cre* to generate double transgenic mice termed *Aqp2Cre RFP* mice. Cre-catalyzed recombination results in removal of the "STOP" sequence and activation of RFP expression in Aqp2-expressing cells and in the cells with a history of Aqp2 expression in *Aqp2Cre RFP* mice. **(*C*)** A working model for specification of principal and intercalated cells. Progenitors within the embryonic kidney first begin to express Aqp2 and RFP driven by the *Aqp2* promoter. Some of RFP labeled progenitor cells maintain the Aqp2 expression and give rise to principal cells, while other RFP labeled progenitor cells lose Aqp2 expression and become intercalated cells characterized by expression of intercalated markers.

Unlike the wide distribution of the principal cells throughout the kidney, the intercalated cells have a more restricted presence. α-Intercalated cells are found in connecting tubules, cortical collecting ducts, outer medulla collecting ducts and the initial part of inner medulla collecting ducts. β-Intercalated cells are abundant only in connecting tubules and cortical collecting ducts (16). Besides these major transporters, other important channels are also found in the collecting duct cells like chloride/bicarbonate exchangers SLC26A7 and SLC26A11, AE4, and Na^+/K^+ATPase (16).

Principal cells and intercalated cells in the collecting ducts act cooperatively to maintain the homeostasis of water and electrolytes. Anti-diuretic hormone (ADH), or vasopressin, increases the membrane localization as well as the protein expression of Aqp2 in the principal cells to increase water reabsorption (17). ADH is released by the pituitary gland in the dehydration status and promotes the conservation of water.

Mutations or malfunctions of these transporters have been observed and characterized in different human diseases (16-21). Patients with *AQP2* mutations or *ADH* receptor mutations develop nephrogenic diabetes insipidus (NDI), which is characterized by the inability to concentrate urine and excessive urine production (17). Gain-of-function mutations in ENaC cause hypertension while loss-of-function mutations in ENaC lead to hypotension (21). The other well-known disease caused by abnormal function of the α-intercalated cells is distal renal tubular acidosis (16). The α-intercalated cells depend on the basolateral AE1 to reabsorb bicarbonates and apical V-ATPase to secret protons into the

urine. Mutations in either AE1 or V-ATPase fail to acidify the urine and decrease the plasma bicarbonates, leading to distal renal tubular acidosis (16). Thus, a better understanding of the function and development of the collecting duct may facilitate the discovery of new therapeutic strategies for kidney disease.

In this project, we employed *in vivo* genetic lineage tracing (described in 1.7) combined with high-resolution image analyses. With the newly constructed Aqp2-lineage tracing mouse model using RFP as the tracing marker, we demonstrated that the $Aqp2^{+}$ progenitor cells are responsible for the generation of connecting tubule and colleting duct during normal development (i.e, without *Dot1l* deletion (Figure 2). The progenitor cells can differentiate into various types of cells including molecularly distinct transitional cells in the connecting tubule, and all the cell types (principal, α-intercalated, and β-intercalated cells) of the collecting duct.

1.5 No progenitor cells identified for the renal collecting duct system.

The kidney contains nephrons and the collecting duct system. Nephrons consist of the glomerulus, proximal tubule, loop of Henle, and distal convoluted tubule. Several renal cell lineage tracing mouse models have been used to identify the stem/progenitor cells responsible for generation of nephron during development. These models include *Six2-Cre (9)*, *Lgr5-EGFP-ires-CreER^{T2} (11)*, and *HoxB7-Cre* mice (22, 23). The *Six2-Cre* mice include a BAC transgenic model carrying a *Tet-off-eGFPCre (TGC)* cassette and knock-in models with *TGC, CreER^{T2}* and *eGFPCreER^{T2}* cassettes residing at the *Six2* initiation codon.

The homeodomain family member Six2 plays a very important role in the maintenance of the progenitor cell pool in the metanephric mesenchyme. Six2 deficiency leads to early termination of nephrogenesis and loss of progenitor cells. McMahon's group provided the first direct evidence that the Six2-expressing cells are multipotent and directly contribute to the main body of nephron, including podocytes, proximal tubule, loop of Henle, and distal convoluted tubule, but not collecting duct, stromal cells, and interstitial cells (9). These authors not only confirmed the multipotency of the Six2 progenitors but also their self-renewal capacity. Other studies have shown that Cited1 is uniquely expressed in the cap mesenchyme like Six2 (24). Using a *Cited1-CreER*^{T2} BAC knock-in mouse model, Caestecker's group reported that Cited1^{+} progenitor cells also contribute to the nephron but not the collecting duct epithelium when traced by LacZ (25). Most recently, Hans Clevers's group performed lineage tracing with mice carrying an *eGFPCreER*^{T2} cassette inserted at the *Lgr5* locus. They used Lgr5 as a marker of a more committed form of progenitor cells within the Six2 population (11). Lgr5^{+} progenitor cells only give rise to the thick ascending limb of Henle's loop and the distal convoluted tubule.

The collecting duct system includes the collecting duct and connecting tubule. Connecting tubule connects the nephron and collecting duct. However, little is known about the progenitors responsible for generating the connecting tubule, collecting duct, or both. This becomes the central question to be addressed in this project.

1.6 *Dot1l* as a primary epigenetic regulator of ENaC in kidney.

Dot1l represents a unique histone H3 lysine 79 methyltransferase. It does not contain a classical enhancer of zeste, and trithorax domain as other methyltransferases do (26). Dot1l is widely expressed and highly conserved and can add one, two, or three methyl groups to lysine 79 at the global domain of histone H3 (26-28). Previous studies from our group have led to the identification of 5 alternative splicing variants (Dot1a-e) in mice (29). In addition to its well-known function in leukemogenesis (30-35), we also have shown that *Dot1l* plays a crucial role in the kidney (36-39). More specifically, *Dot1l* is under the regulation of aldosterone, a steroid hormone that plays a key role in sodium metabolism and blood pressure control through the epithelial Na^+ channel (ENaC) (40-42). The channel consists of three homologous subunits α-, β-, and γENaC and plays a key role in Na^+ homeostasis and blood pressure control (41-46).

We have reported that *Dot1l* represses αENaC (39, 40, 47-49). This repression involves Dot1l-mediated H3 K79 hypermethylation of the αENaC promoter (40). The execution and relief of this repression require the interactions of Dot1l with its binding partners AF9 and AF17 (39). AF9 and AF17 are transcription factors that were reported to bind to Dot1l in a yeast two-hybrid assay(39). AF9 decreases αENaC transcription by recruiting Dot1l to the promoter region of αENaC (39). Phosphorylation of AF9 at S435 by Sgk1 compromises Dot1l-AF9 interaction, resulting in H3 K79 hypomethylation at the αENaC promoter and upregulation of αENaC (48). Aldosterone activates αENaC in part by increasing Sgk1 expression and thus phosphorylation of AF9 as well as by decreasing Dot1l

and AF9 expression (48). In contrast to AF9, AF17 facilitates Dot1l nuclear export by competing with AF9 for binding to Dot1l (47, 49). Thus, AF17 upregulates αENaC by exhausting Dot1l at the αENaC promoter region. Indeed, AF17-deficient mice develop hypotension due to decreased αENaC expression and activity (50). Consistently, mice with Dot1l inactivated in the connecting tubule/collecting duct displayed increased αENaC expression (36), blood sodium concentration, and blood pressure (data not shown). These results are consistent with our *in vitro* findings that Dot1l is a negative regulator of ENaC.

1.7 *In vivo* genetic lineage tracing, a powerful tool to identify the stem/progenitor cells

Identification and understanding of the stem and progenitor cells within the adult organ hold promise to translate the stem cell research to clinical applications. The lineage-tracing technique represents the most powerful tool to identify the stem/progenitor cells in their native environment and decipher the origins of the tissue.

The key components of the genetic lineage tracing technique include the use of Cre recombinase and Cre-dependent reporters. Cre recombinase is an enzyme that catalyzes the recombination of DNA between two loxP sites. A LoxP site consists of 34 base pair (bp) with two 13 bp palindromic sequences separated by an 8bp spacer region. A floxed allele means that the allele is placed between two loxP sites. Cre recognizes the loxP sites and mediates the deletion or reversion

of the floxed DNA sequence, when the two loxP sites are in the same or opposite direction (51-53), respectively.

In the genetic lineage tracing experiment, one mouse line carries a transgene or a knock-in construct that drives Cre expression under a tissue- or cell-specific promoter. This line is often referred as a deletor or Cre driver. The Cre driver is crossed to a second mouse line harboring a Cre-dependent reporter, such as red fluorescent protein (RFP). RFP is under control of a ubiquitous promoter, usually consisting of a **C**MV-IE enhancer/chicken beta-**a**ctin/rabbit beta-**g**lobin hybrid promoter (CAG). Between the RFP coding sequence and CAG promoter is a loxP-flanked “STOP” cassette, which prevents transcription of the reporter (54). In mice harboring both a Cre driver and RFP reporter, Cre recombinase-mediated recombination results in deletion of the “STOP” cassette and expression of RFP in the Cre-expressing tissue(s) or cells. Because CAG is ubiquitously active and can be prevented by the “STOP” cassette, RFP expression is achieved only in the tissue(s)/cells that express Cre recombinase to remove the “STOP” cassette. Once a cell activates the RFP, its offspring also have a permanently deleted “STOP” cassette and persistent expression of RFP, leading to a population of RFP-traced cells. This technique is extremely useful in stem cell research, especially in organs with complex cellular hierarchies like kidney (52, 53).

Chapter 2

Materials and Methods

2.1 Antibodies.

The primary antibodies used are rabbit anti-H3m2K79 (abcom, ab3594-100), rabbit anti-AE1 (Alpha Diagnostic, 396768A3), rabbit anti-Aqp1 (Millipore, LV1598400), rabbit anti-NCC (Millipore, AB3553), mouse anti-RFP (Cell Biolabs, AKR-021), rabbit anti-RFP (Clontech, 632496), and nine antibodies from Santa Cruz: goat anti-uromodulin (sc-19554), goat anti-megalin (sc-16478), goat anti-calbindin (sc-7691), goat anti-Aqp2 (sc-9882), goat anti-Aqp3 (sc-9885), goat anti-pendrin (sc-16894), rabbit anti-Aqp2 (sc-28629), mouse anti-V-ATPase B1 and B2 (sc-55544), and mouse anti-CAII (sc-48351). The secondary antibodies from Invitrogen are Alexa Fluor 488-conjugated goat anti-mouse IgG (774904), Alexa Fluor 647-conjugated donkey anti-rabbit IgG (A31573), Alexa Fluor 488-conjugated donkey anti-goat IgG (51475A), Alexa Fluor 594-conjugated donkey anti-mouse IgG (796011), and Alexa Fluor 594-conjugated donkey anti-rabbit IgG (A10042).

2.2 Generation, genotyping, and characterization of *Aqp2Cre RFP* mice.

Aqp2Cre mice have been previously reported (55). Ai14 mice (Jackson Lab) harbor a loxP-flanked STOP cassette, which prevents transcription of a CAG promoter-driven RFP (54). Ai14 mice were crossed with the *Aqp2Cre* line to generate double transgenic animals, which is termed *Aqp2Cre RFP*. Genotyping was performed as described. Because both Ai14 and *Aqp2Cre* strains are maintained in C57BL6 background, *Aqp2Cre RFP* mice should be genetically

pure. They were maintained with the RFP allele being homozygous and *Aqp2Cre* heterozygous. Mice at age of 2-5 months were used.

2.3 Immunofluorescence studies.

Kidneys were fixed in 4% paraformaldehyde overnight at 4°C, embedded in paraffin, and cut into thin (2 μm) and thick (8 μm) sections for epifluorescence and confocal microscopy, respectively. The actual thickness of the thick sections determined by confocal microscopy ranges from 7 to 10 μm.

Paraffin sections were deparaffinized for 3 X 5 minutes in xylene. Deparaffinized sections then were hydrated with 100%, 95%, 75%, 50% ethanol and water for 5 minutes each time. Prior to blocking, antigen retrieval was performed. Sections were immersed in antigen retrieval buffer (9 ml 0.1M citric acid, 41 ml 0.1M sodium citrate, and 450 ml H_2O, pH=6.0) and boiled for 16 minutes in a microwave. After cooling to room temperature, paraffin sections were blocked with 5% BSA/0.5% Triton X-100 in PBS for 1 hour. Primary antibodies from goat, rabbit or mouse were diluted in 5% BSA/0.5% Triton X-100 in PBS at a concentration of 1:50~1:100 and incubated overnight at 4°C. Following three 5 minute washes with PBS, the sections were incubated with Alexa Fluor 488-conjugated donkey anti-goat IgG, Alexa Fluor 647 donkey anti-rabbit IgG, or Alexa Fluor 594 donkey anti-mouse IgG at the concentration of 1:500~1:1000. After three 5 minute washes with PBS, the sections were counterstained with DAPI and mounted.

All slides were examined under an epifluorescence microscope (Olympus IX71) or confocal microscope (Nikon eclipse Ti). Since DAPI signaling is not on the same focal plane as RFP and other markers, we composed 7 images obtained by confocal microscope with 0.5 μm optical sections to generate a composite view for each confocal picture shown in the figures. Adobe Photoshop CS4 was used to assign each marker a color, which may be different from that observed under the microscope for consistency between experiments. We examined 3-4 mice. Five to ten fields were taken from the cortex, outer medulla, and inner medulla in each mouse. Cell counting was conducted as we have reported (28) and restricted to RFP^+ tubules. In each case, we counted >100 RFP^+ tubules with ~1000 cells from 3-4 mice. DAPI staining was used to aid the counting. The percentage of derived intercalated cell was defined as X^+RFP^+ / (X^+RFP^+ + X^+RFP^-) cells, where X indicates an intercalated cell marker.

2.4 Kidney primary cell isolation.

Two-month-old mice were anesthetized and sacrificed by cervical dislocation. Kidneys were removed and immediately placed in cold Hanks Balanced Salt Solution (HBSS) (Invitrogen) with 1% antibiotic/antimycotic solution (Sigma). After the renal papilla and inner medulla were removed, the renal cortical section was minced into small pieces with a sterilized blade and incubated at 37°C for 30 minutes in HBSS with 0.5mg/ml collagenase type II (Invitrogen) with agitation at every 10 minutes. An equal volume of horse serum (Invitrogen) was used to inactivate the enzymes in the cell suspension. After the cell suspension was

gently mixed and seated for 1-3 minutes, the supernatant was transferred to a 15-ml tube and centrifuged for 7min at 200g at 4°C. After the pellet was washed with HBSS and centrifuged again, it was suspended and cultured in a modified DMEM/F-12 medium (56) (Invitrogen) with 0.01ug/ml hEGF (R&D), 2 ug/ml APO transferrin (Sigma), 0.11 μmol/ml hydrocortisone (Sigma), 1X insulin/transferrin/selenium (Invitrogen), and 1% antibiotic/antimycotic solution.

2.5 Immortalization and establishment of primary cells.

After the primary cells formed spheres, which took about 1 week, the medium was replaced with a pre-conditioned medium containing retroviruses for infection. The preconditioned medium was prepared as follows. First, fibroblast line PA317 LXSN16E6E7 (57) (ATCC) harboring the human papilloma antigen E6E7 was cultured with DMEM/F12 to confluency. The medium was harvested and filtered through a 0.45-μm filter (VWR) to remove PA317 LXSN16E6E7 cells, followed by addition of polybrene (Sigma) at the final concentration of 8 μg/ml. To increase the efficacy of infection and immortalization, the primary cells were infected at least two times. Cells infected by the viruses were selected with G418 (Sigma) at various concentrations (100, 200, and 400 μg/ml). Primary cells without infection were used as a negative control for G418 resistance. G418-resistant cells were expanded in DMEM/F12 medium to confluency. The cells were detached by TryPLE Express (Invitrogen) and filtered through a 40-μm cell strainer (Corning) to obtain a single-cell suspension. RFP positive cells were then sorted by fluorescence activated cell sorting at the Cytometry and Cell Sorting Core, Baylor

College of Medicine. Each RFP^+ single cell was placed into a single well of 96-well plate. After a series of expansions, single-cell-derived clones were selected and characterized by immunofluorescence and immunoblotting analyses as we reported (38).

2.6 Generation of inducible *Aqp2ER^{T2}CreER^{T2}* construct.

The plasmid pcDNA 3.1(+) was used as the parental vector. We first inserted a 2.5 kb DNA fragment at the 3' arm to generate WZ692. The 2.5kb genomic DNA fragment starting from the first codon immediately after the start codon of mouse Aqp2 was amplified and cloned into pcDNA 3.1(+) at PciI and BstZ171. The PCR product was obtained with the following two primers: WZ1499 and WZ1500. A 2.9kb fragment containing *ER^{T2}CreER^{T2}* cassette was released from pCAG-ER^{T2}CreER^{T2} (Addgene Plasmid #13777) with EcoRI and NotI and subsequently cloned into WZ692 at these sites to generate WZ693a. To insert the 5' arm, we used 4 primers to generate two overlapping PCR fragments. The first fragment was generated with WZ1502 and WZ1494 (All primers are listed in Table 1), using mouse genomic DNA as template. This fragment contains 4.1 kb genomic DNA upstream of the start codon of the mouse *Aqp2* gene and 30 bp encoding the first 10 amino acids of ERT2 as part of the overlapping region of the second fragment. The second fragment was produced with the primers WZ1495 and WZ1496 using pCAG-ERT2CreERT2 as template. This 1.6 kb PCR product harbors the whole ER^{T2} and partial Cre coding region. The final 5.7 kb insert was obtained using WZ1502 and WZ1496 and the two fragments as the templates.

To create the final target vector WZ694C2, WZ693a was digested with EcoRI and AgeI to obtain a 9.5-kb vector fragment, which was then ligated to the 5.7 kb fragment after EcoRI and AgeI digestion. DNA sequencing verified the authenticity of all inserted fragments.

Primer name	Sequence
WZ1494	5'-AAGGTTGGCAGCTCTCATGTCTCCAGCCATGCTGCTCGGCCTTCTGAGCGCTGGCCAGTGGTCT-3'
WZ1495	5'-AAGGTTGGCAGCTCTCATGTCTCCAGCCATGCTGCTCGGCCTTCTGAGCGCTGGCCAGTGGTCT-3'
WZ1496	5'-TACACCAGAGACGGAAATCCATCGCTCG-3'
WZ1499	5'-ATCTGTGTATACTGGGAACTCCGGTCCATAG-3'
WZ1500	5'-CAGACTACATGTTAGGTCATACTGATACAACAGGATGC-3'
WZ1502	5'-ATCTGTGAATTCCTGGCTCCCTAAACCTCCTATG-3'

Table 1: Primers used in generation of the inducible *Aqp2ER^{T2}CreER^{T2}* construct.

2.7 Metabolic balance studies.

Twenty-four-hour urine collection was carried out after the mice were acclimated for 3-7 days in Tecniplast metabolic cages (Exton, PA, USA) with free access to water and food (28, 50).

Blood pressure was measured by CODA tail-cuff blood pressure system (Kent Scientific, Torrington, CT). Mice were trained with the animal holders and pretested for blood pressure measurement with the system several times. Each time, mice are restrained in the holders with the tail extended onto the warming platform. The temperature was set at level 2 (35°C). A nose cone was used to adjust the movement of the mice, which ensures the mice are comfortable while also being confined. The Occlusion Cuff (O-Cuff) was placed onto the base of the tail of the mice without pressurizing it, followed by VPR cuff (V-Cuff) with the larger end facing the Occlusion Cuff. CODA software was used to determine both the systolic and diastolic pressure of the mice. Each mouse was assigned to a different CODA channel and monitored. When starting the measurement, a total 20 cycles were set to run in each experimental session. The blood pressure of each mouse was graphically displayed in real-time. Data from each session were collected and analyzed.

2.8 Blood and urine measurements.

Urinary parameters including Na^+, K^+, and creatinine were measured with Roche Cobas Integra 400 plus at the University of Texas MD Anderson Cancer Center.

Urine osmolarity was determined by vapor pressure (WescorVapro Vapor Pressure Osmometer 5520, Scimetrics, Houston, TX, USA). Before measurement, the urine was centrifuged to remove any contaminants. After calibrating the osmometer with the standard solution in the order of 290 mmol/kg and 1000 mmol/kg, 10 μl urine sample was transferred to a solute-free paper disc in the sample holder. Measurement was initiated by pushing and locking the sample holder into the osmometer. It takes about 80 seconds for each measurement.

Blood parameters were assessed using VetScani-STAT 1 (ABAXIS). About 100 μl blood was collected from the anesthetized mouse heart by insulin syringe. The blood was subsequently loaded into the i-STAT *EC+* cartridge. After inserting the cartridge into the analyzer, information about blood gas, hematology, and electrolytes was automatically delivered in 2 minutes.

2.9 Statistical analysis.

We reported quantitative data as mean±SEM and used Student t-test with the statistical significance set at $P<0.05$.

All mouse studies were conducted in accordance with NIH Guideliness for the Care and Use of Laboratory Animals and were approved by the University of Texas Health Science Center at Houston Animal Welfare Committee.

Chapter 3

Results

3.1 The *Aqp2Cre* transgene does not significantly impact kidney development and function.

Our previous studies have shown that *Dot1l* histone methyltransferase downregulates the expression and activity of epithelial sodium channel (ENaC) (39, 40, 47-49). ENaC is found in the connecting tubule/collecting duct tubules where Aqp2 is exclusively expressed within kidney (16, 17). To characterize the *in vivo* function of *Dot1l*, we first generated *Dot1l*$^{f/f}$ mice, which allows inactivation of *Dot1l* upon Cre-mediated recombination (33).

To generate connecting tubule/collecting duct-specific *Dot1l* conditional knockout mice, we crossed *Dot1l*$^{f/f}$ mice with an *Aqp2Cre* transgenic line. This line carries a phage-derived artificial chromosome (PAC) harboring an *Aqp2Cre* construct. The *Aqp2Cre* transgene contains 125-kb 5' and 31-kb 3' of the *Aqp2* gene to avoid disrupting any potential regulatory elements of *Aqp2,* and the Cre recombinase was inserted at the ATG codon of *Aqp2* in this transgene (55). The resulting offspring are referred to as *Dot1l*$^{f/f}$ *Aqp2Cre* in the entirety of the thesis.

To test whether the *Aqp2Cre* transgene disturbs water and sodium handling and acid-base status, we collected the urine samples and measured urinary parameters with freshly collected samples from *Dot1l*$^{f/f}$ and *Dot1l*$^{+/+}$ *Aqp2Cre* mice. There was no significant difference in any of the urinary parameters tested between the two genotypes (Figure 3). These results demonstrate that the *Aqp2Cre* transgene does not significantly impact kidney development and function. Similarly, careful examination revealed no visualized differences in kidney morphology and histology between *Dot1l*$^{f/f}$ and *Dot1l*$^{+/+}$.

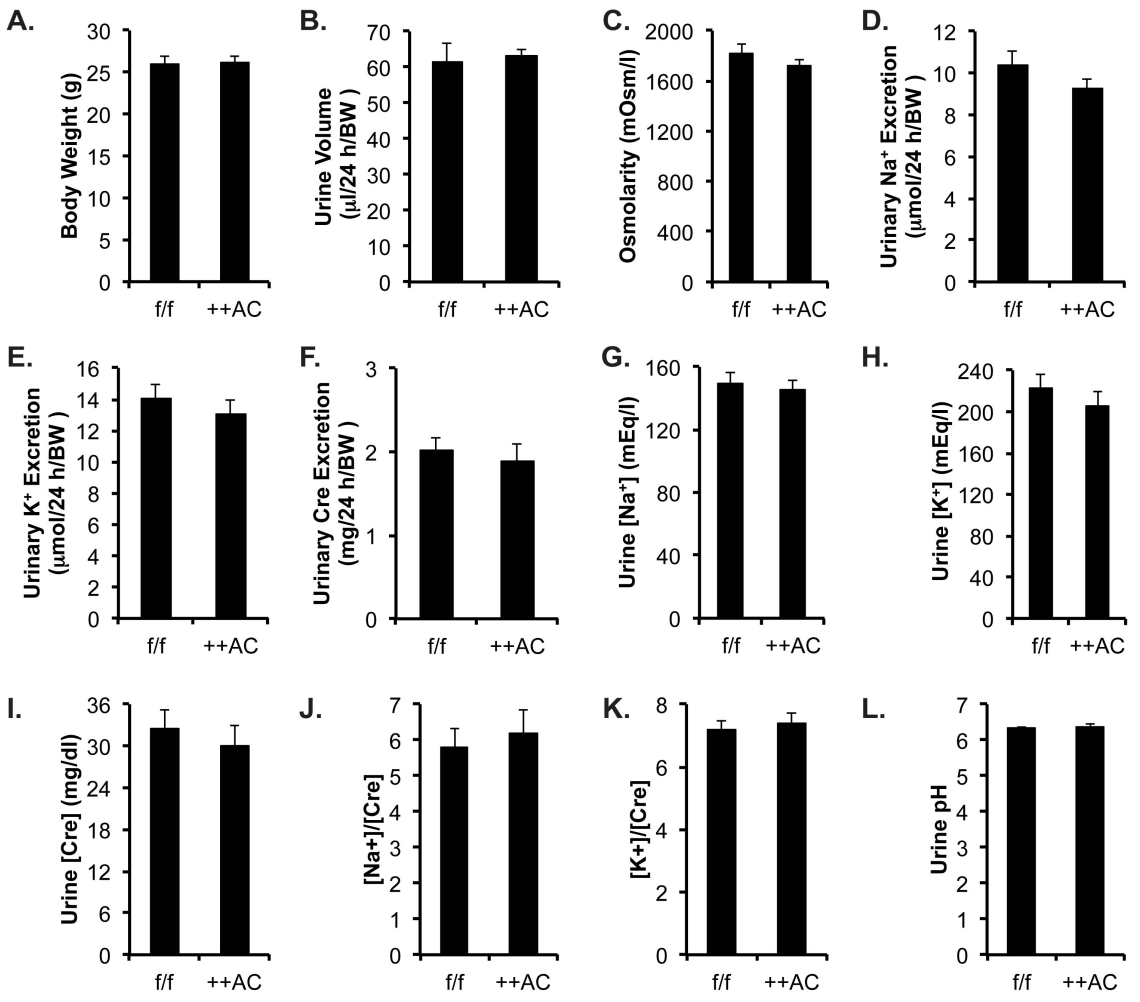

Figure 3. The *Aqp2Cre* transgene does not significantly affect renal function.

Urine analyses of *Dot1l*$^{f/f}$ and *Dot1l*$^{+/+}$ *Aqp2Cre* mice (*n*=8 mice per group) were conducted to measure the parameters as indicated. Urine volume was measured from samples collected for 24-h. The concentrations of urinary parameters were determined with fresh samples collected by bladder voiding. No *P*<0.05 versus *Dot1l*$^{f/f}$ was found with *Aqp2Cre* mice, indicating that apparently Dot1l deletion does not have a severe impact on kidney development (28).

3.2 *Aqp2Cre* drives Cre expression exclusively in Aqp2$^+$ cells.

To determine if Cre is expressed specifically in Aqp2$^+$ expressing cells, we performed double immunofluorescence studies with adult kidneys from *Dot1l*$^{f/f}$ and *Dot1l*$^{f/f}$ *Aqp2Cre* mice. In the double immunofluorescence experiments, an antibody specific for Aqp2 was used in combination with an antibody against Cre. As shown in Figure 2 in reference (28), strong nuclear staining of Cre was observed in most or all of Aqp2$^+$ cells in *Dot1l*$^{f/f}$ *Aqp2Cre.* However, all Aqp2$^-$ cells in either *Dot1l*$^{f/f}$ or *Dot1l*$^{f/f}$ *Aqp2Cre* kidneys have no detectable Cre staining. These results suggest that we have successfully developed *Dot1l*$^{f/f}$ *Aqp2Cre* mice and that *Aqp2Cre* drives persistent Cre expression exclusively in Aqp2$^+$ cells.

3.3 Disruption of *Dot1l* abolishes all H3 K79 methylation events.

To determine whether Cre-mediated disruption of *Dot1l* abolishes histone H3 K79 mono-, di-, and trimethylation (H3m1K79, H3m2K79, and H3m3K79) in Aqp2$^+$ expressing cells, a set of double immunofluorescence studies were conducted, using adult kidneys from *Dot1l*$^{f/f}$ and *Dot1l*$^{f/f}$ *Aqp2Cre* mice. For each of these double immunofluorescence experiments, we used the anti-Aqp2 antibody to label the Aqp2$^+$ cells, and an antibody specific for H3m1K79, H3m2K79, or H3m3K79 to check the methylation status at histone H3 K79.

All methylation events (mono-, di-, and tri-methylation) at H3 K79 are robustly detected in various Aqp2$^-$ cells in *Dot1l*$^{f/f}$ *Aqp2Cre* as well as in all types of cells including Aqp2-expressing cells in *Dot1l*$^{f/f}$ mice. However, these methylation

events are completely abolished in Aqp2-expressing cells in *Dot1l*$^{f/f}$ *Aqp2Cre* mice (Figure 4). These results demonstrate that *Dot1l* is solely responsible for all of these modifications *in vivo* in mouse kidney and that loss of H3m2K79 may be used as a marker to trace the Aqp2^{+} lineage in *Dot1l*$^{f/f}$ *Aqp2Cre* mice.

3.4 Aqp2-expressing cells give rise to intercalated cells in *Dot1l*$^{f/f}$ *Aqp2Cre* mice.

Through a similar set of double immunofluorescence staining experiments, we surprisingly found that deletion of *Dot1l* in the principal cells (i.e. Aqp2^{+} cells) leads to loss of H3m2K79 not only in principal cells, but also in intercalated cells. Using multiple intercalated cell markers (V-ATPase B1B2 (58) for all intercalated cells, AE1 for α-intercalated cells, and Pendrin for β-intercalated cells), we discovered that about 75% of intercalated cells have no detectable H3m2K79 as well (Figure 5). The undetectable methylation events in the intercalated cells are not due to promiscuous Cre expression in these cells, since we are not able to detect any Cre positive intercalated cells (Figure 6 in reference (28)). Hence, we proposed that Aap2^{+} progenitors express Cre recombinase, leading to abolition of Dot1l-mediated H3m2K79. These progenitor cells can differentiate either into principal cells or intercalated cells. Principal cells maintain the ability to persistently express Cre as well as Aqp2. However, once Aqp2^{+} progenitor cells

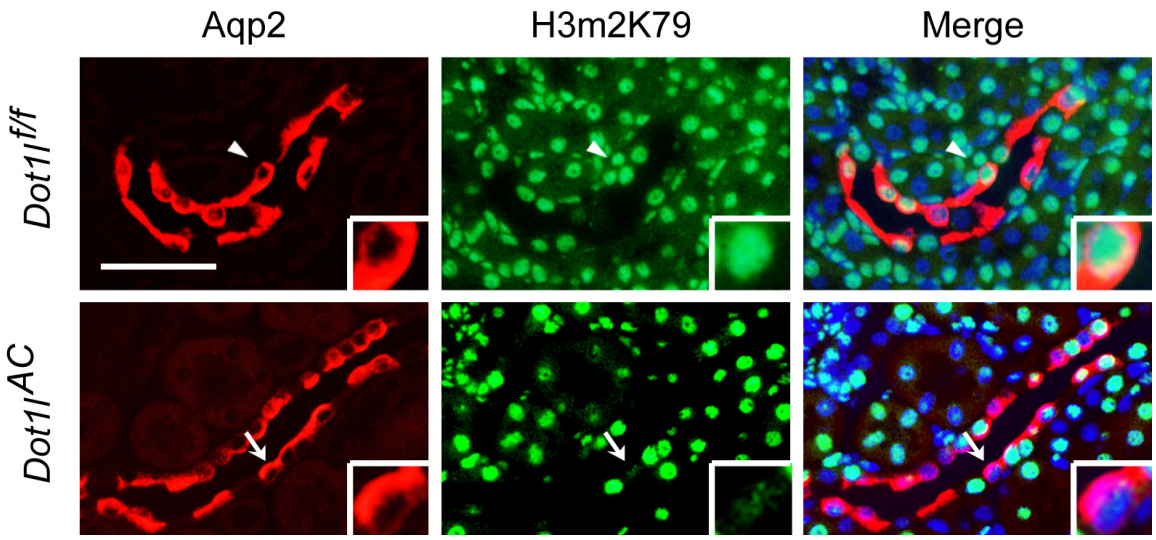

Figure 4. Disruption of *Dot1l* abolishes H3m2K79 methylation in *Dot1l*$^{f/f}$ *Aqp2Cre* mice (*Dot1l*^{AC}).

Representative epifluorescence images showing expression of Aqp2 (red) and H3m2K79 (green) in both *Dot1l*$^{f/f}$ and *Dot1l*$^{f/f}$ *Aqp2Cre* mice. Deletion of *Dot1l* abolished H3m2K79 in Aqp2^{+} cells in *Dot1l*$^{f/f}$ *Aqp2Cre* mice but not in control kidneys. Nuclei labeled with DAPI were shown in blue. Arrows and arrowheads: Cells that were amplified in the inserts displayed intact or disrupted nuclear H3m2K79. Scale bar: 50μM and 12.5μM for inserts. This figure was revised from the Figure 2 that was published in the Journal of the American Society of Nephrology. Wu H*, Chen L*, Zhou Q, Zhang X, Berger S, Bi J, Lewis DE, Xia Y, Zhang W: Aqp2-expressing cells give rise to renal intercalated cells. *J Am Soc Nephrol* 24: 243-252, 2013. Copyright by the American Society of Nephrology.

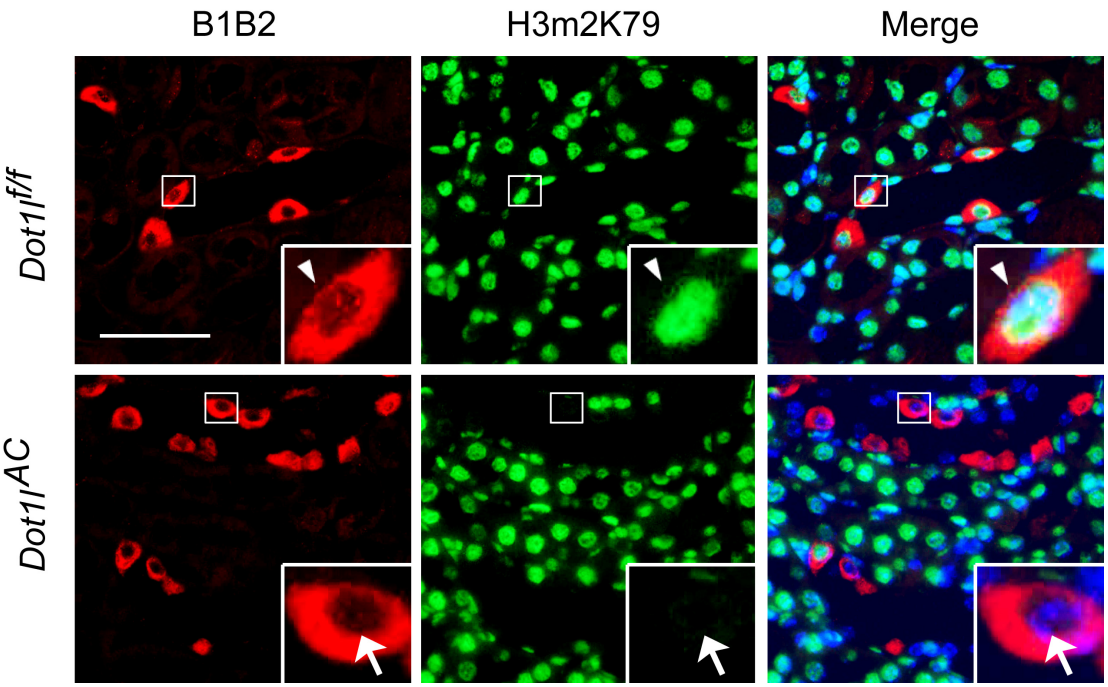

Figure 5. Loss of H3m2K79 in intercalated cells in *Dot1l*$^{f/f}$ *Aqp2Cre* mice (*Dot1l*^{AC}).

Representative epifluorescence images showing expression of intercalated cell marker B1B2 (red) and H3m2K79 (green) in both *Dot1l*$^{f/f}$ and *Dot1l*$^{f/f}$ *Aqp2Cre* mice. Most of the intercalated cells lack detectable H3m2K79 in *Dot1l*$^{f/f}$ *Aqp2Cre* mice (*Dot1l*^{AC}, bottom), but not in the control mice (*Dot1l*$^{f/f}$, top). DAPI-labeled nuclei were shown in blue. Arrows and arrowheads: Cells that were amplified in the inserts displayed intact or disrupted nuclear H3m2K79. Scale bar: 50μM and 12.5μM for inserts. This figure was revised from the Figure 4 that was published in the Journal of the American Society of Nephrology. Wu H*, Chen L*, Zhou Q, Zhang X, Berger S, Bi J, Lewis DE, Xia Y, Zhang W: Aqp2-expressing cells give rise to renal intercalated cells. *J Am Soc Nephrol* 24: 243-252, 2013. Copyright by the American Society of Nephrology.

convert into intercalated cells, they bear two markers: abolished H3m2K79 and failure to persistently express Cre due to inactivation of *Aqp2* promoter. In brief, we concluded that Aqp2$^+$ progenitor cells give rise to not only principal cells, but also intercalated cells, during kidney development in the **absence of *Dot1l***.

However, two important questions remain unclear. 1) Do Aqp2$^+$ progenitors contribute to **connecting tubules**? And 2) is derivation of intercalated cells from Aqp2$^+$ progenitors a **natural process** rather than just a simple artifact of *Dot1l* deletion? Thus, we exploit a well-established red fluorescent protein (RFP) reporter line to trace Aqp2$^+$ lineage in *Dot1l*$^{+/+}$ background.

3.5 Generation of a new Aqp2-lineage tracing mouse model.

To address these questions raised by using loss of H3m2K79 as a lineage-tracing marker, we imported Ai14 mice from Jackson Laboratory. Ai14 mice harbor a targeted mutation of the *ROSA26* locus with a *loxP* site flanked by a "STOP" cassette, which prevents the transcription of a CAG promoter-driven RFP.

Accordingly, Ai14 mice were bred with *Aqp2Cre* to generate double transgenic mice termed *Aqp2Cre RFP* mice. As shown in Figure 6, immunofluorescence staining revealed no visible RFP in Ai14 mice because they do not contain the *Aqp2Cre* transgene. In contrast, cre-catalyzed recombination results in removal of the "STOP" sequence and activation of RFP expression in Aqp2-expressing cells and in the cells with a history of Aqp2 expression in *Aqp2Cre RFP* mice (Figure 7). These results not only demonstrate the absolute dependency of RFP

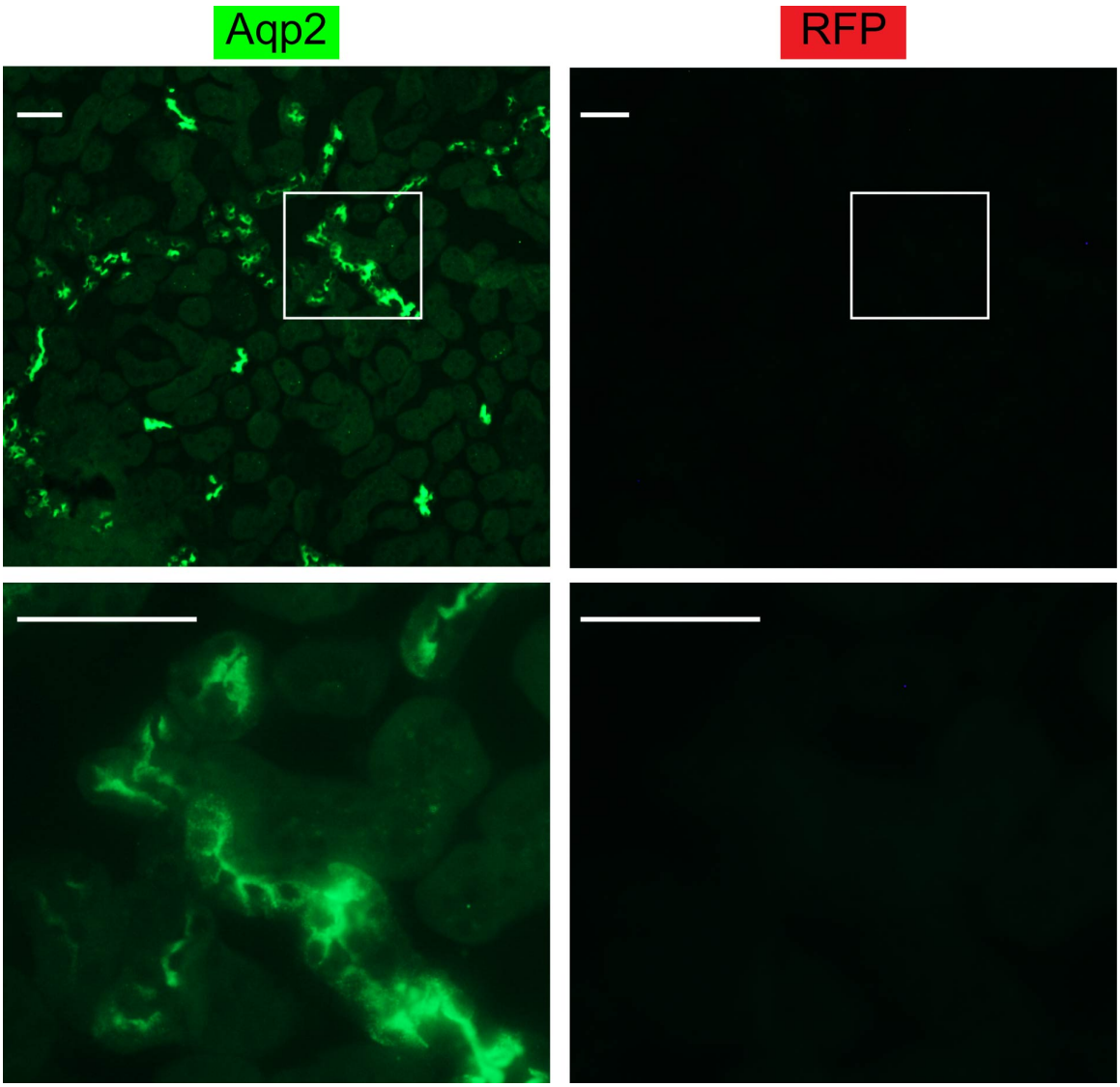

Figure 6. RFP is not expressed in Ai14 kidney.

Representative double immunofluorescence staining images showing staining of Aqp2 (green) and RFP (red) in Ai14 kidney. Boxed areas were 4X magnified and shown at the bottom. RFP signals were undetectable, indicating the dependency of Cre-mediated removal of the STOP cassette upstream the RFP coding sequence (tdTomato). Scale bar: 100 μm.

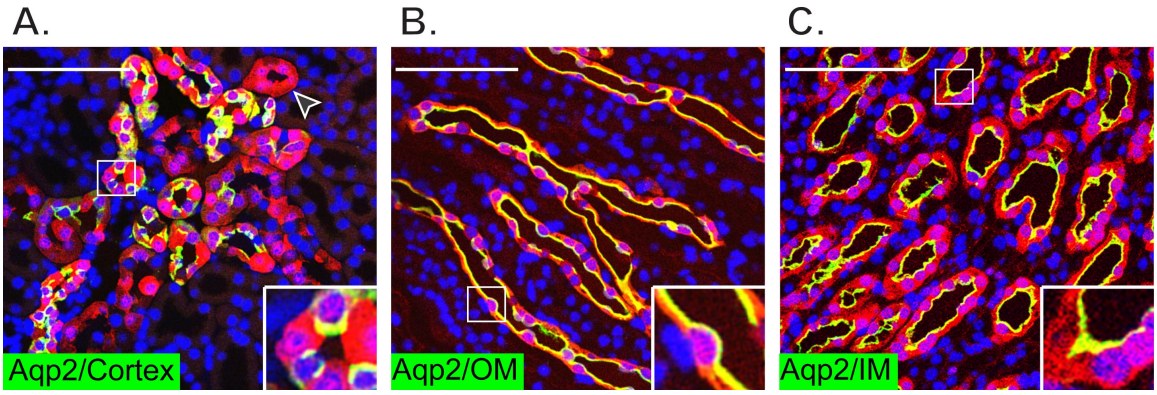

Figure 7. Almost all Aqp2$^+$ cells are RFP$^+$.

Representative merged confocal images showing RFP co-expression with Aqp2 in the areas as indicated in *Aqp2Cre RFP* kidney. Boxed areas were 3X magnified in the inserts. OM: outer medulla. IM: inner medulla. Black arrowhead: CNT2 or CNT3 tubules (see Figure 30 and text) lacking detectable Aqp2$^+$ cells, but contain multiple RFP$^+$ cells. Scale bar: 100 μm.

expression on *Aqp2Cre* transgene, but also confirm the specificity of the RFP antibody.

3.6 RFP faithfully recapitulates the endogenous expression of Aqp2.

To test if *Aqp2Cre* transgene is able to reproduce the expression profile of the endogenous Aqp2, we performed double immunofluorescence staining to determine if RFP is co-expressed with Aqp2. Kidney sections were stained with the antibodies specific for RFP and Aqp2, respectively, and examined by epifluorescence and confocal microscopy. Figure 7 shows the representative confocal images from the cortex, medulla and papilla of an *Aqp2Cre RFP* kidney. Aqp2 expression is restricted to connecting tubule and collecting duct throughout the whole kidney. Aqp2 staining signals were concentrated at the apical region of collecting duct and connecting tubule. The vast majority, if not all, of $Aqp2^+$ cells were positive for RFP, indicating a high efficiency of Cre-mediated recombination and a high fidelity of the *Aqp2Cre* and thus RFP in mimicking Aqp2 expression.

More careful examination of these images revealed that the both $Aqp2^+RFP^+$ and $Aqp2^-RFP^+$ cells coexist in the same collecting ducts in the whole kidney. According to our hypothesis and as detailed later in the thesis, these $Aqp2^-RFP^+$ cells were intercalated cells (see below). Surprisingly, some $Aqp2^-RFP^+$ cells were presented in tubules that contained no $Aqp2^+$ cells at all. These tubules existed exclusively in the cortex and were identified as segments of connecting tubule (see below).

To demonstrate if *Aqp2Cre* mimics the silencing of the endogenous *Aqp2* in various segments of nephron, we conducted a series of double immunofluorescence staining to assess co-expression of RFP with other segment-specific markers.

Aqp1 labels the proximal tubules, medullary descending thin limb, and blood vessels (59, 60). Megalin and THP are expressed in proximal tubule and thick ascending limb of loop of Henle, respectively (11). These three markers are expected to have no overlap with Aqp2 and RFP. Indeed, as shown in Figure 8, no $Aqp1^+$, $Megalin^+$, and THP^+ cells were RFP^+.

Calbindin D28K and Aqp2 share a partial overlapping expression domain. Calbindin is limited to the distal convoluted tubule (11), connecting tubule (61), and proximal part of collecting duct (62), all of which are located in the cortex. As expected, Calbindin $D28K^+$ cells appeared only in the cortex, most of which were also RFP^+ (Figure 9). This indicates faithful recapitulation of the partial overlapping of Aqp2 with calbindin D28K in connecting tubule and proximal part of collecting duct.

Collectively, these findings demonstrate that 1) RFP faithfully recapitulates the spatial activation of the endogenous Aqp2 in connecting tubule/collecting duct and the silencing of the endogenous *Aqp2* in most, if not all, of the tubular cells from proximal tubule to distal convoluted tubule and 2) the *Aqp2Cre* does not impact the expression pattern of these segment-specific markers tested.

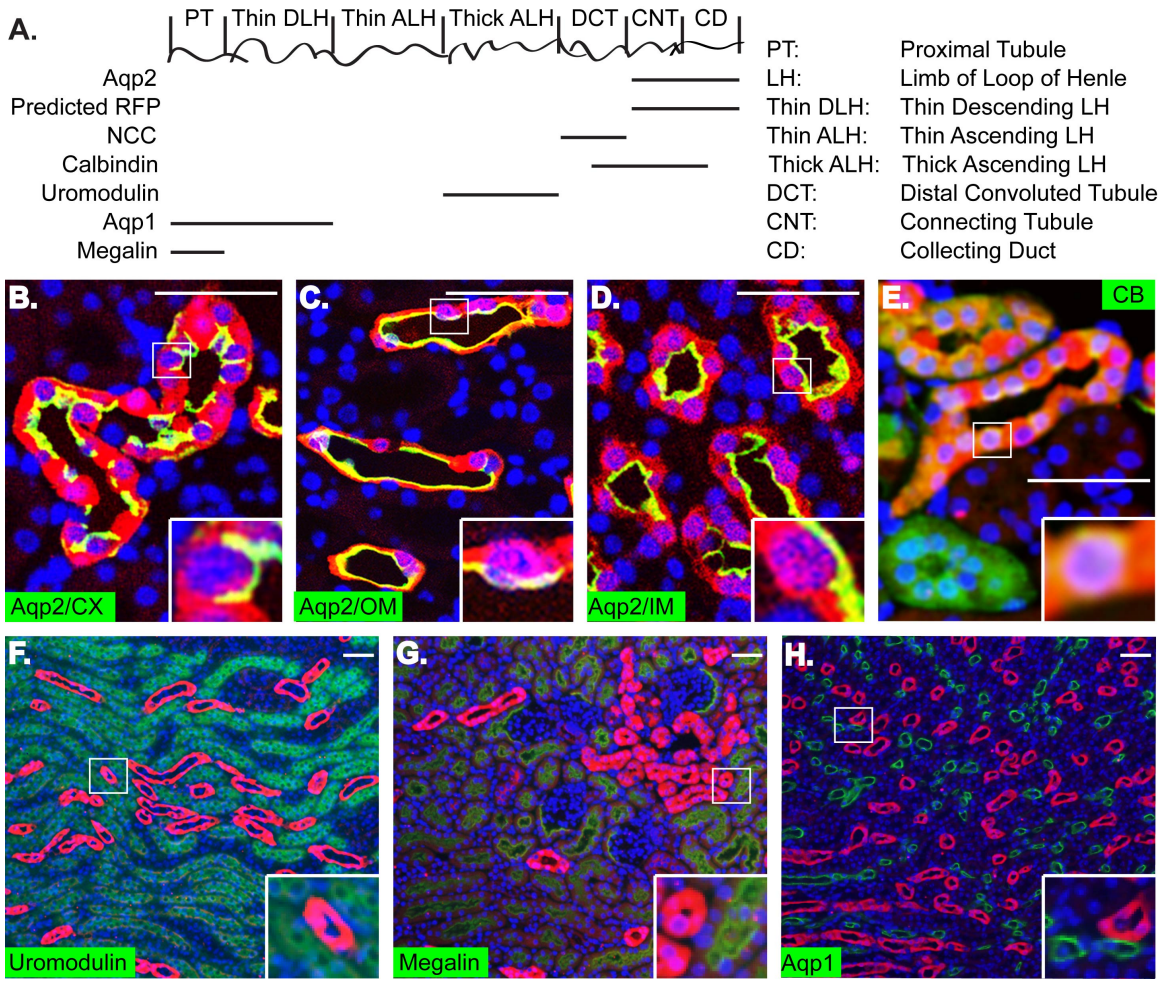

Figure 8. RFP faithfully recapitulates the expression of the endogenous Aqp2 in *Aqp2Cre RFP* kidney.

A nephron diagram showing the segment-specific markers. Aqp2 is partially overlapped with calbindin, but not with all other markers (***A***). Representative merged images showing RFP co-expression with Aqp2 (***B-D***), partially with calbindin (***E)*** in some cortical tubules, but not with other markers as indicated (***F-H***). Images were captured by confocal (***B***-***D***) and epifluorescence microscopies (***E***-***H***). RFP was shown in red. All markers were in green. Boxed areas highlighting RFP co-expression with (***B-E***) or segregation from (***F***-***H***) the corresponding markers were 3X magnified in the inserts. CX: cortex. OM: outer medulla. IM: inner medulla. CB: Calbindin. Scale bar: 100 μm.

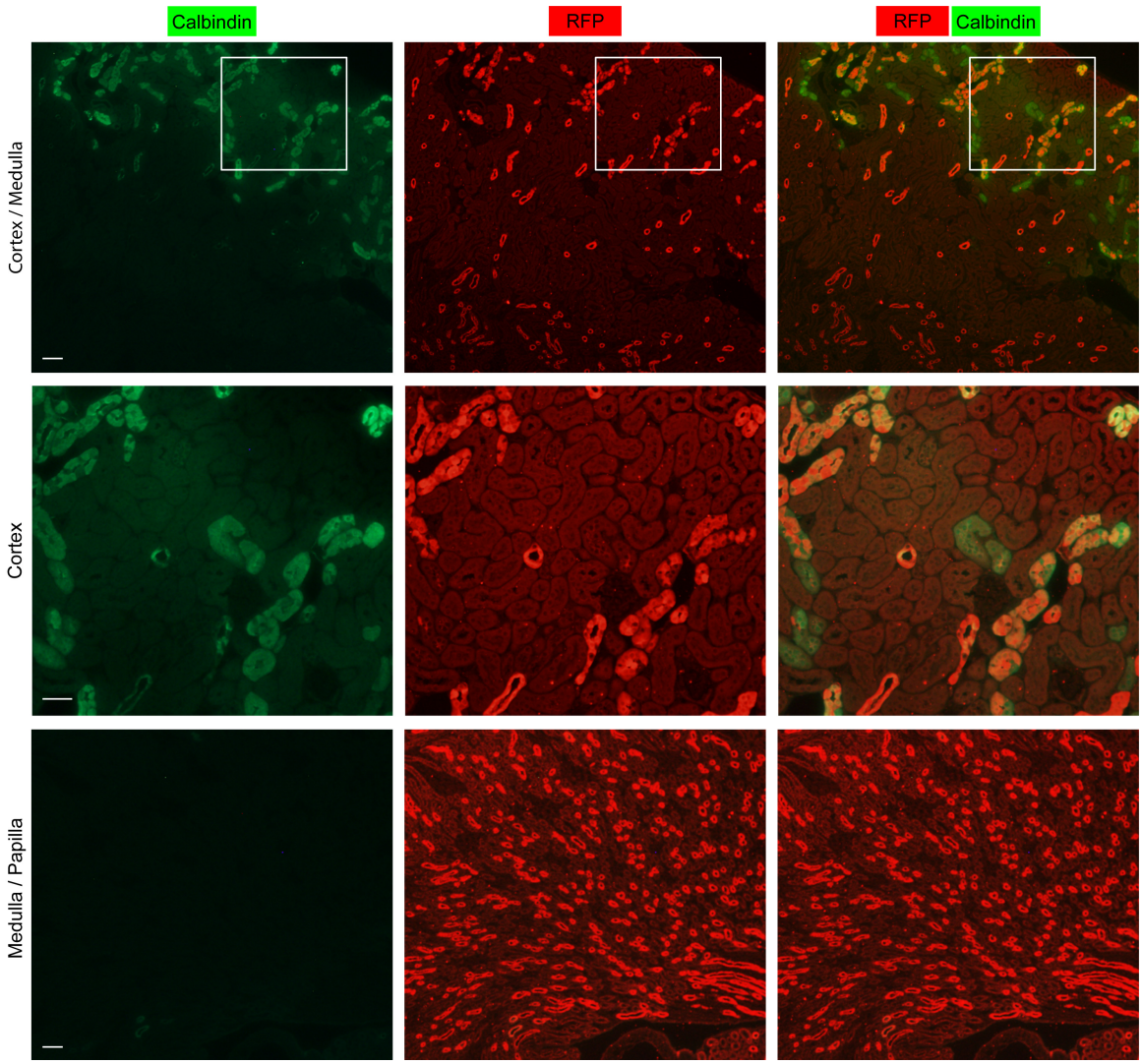

Figure 9. Aqp2 and Calbindin D28K (Calbindin) have partially overlapped expression domains in the cortex in *Aqp2Cre RFP* kidney.
Representative double immunofluorescence staining images showing staining of Calbindin (green) and RFP (red) in *Aqp2Cre RFP* kidney from cortex to medulla/papilla. Boxed areas were 4X magnified and shown below as indicated (cortex). Calbindin^{+} cells were restricted in the cortex, with most of them were also RFP^{+}. Calbindin^{+} cells were absent in the medulla/papilla. Scale bar: 100 μm.

3.7 All principal cells are derived from Aqp2$^+$ progenitors.

To test if all the principal cells originated from Aqp2$^+$ progenitors during development, we examined co-labeling of RFP and Aqp3 by immunofluorescence staining. Like Aqp2, Aqp3 is also a well-established principal cell marker. It resides at the basolateral plasma membrane of principal cells and mediates the exit pathway for apically reabsorbed water. All principal cells identified by basolateral Aqp3 were also marked by RFP (Figure 10), confirming that all principal cells are derived from Aqp2$^+$ progenitors. It should be noted that, in the cortex, there were multiple tubules, in which the vast majority, if not all, of the cells were labeled by RFP, but none of these cells were stained by Aqp3 (Figure 10). These tubules are reminiscent of those Aqp2$^-$RFP$^+$ tubules described before and represent the transitional segments of connecting tubule (see below).

3.8 Most intercalated cells arise from Aqp2$^+$ progenitors with intact *Dot1l* function.

To establish that Aqp2$^+$ progenitor cells differentiate into intercalated cells as well as principal cells during normal development, rather than as a consequence of *Dot1l* disruption, we performed double immunofluorescence staining with anti-RFP to label the Aqp2-lineage and an antibody recognizing V-ATPase subunits B1 and B2 (referred as B1B2 hereafter) to identify the intercalated cells. Confocal images revealed two populations of intercalated cells throughout the

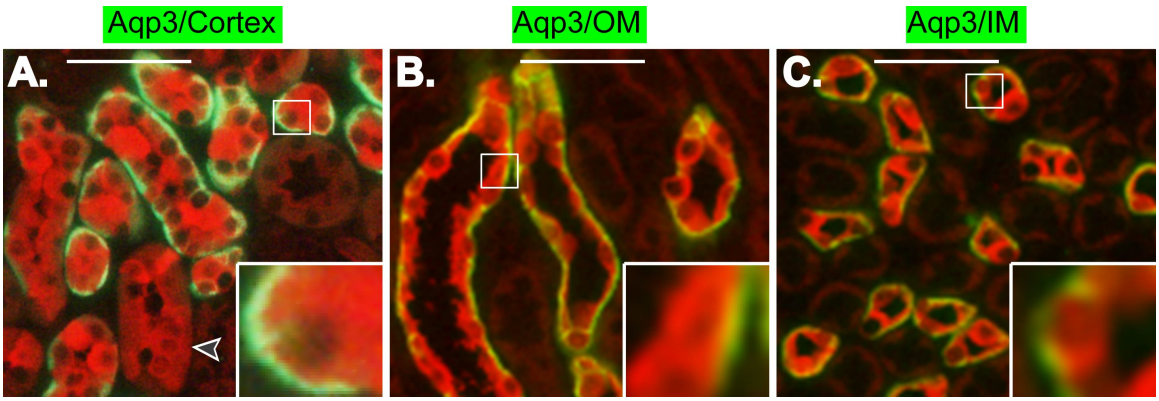

Figure 10. All principal cells are derived from Aqp2$^+$ progenitors.

Representative merged double immunofluorescence staining images showing RFP co-expression with principal cell marker Aqp3 in the regions as indicated (***A-C***). RFP and Aqp3 were shown in red and green, respectively. Boxed areas were 4X magnified in the insert. OM: outer medulla. IM: inner medulla. Black arrowhead: CNT2 or CNT3 tubules (see Figure 30 and text) lacking detectable Aqp3$^+$ cells but containing multiple RFP$^+$ cells (***A***). Scale bar: 100 μm.

kidney: RFP^+B1B2^+ and RFP^-B1B2^+. Among all the $B1B2^+$ cells, RFP^+B1B2^+ cells account for 82-89% in the cortex, outer and inner medulla (Figure 11).

Next, we examined co-expression of RFP with CAII, AE1, and Pendrin. AE1 is a specific marker of α-intercalated cells (63) and Pendrin marks β-intercalated cells and non-A-non-B intercalated cells in the cortical collecting duct (64). About 62-88% of $CAII^+$, 82-91% of all $AE1^+$ and 91% of all $Pendrin^+$ cells throughout the whole kidney were also labeled by RFP (Figure 12-14). Consistent with a previous report (65), $Pendrin^+$ cells were rarely seen in the medulla and papilla. The occasional $Pendrin^+$ cells in the medulla were also RFP^+ (Figure 14). In brief, our data demonstrate that most of the intercalated cells, regardless of their subtypes, originate from Aqp2-lineage cells in the presence of intact *Dot1l* function.

3.9 The *Aqp2Cre* transgene is not promiscuously activated to drive Cre expression in intercalated cells.

RFP expression is based on the dynamics of Cre enzymatic activity. Activation of the *Aqp2Cre* transgene in the $Aqp2^+$ progenitor cells, before the fate determination of both principal cells and intercalated cells to induce recombination for permanent activation of RFP, is critical in drawing our conclusion. If the transgene is faithful, it should be only persistently active in $Aqp2^+$ principal cells and permanently silenced in $Aqp2^-$ intercalated cells, leading to detectable and undetectable Cre expression, respectively (Figure 15A).

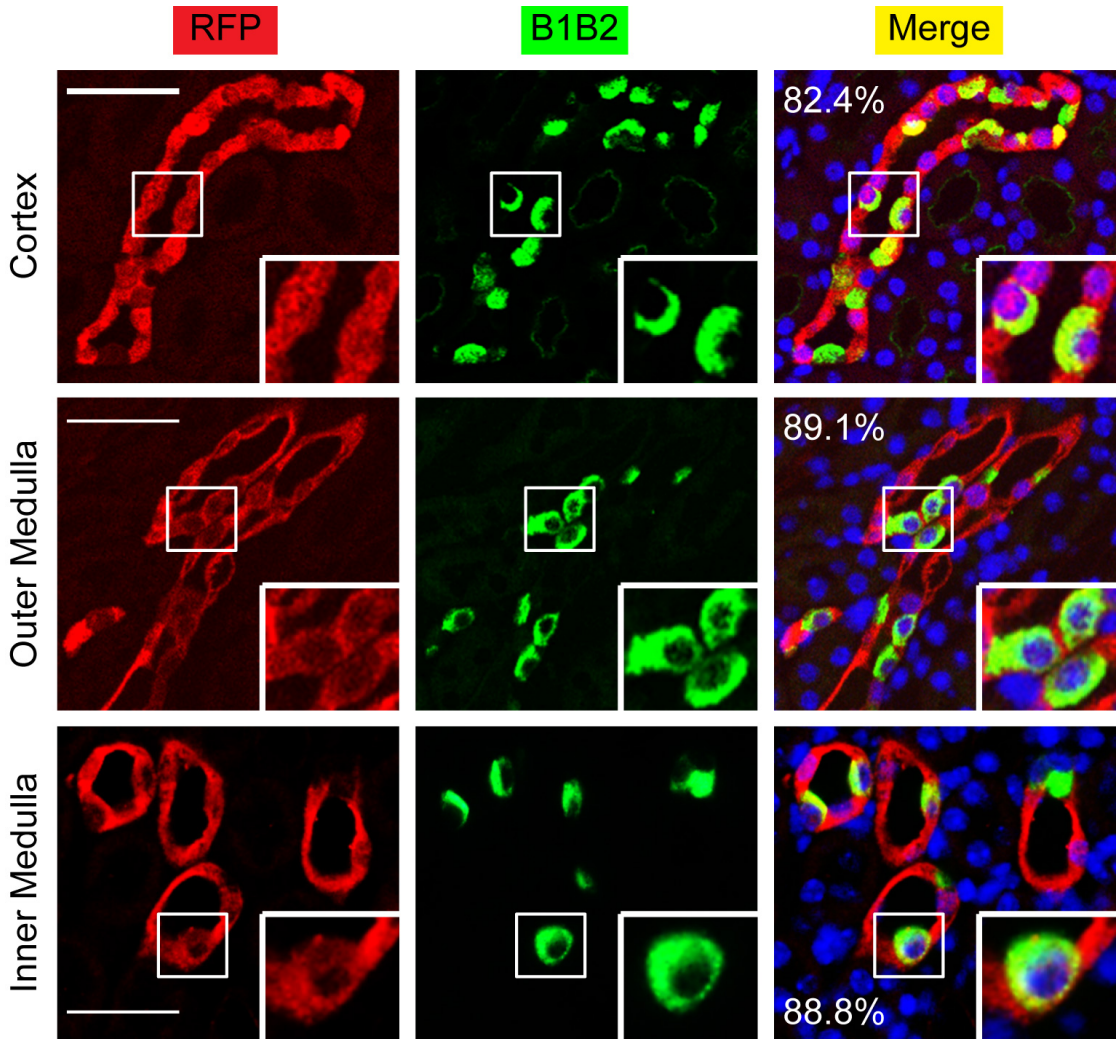

Figure 11. Most intercalated cells originate from Aqp2$^+$ progenitors.

Representative confocal images showing co-expression of RFP (red) with intercalated cell marker V-ATPase B1 and B2 (B1B2, green) in *Aqp2Cre RFP* mice. Boxed areas were 2X magnified in the inserts. %: percentage derived of intercalated cell as defined by RFP$^+$B1B2$^+$ cells in all of B1B2$^+$ cells in all tubules containing at least one RFP$^+$ cell. The images were chosen to clearly demonstrate co-expression of RFP with the intercalated cell marker, but not to necessarily represent the % of the derived intercalated cells. Scale bar: 100 μm.

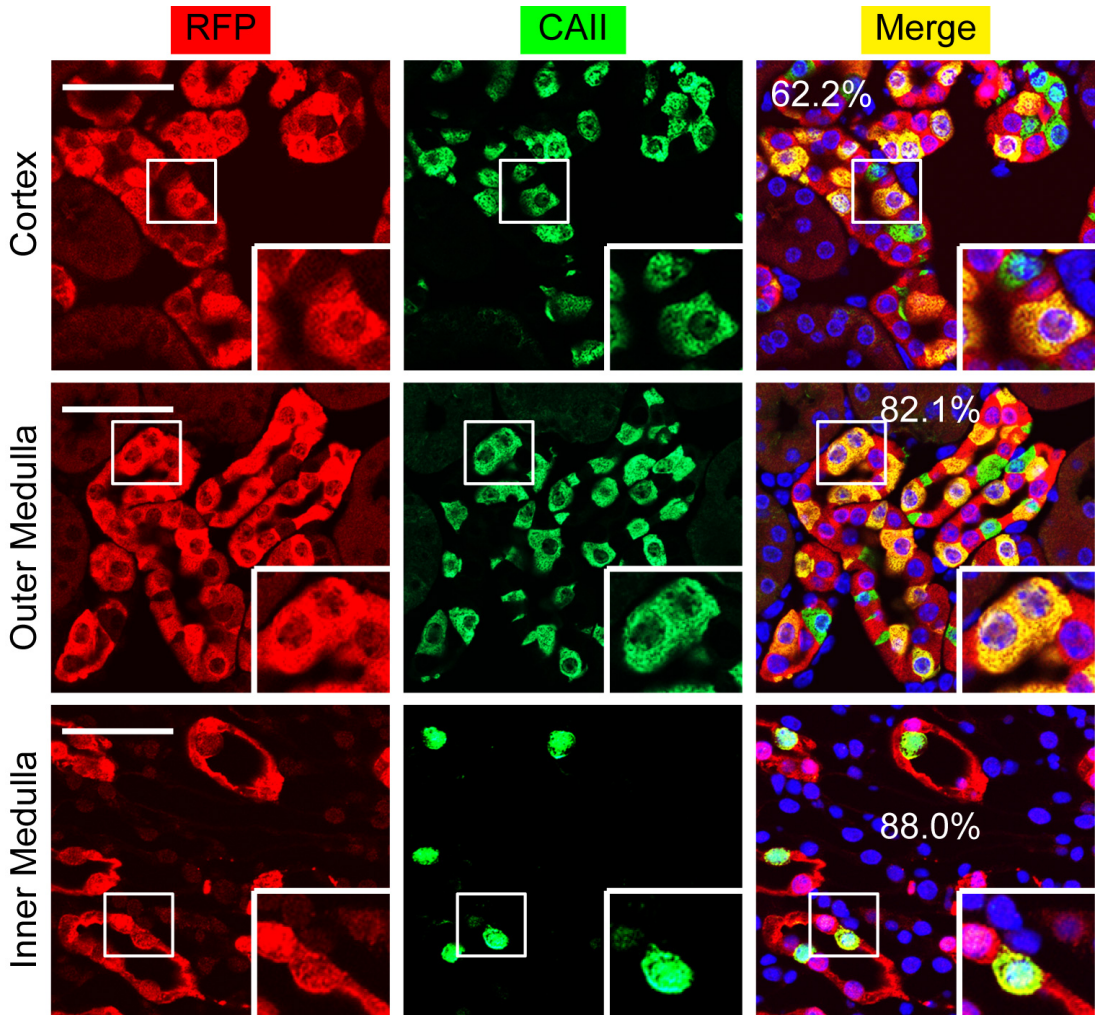

Figure 12. Most intercalated cells originate from Aqp2$^+$ progenitors.

Representative confocal images showing co-expression of RFP (red) with intercalated cell marker CAII (green) in *Aqp2Cre RFP* mice. Boxed areas were 2X magnified in the inserts. %: percentage derived of intercalated cell as defined by RFP$^+$CAII$^+$ cells in all of CAII$^+$ cells in all tubules containing at least one RFP$^+$ cell. The images were chosen to clearly demonstrate co-expression of RFP with the intercalated cell marker, but not to necessarily represent the % of the derived intercalated cells. Scale bar: 100 μm.

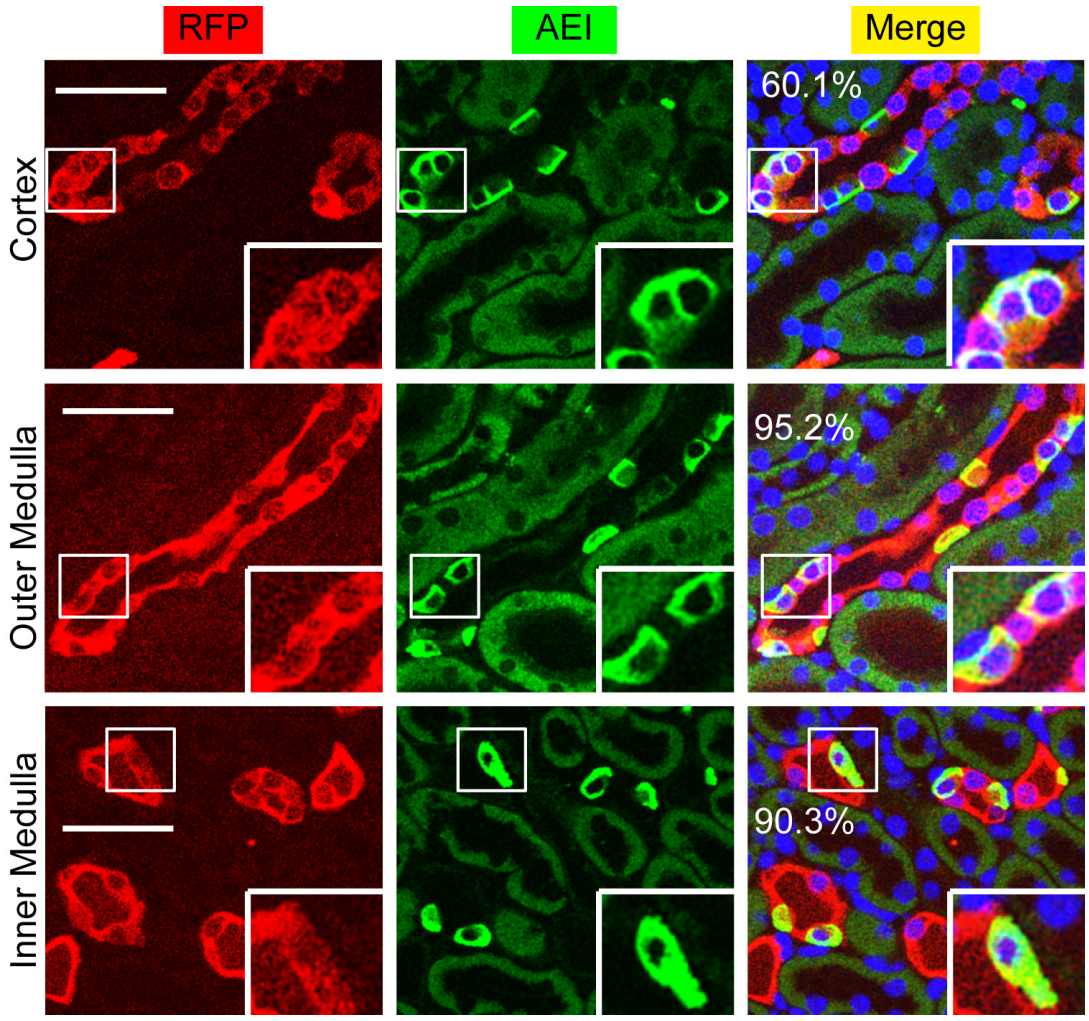

Figure 13. Most α-intercalated cells originate from Aqp2$^+$ progenitors.

Representative confocal images showing co-expression of RFP (red) with α-intercalated cell marker AE1 (green) in *Aqp2Cre RFP* mice. Boxed areas were 2X magnified in the inserts. %: percentage derived of intercalated cell as defined by RFP$^+$AE1$^+$ cells in all of AE1$^+$ cells in all tubules containing at least one RFP$^+$ cell. The images were chosen to clearly demonstrate co-expression of RFP with the intercalated cell marker, but not to necessarily represent the % of the derived intercalated cells. Scale bar: 100 μm.

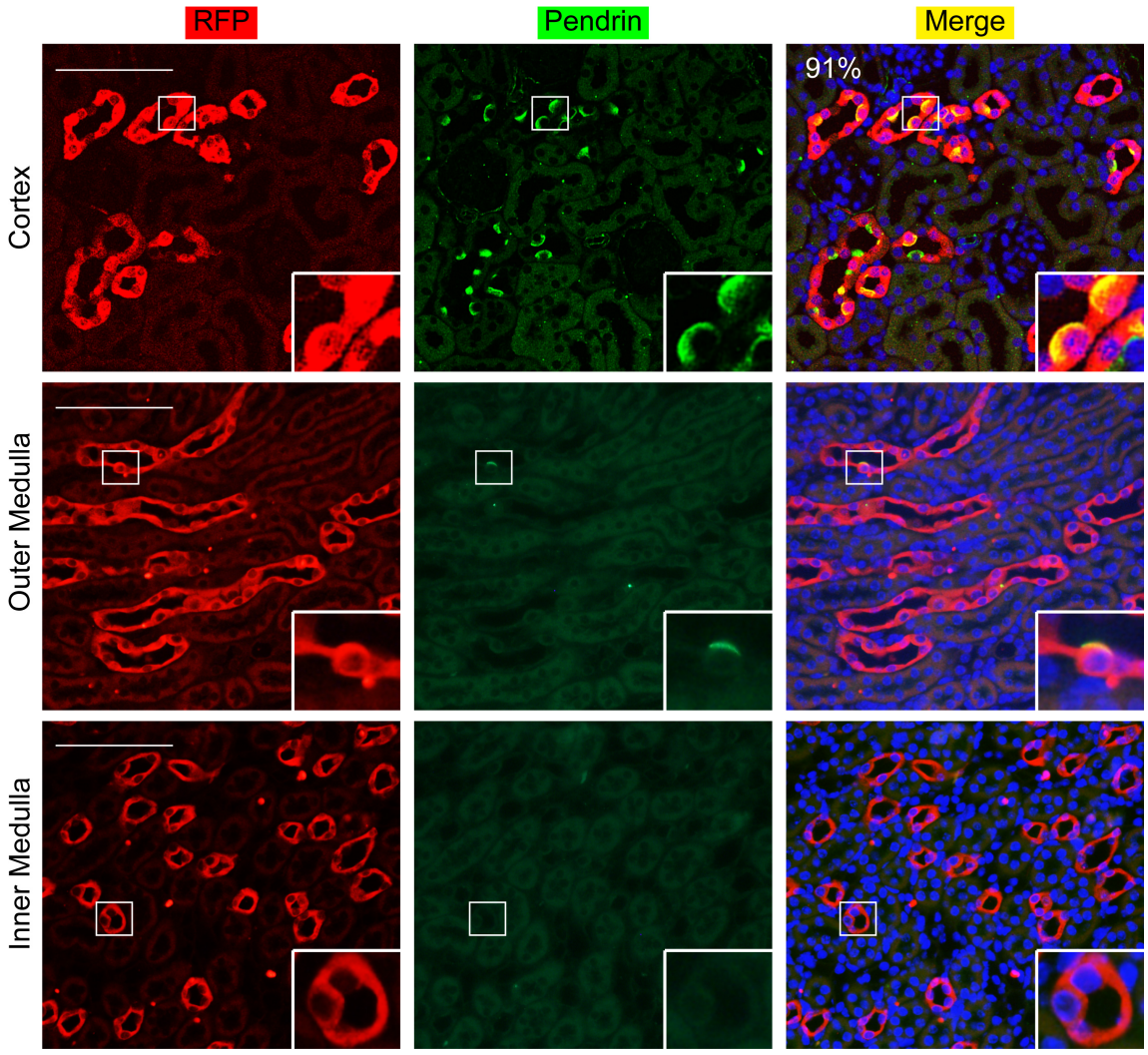

Figure 14. Most β-intercalated cells originate from Aqp2$^+$ progenitors.

Representative confocal images showing co-expression of RFP (red) with β-intercalated cell marker Pendrin (green) in *Aqp2Cre RFP* mice. Boxed areas were 2X magnified in the inserts. %: percentage derived of intercalated cell as defined by RFP$^+$Pendrin$^+$ cells in all of Pendrin$^+$ cells in all tubules containing at least one RFP$^+$ cell. The images were chosen to clearly demonstrate co-expression of RFP with the intercalated cell marker, but not to necessarily represent the % of the derived intercalated cells. Scale bar: 100 μm.

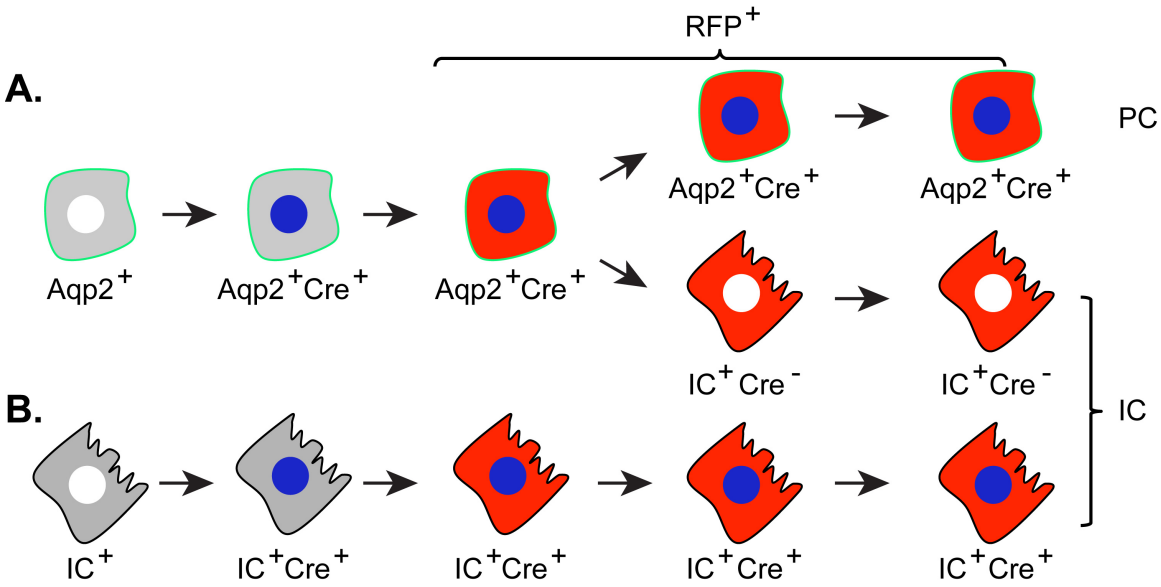

Figure 15. A model for activation of *Aqp2Cre* transgene in the Aqp2$^+$ progenitors.

A-B. Diagrams of principal cell-specific (***A***) and non-specific (***B***) activation of *Aqp2Cre* transgene. If the *Aqp2Cre* transgene is faithful, it should be only active in principal cells and permanently silenced in intercalated cells, leading to detectable and undetectable Cre expression, respectively (***A***). Alternatively, if the transgene lacks the faithfulness, it remains active to direct Cre expression in intercalated cells (B). Green border: Aqp2$^+$ or PC. Black border: Aqp2$^-$ or IC. Red: RFP$^+$. White nuclei: Cre$^-$. Blue nuclei: Cre$^+$.

Alternatively, if the transgene lacks the faithfulness, it remains active to direct persistent Cre expression in intercalated cells as well as in principal cells (Figure 15B). To clarify these possibilities, we evaluated Cre co-expression with the intercalated cell markers. While Cre staining was visible in all the nuclei of principal cells, none of the $CAII^+$, $AE1^+$, and $Pendrin^+$ intercalated cells were Cre^+ (Figure 16). To further confirm the results, we performed triple immunofluorescence staining with Aqp2, Cre, and B1B2. Without exception, Cre was exclusively detected in the $Aqp2^+$ cells and none of the $B1B2^+$ cells had detectable Cre staining (Figure 17). We conclude that the *Aqp2Cre* transgene, like the endogenous *Aqp2*, is silenced in intercalated cells. RFP expression in intercalated cells results from the transgene activation before intercalated cell specification from the $Aqp2^+$ progenitors.

3.10 $Aqp2^+$ progenitors appear as early as E15.5.

The Aqp2 transcript is detected by RT-PCR at embryonic day E15.5, but not at E13.5 and E14.5 (66), suggesting that E15.5 may be the earliest time point at which Aqp2 protein becomes detectable. To verify the Aqp2 expression in the developing kidneys and to document the temporal faithfulness of RFP, we performed immunofluorescence staining of *Aqp2Cre RFP* kidneys from E15.5 to P7. $Aqp2^+$ cells were observed at both E15.5 and E16.5, and were also RFP^+ (Figure 18). Almost all of $Aqp2^+$ cells had RFP expression in all other stages examined (P1, P4, and P7, Figure 19 and Figure 20).

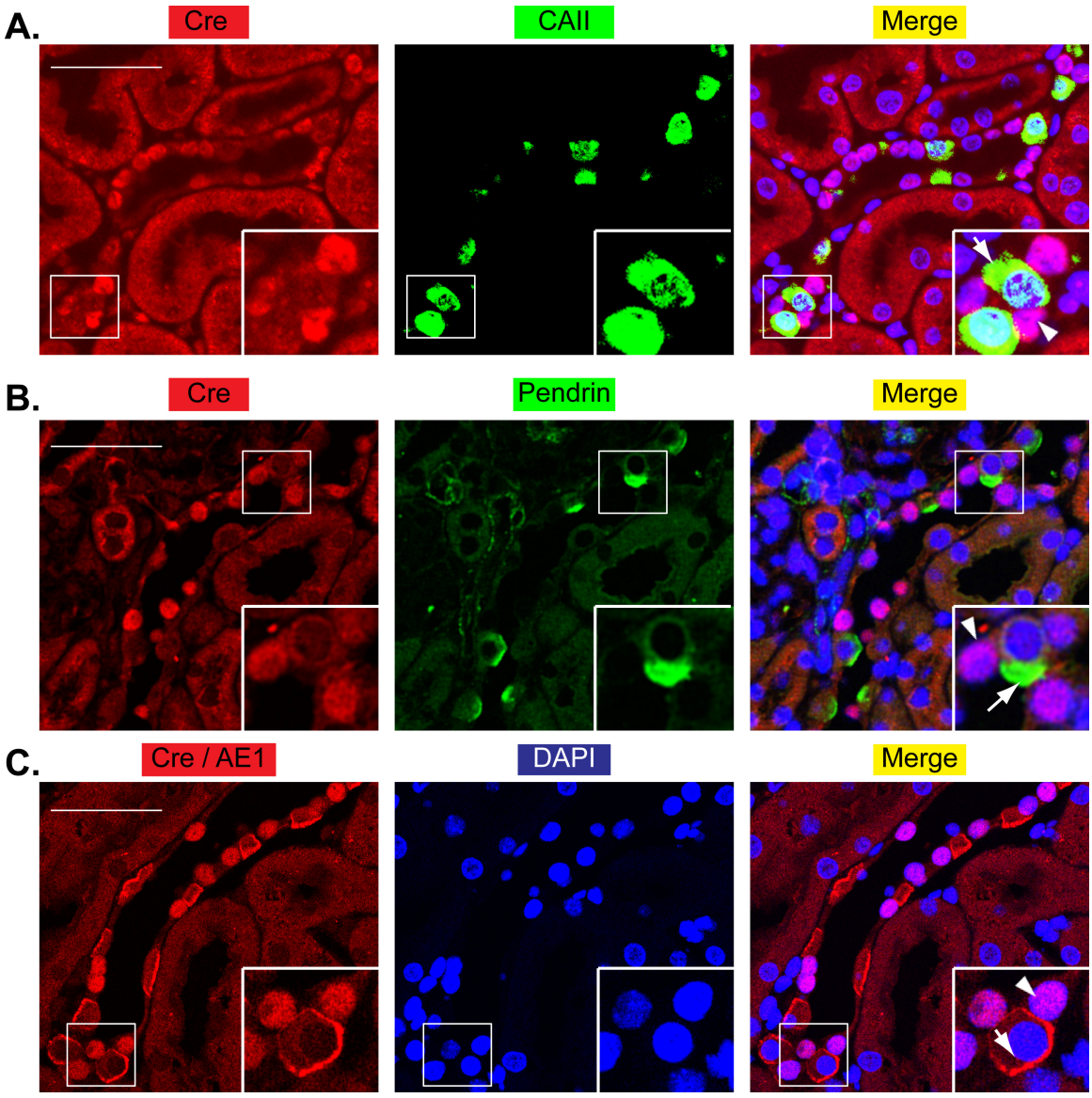

Figure 16. *Aqp2Cre* transgene is not promiscuously activated to persistently drive Cre expression in intercalated cells.
A-C. Representative confocal images showing no co-expression of Cre (red) with intercalated cell marker CAII (green), β-intercalated cell marker Pendrin (green), and α-intercalated cell marker AE1 (red) in *Aqp2Cre RFP* mice. Boxed areas were 2X magnified in the inserts. Note, the rabbit antibodies for Cre and AE1 were used, leading to the same color (red) for these two proteins. However, they were located in the nucleus and basolateral membrane, respectively. Scale bar: 100 μm.

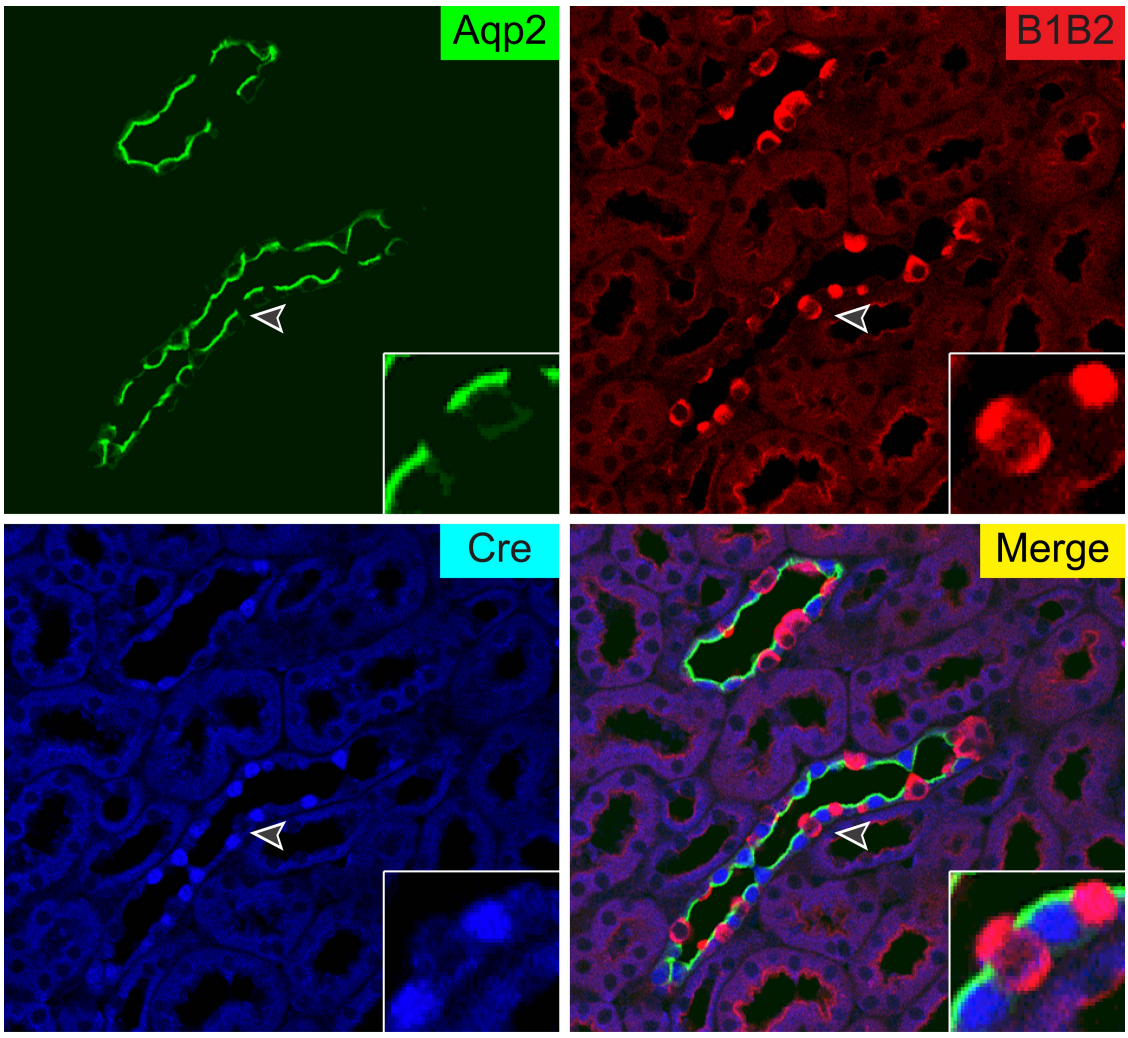

Figure 17. Triple IF confirms no promiscuous expression of Cre in intercalated cells in *Aqp2Cre RFP* mice.

Representative confocal images showing co-expression of Cre (blue) with principal marker Aqp2 (green), but not with intercalated cell marker B1B2 (red) in *Aqp2Cre RFP* mice. Boxed areas were 4X magnified from the indicated area by the arrowhead. Scale bar: 100 μm.

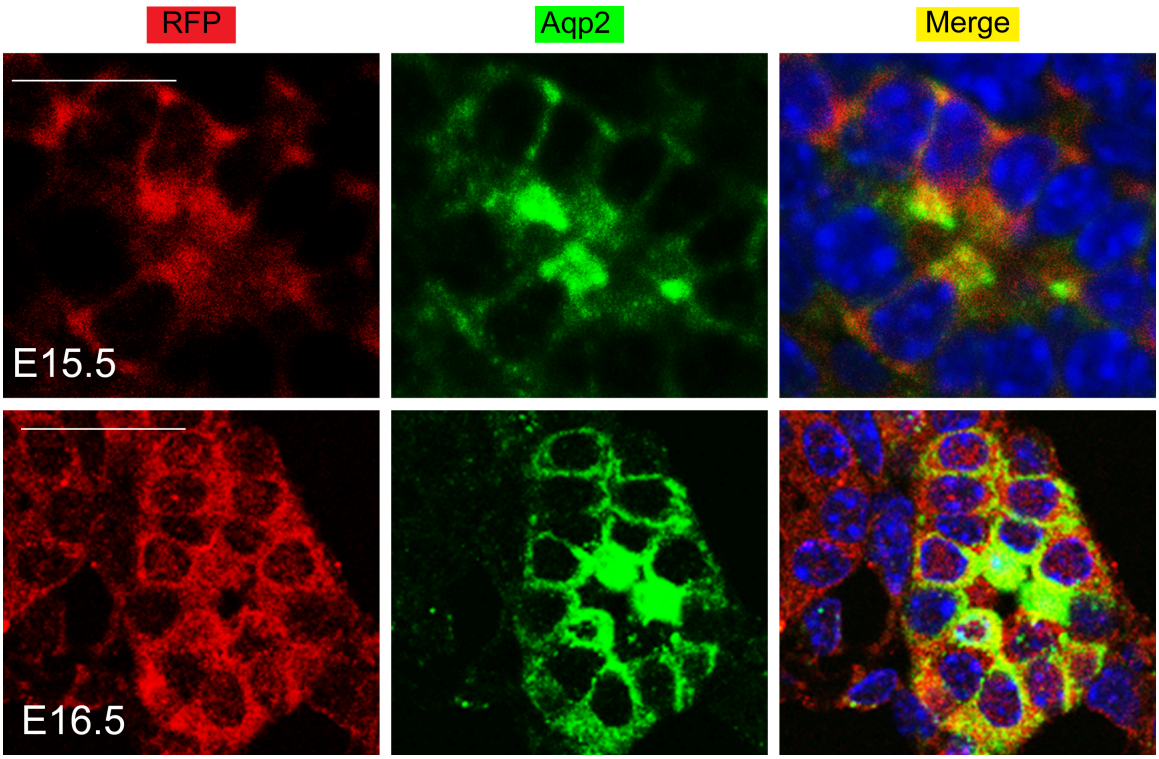

Figure 18. Aqp2^{+} progenitors appear as early as E15.5.

Representative confocal images showing co-expression of Aqp2 (green) with RFP (red) in E15.5 and E16.5 *Aqp2Cre RFP* kidneys. Nuclei were stained with DAPI (blue). Scale bar: 100 μm.

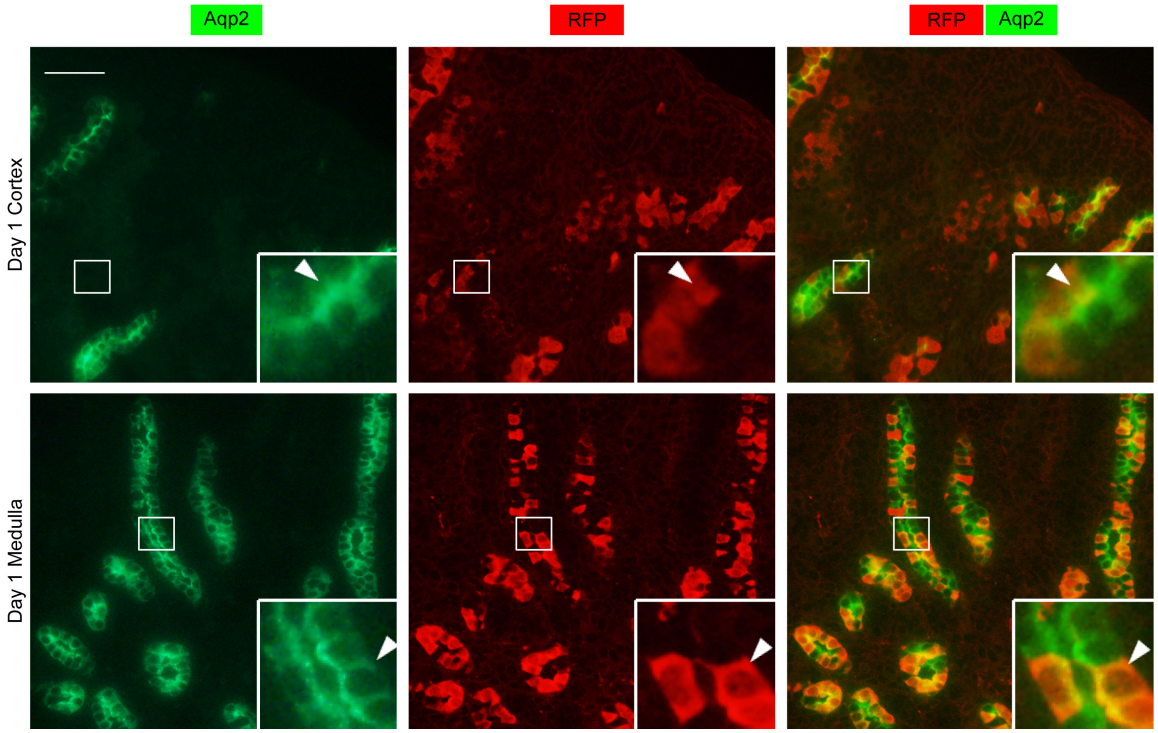

Figure 19. Co-expression of RFP with Aqp2 in neonatal *Aqp2Cre RFP* kidneys at P1.

Representative double epifluorescence images showing staining of Aqp2 (green) and RFP (red) in *Aqp2Cre RFP* kidneys. Boxed areas were amplified in the inserts. Arrowheads: $RFP^{+}Aqp2^{+}$ cells. Scale bar: 100 μm.

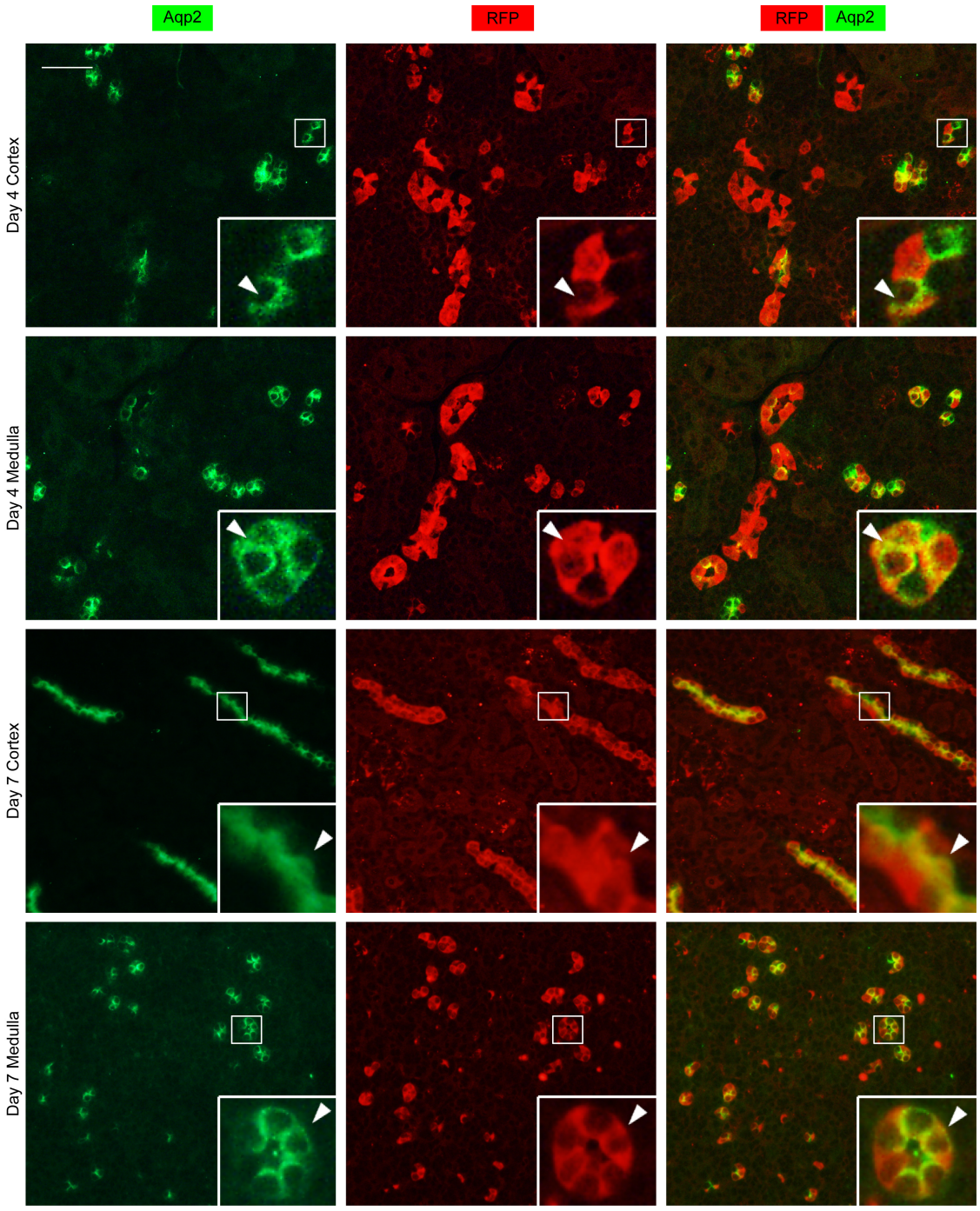

Figure 20. Co-expression of RFP with Aqp2 in *Aqp2Cre RFP* kidneys at P4 and P7.

Representative double epifluorescence images showing staining of Aqp2 (green) and RFP (red) in *Aqp2Cre RFP* kidneys as indicated. RFP^+Aqp2^+ cells were progressively expanded in the whole kidney from P1 (see Figure 19) to P7. Boxed areas were amplified in the inserts. Arrowheads: RFP^+Aqp2^+ cells. Scale bar: 100 μm.

It should be noted that substantial Aqp2$^+$ cell numbers had no detectable RFP expression at P1 (Figure 19). Given that the kidney undergoes robust nephrogenesis, which is still not fully developed at this stage (67), we interpreted that as a consequence of the low recombination events in those Aqp2$^+$ cells. Taken together, based on the tight correlation between RFP expression and the endogenous Aqp2 staining, we conclude that 1) *AqpCre* and thus RFP faithfully recapitulate the spatiotemporal expression profile of the endogenous *Aqp2;* 2) RFP is an accurate reporter of endogenous Aqp2 expression in *Aqp2Cre RFP* kidneys; and 3) Aqp2$^+$ progenitors are detectable as early as E15.5.

3.11 Aqp2$^+$ progenitors begin to express Foxi 1 and V-ATPase B1B2 at E15.5 and CAII at E16.5.

To determine the time frame when Aqp2$^+$ cells begin to differentiate into intercalated cells, we performed a staining series of the E15.5 and E16.5 kidney sections with various makers of intercalated cells. It has been reported that while V-ATPase subunit B1 is expressed after induction of Foxi1 at E15.5, V-ATPase subunit B2 becomes detectable as early as E13.5. Consistent with these observations, we also detected strong B1B2 positive staining at E15.5. Surprisingly, most of B1B2$^+$ cells were also Aqp2$^+$ (Figure 21A). These results suggest that the progenitor cells bear some properties of both PC and IC, characterized by expression of Aqp2 and B1B2, respectively. Furthermore, Foxi1, a well-established intercalated cell marker (68), was also detectable and co-expressed with RFP (Figure 21B). CAII$^+$ cells were not seen at E15.5 (data not

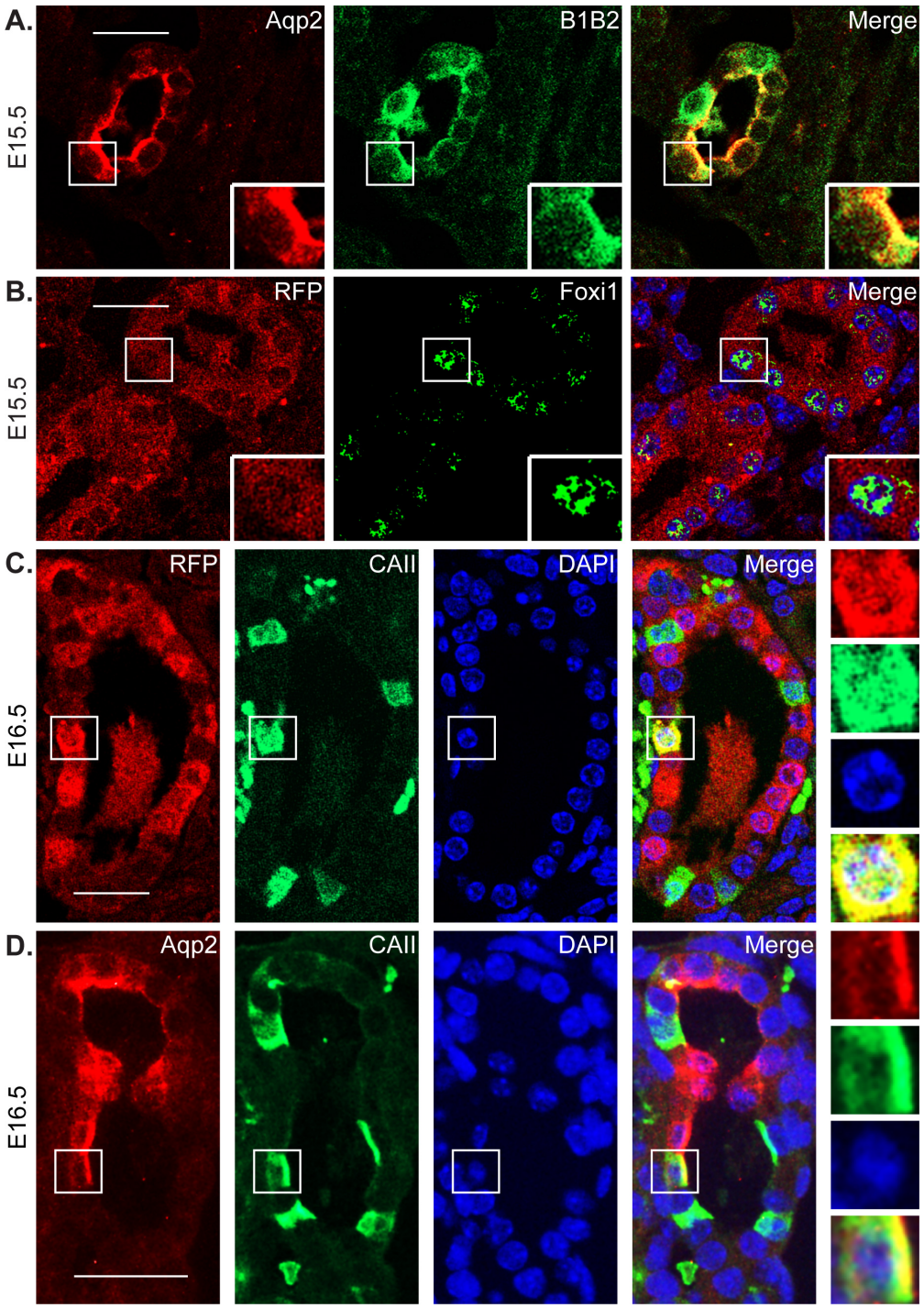

Figure 21. Aqp2-expressing progenitor cells begin to express Foxi1 and V-ATPase B1B2 at E15.5 and CAII at E16.5.

Representative double (***A-D***) IF images showing staining of E15.5 and E16.5 *Aqp2Cre RFP* kidneys as indicated. Boxed areas highlighting the double positive cells were amplified in inserts (***A-B***) or shown at the right (***C-D***). Nuclei were stained with DAPI (blue). Scale bar: 100 μm. For CAII expression in late developing kidneys, see Figure 22 and Figure 23.

shown), but became detectable at E16.5 (Figure 21C). A small proportion of $CAII^+$ cells were also RFP^+. To determine if these cells have lost their $Aqp2^+$ phenotype, coexpression of Aqp2 with CAII was pursued. In a singe tubule, we observed 4 types of cells: $Aqp2^+CAII^-$, $Aqp2^-CAII^+$, $Aqp2^+CAII^+$, and $Aqp2^-CAII^-$ (Figure 21 D). The last two may represent the intermediate states of the derivation of "intercalated cells" from "principal cells". Alternatively, some $CAII^+$ cells may be derived from non-$Aqp2^+$ progenitor cells. RFP^+CAII^+ cells were progressively expanded in the whole kidney from P1 to P7 (Figure 22 & 23). Collectively, these findings demonstrated that $Aqp2^+$ progenitors begin to specify the fate of intercalated cells gradually by gaining B1B2 as early as E15.5 and CAII at E16.5.

3.12 Aqp2+ progenitors begin to express α-intercalated cell marker AE1 and β-intercalated cell marker Pendrin at P1.

Despite co-expression of RFP with Foxi1 and CAII during embryogenesis, no RFP co-expression with AE1 or Pendrin in the same cells was observed by E16.5 (Figure 24A & C). In E15.5 and E16.5 kidneys, no parenchymal staining of AE1 can be identified. All $AE1^+$ cells were erythrocytes since they lacked DAPI-stained nuclei and the antiserum recognized both the α-intercalated cell-specific and the erythrocyte isoforms of AE1 (68). RFP^+AE1^+ cells began to appear in the cortex and medulla at P1 (Figure 24B). They gradually increased in numbers in both cortex and medulla at P4 and P7 (Figure 25). Similarly, $Pendrin^+$ cells were observed at E16.5 (Figure 24C), consistent with a previous report (65). However,

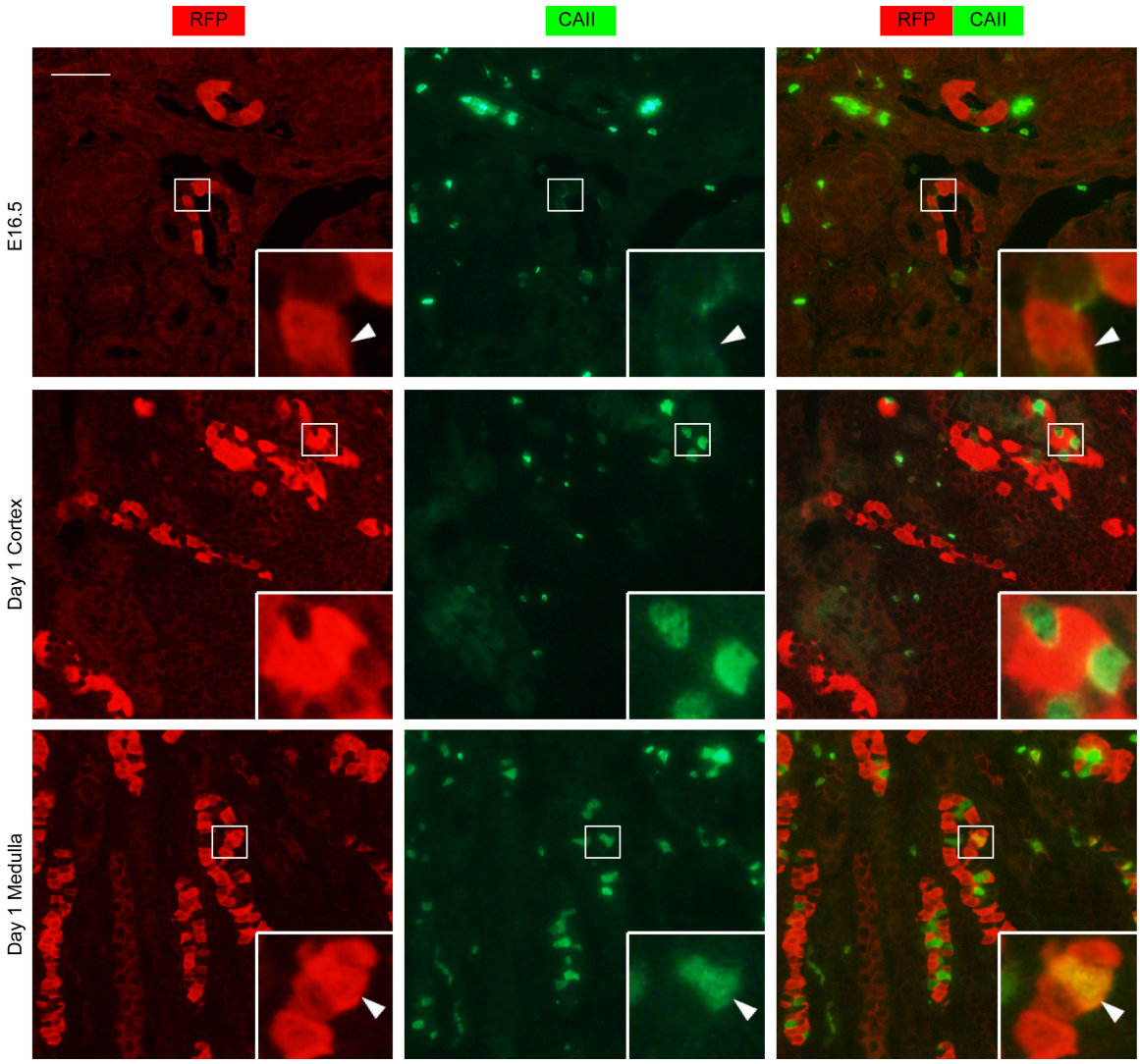

Figure 22. Co-expression of RFP with CAII in neonatal *Aqp2Cre RFP* kidneys at E16.5 and P1.

Representative double epifluorescence images showing staining of CAII (green) and RFP (red) in *Aqp2Cre RFP* kidneys as indicated. $RFP^{+}CAII^{+}$ cells were progressively expanded in the whole kidney from P1 to P7 (See Figure 23). Boxed areas were amplified in the inserts. Arrowheads: $RFP^{+}CAII^{+}$ cells. Scale bar: 100 μm.

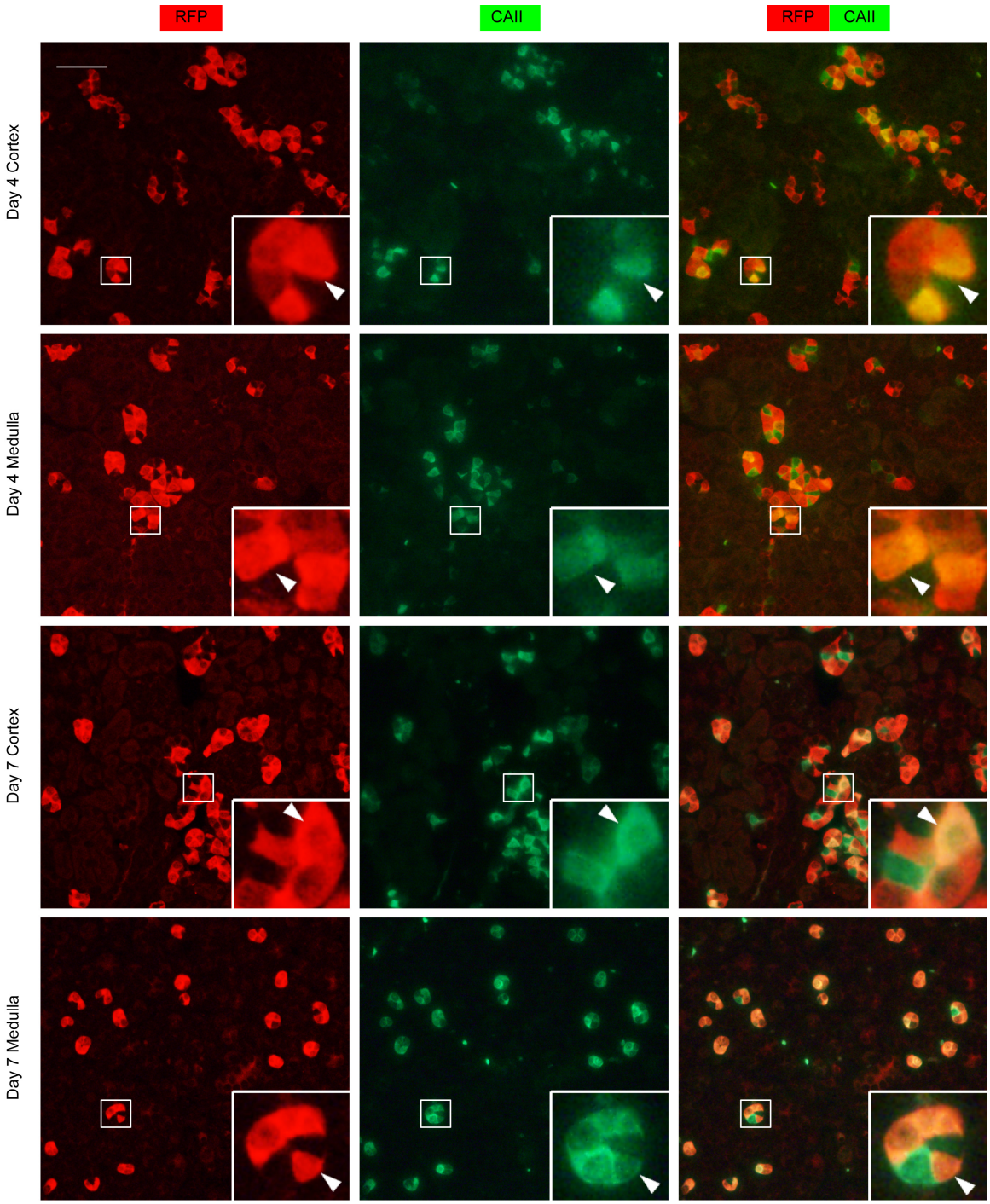

Figure 23. Co-expression of RFP with CAII in *Aqp2Cre RFP* kidneys at P4 and P7.

Representative double epifluorescence images showing staining of CAII (green) and RFP (red) in *Aqp2Cre RFP* kidneys as indicated. $RFP^{+}CAII^{+}$ cells were progressively expanded in the whole kidney from P1 to P7. Boxed areas were amplified in the inserts. Arrowheads: $RFP^{+}CAII^{+}$ cells. Scale bar: 100 μm.

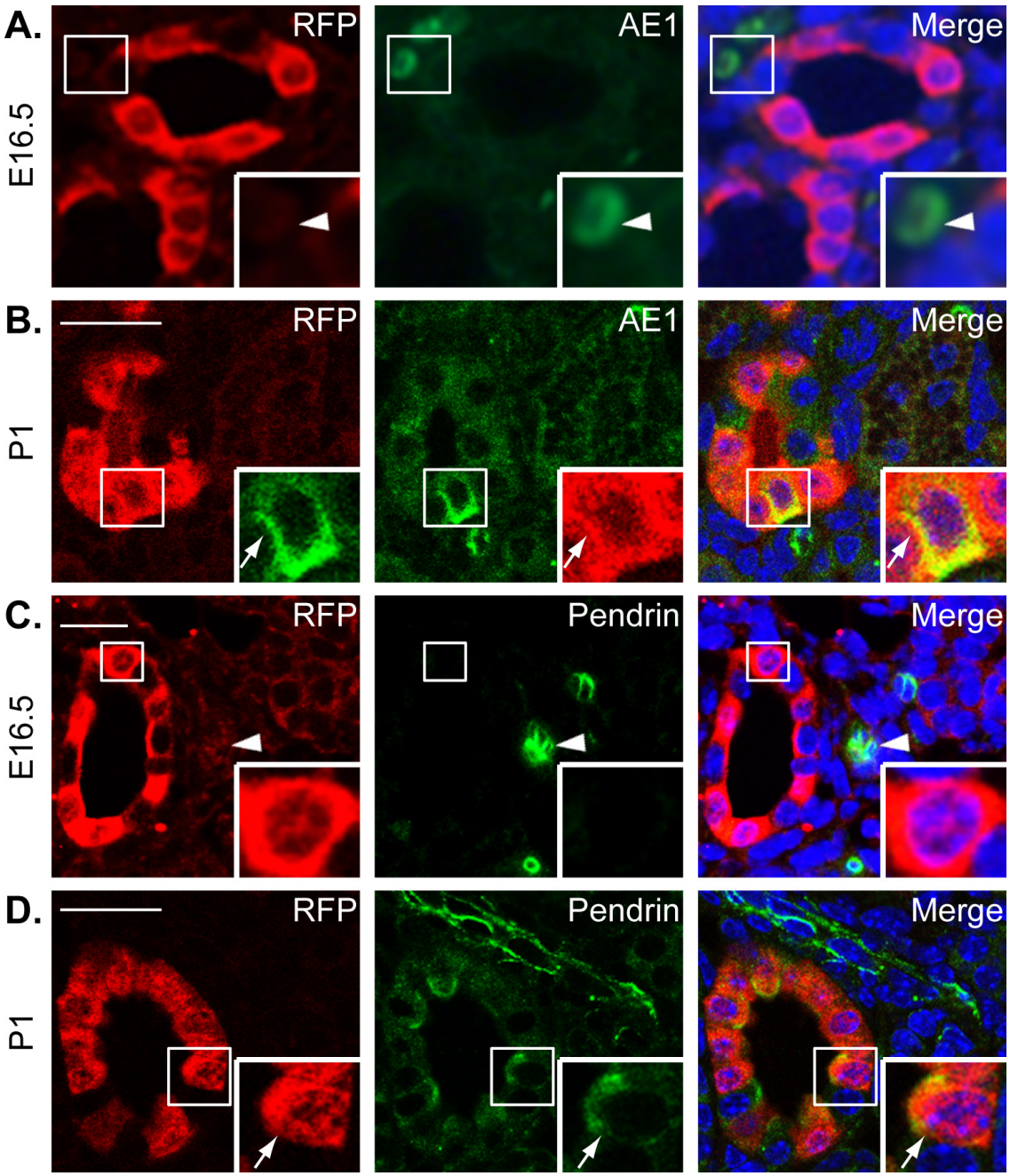

Figure 24. Aqp2-expressing progenitor cells differentiate into α-IC and β-IC at P1.

Representative IF images showing co-expression of RFP with α-IC marker AE1 (***A-B***) and β-IC marker Pendrin (***C-D***) at P1, but not at E16.5 *Aqp2cre RFP* kidneys. At E16.5 in ***A***, all $AE1^+$ cells were identified as erythrocytes due to lack of DAPI-stained nucleus. The scattered $Pendrin^+$ cells in ***C*** were most likely of non-Aqp2-expressing lineage because they were RFP^- cells. Boxed areas were magnified in the inserts. Arrowhead: erythrocytes (***A***) and $RFP^-Pendrin^+$ cells (***C***). Arrow: RFP^+AE1^+ (***B***) and $RFP^+Pendrin^+$ (***D***). Scale bar: 100 μm and 25 μm for the inserts.

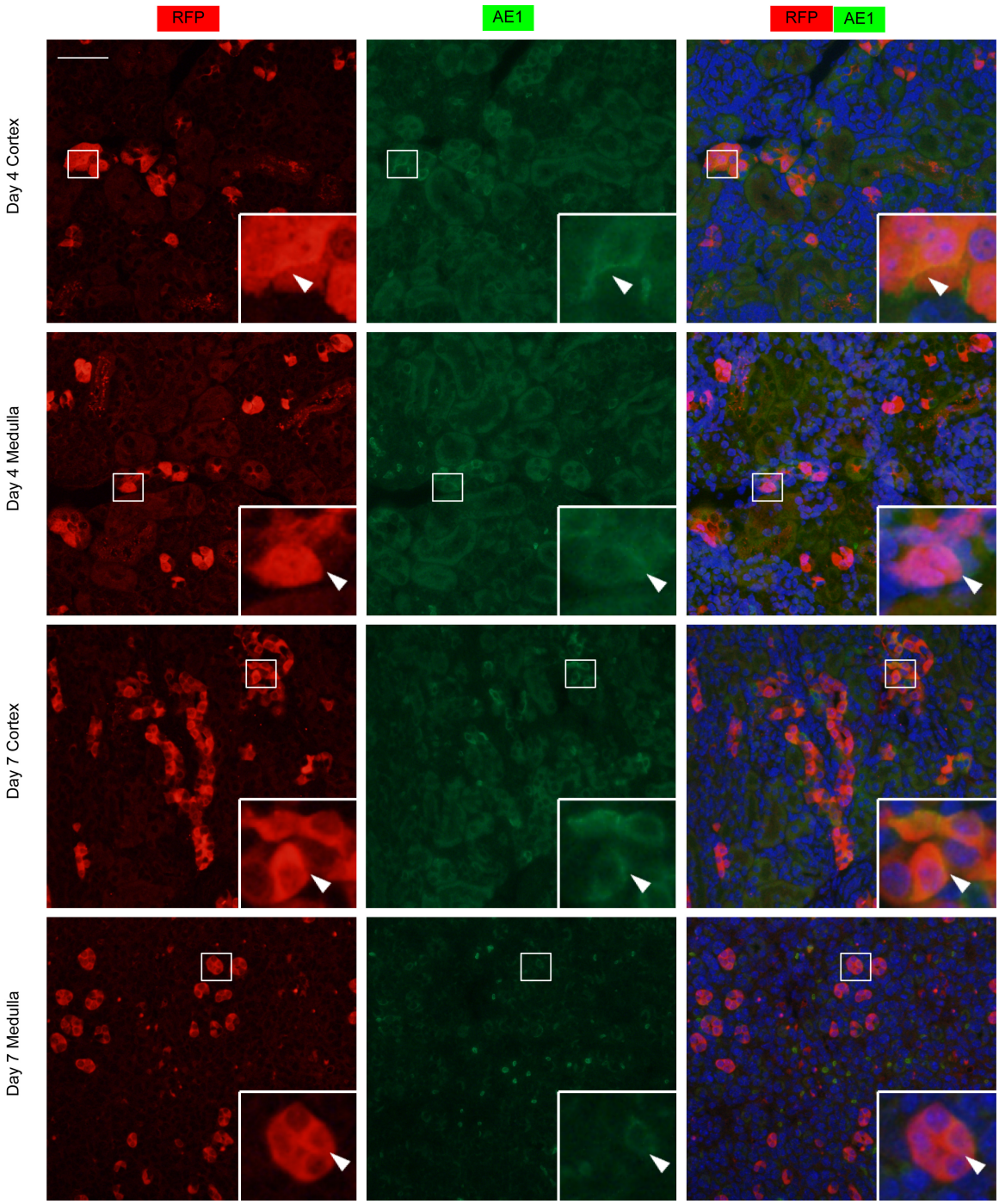

Figure 25. Co-expression of RFP with AE1 in *Aqp2Cre RFP* kidneys at P4 and P7.

Representative double epifluorescence images showing staining of AE1 (green) and RFP (red) in *Aqp2Cre RFP* kidneys as indicated. RFP^+AE1^+ cells began to appear in the cortex and medulla at P1 (Figure 24). They gradually increased in numbers in both cortex and medulla at P4 and P7. Boxed areas were amplified in the inserts. Arrowheads: RFP^+CAII^+ cells. Scale bar: 100 μm.

none of them were RFP^+ or resided within the RFP-labeled tubules. $RFP^+Pendrin^+$ cells were first occasionally observed in the cortex and medulla at P1 (Figure 24D), with a slight expansion at P4. At P7, $RFP^+Pendrin^+$ cells continued to expand in the cortex and were largely lost in the medulla (Figure 26). In conclusion, these data indicated that $Aqp2^+$ progenitors further differentiate into α-intercalated and β-intercalated cells at around P1.

3.13 $Aqp2^+$ cells are highly differentiated at E15.5.

The stepwise derivation of the intercalated cells from the $Aqp2^+$ progenitors indicated the possibility of a similar maturation pattern for the principal cells during development. To determine whether $Aqp2^+$ progenitors differentiate into principal cells in a similar way as intercalated cells and to assess the maturity of the $Aqp2^+$ cells at the earliest detectable time point, E15.5, we investigated if the Aqp2-expressing cells gain other principal cell markers (Aqp3, βENaC and γENaC). Double immunofluorescence staining with each of these principal cell markers along with Aqp2 or RFP was carried out on the E15.5 *Aqp2Cre RFP* kidneys. Remarkably, some of the $Aqp2^+$ or RFP^+ cells have acquired all of the three principal cell markers examined (Figure 27A-E). Some β- and γENaC-labeled tubules did not contain any cells positive for Aqp2 or RFP (data not shown). These tubules are most likely precursors of distal convoluted tubules derived from the metanephric mesenchyme because ENaC genes are also expressed in distal convoluted tubules (69). Therefore, we conclude that unlike

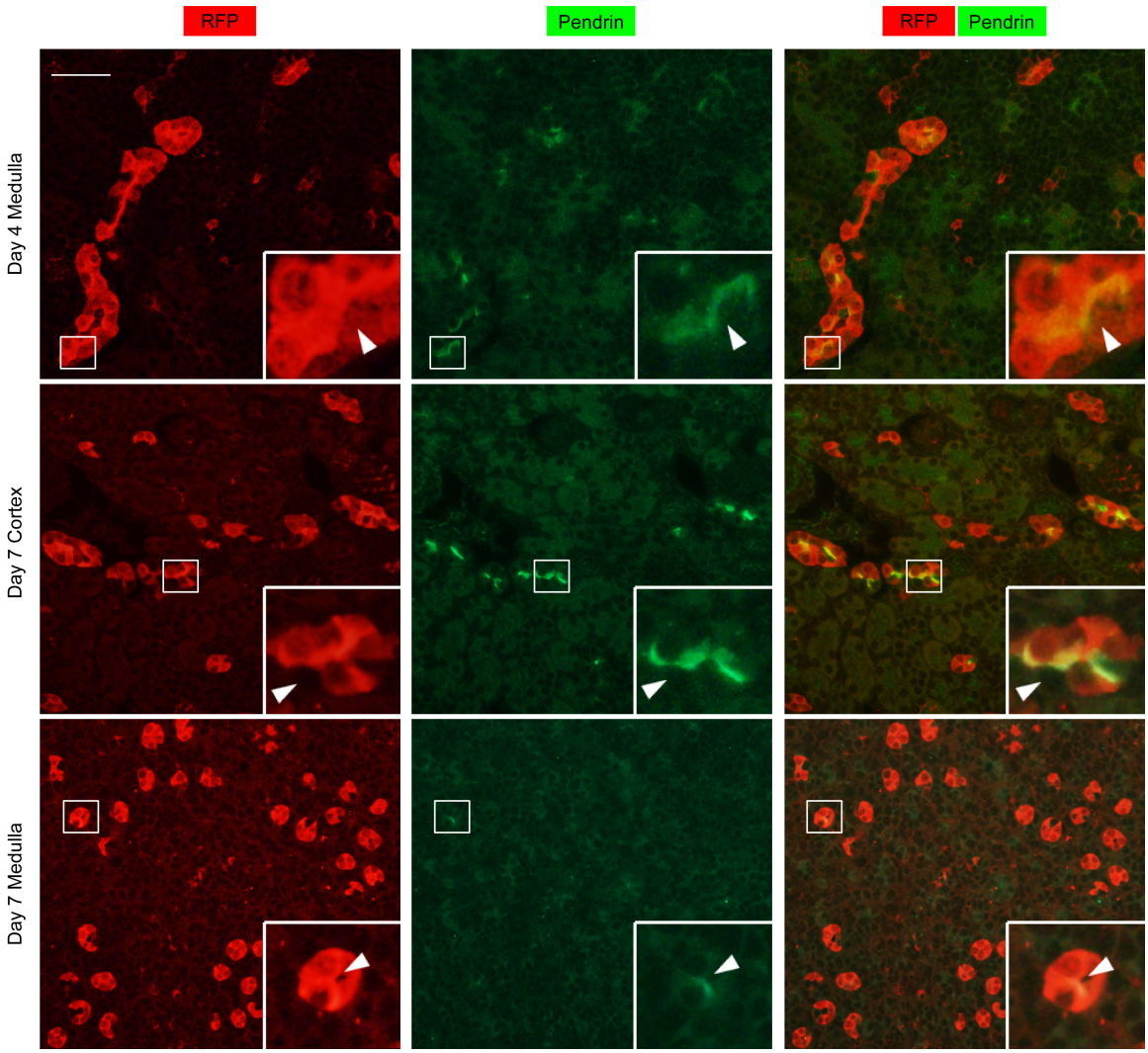

Figure 26. Co-expression of RFP with Pendrin in *Aqp2Cre RFP* kidneys at P4 and P7.

Representative double IF images showing staining of RFP (red) and Pendrin (green) in *Aqp2Cre RFP* kidneys as indicated. $RFP^+Pendrin^+$ cells were first occasionally observed in the cortex and medulla at P1 (Figure 24), with a slight expansion at P4. Boxed areas were magnified in the inserts. Arrowhead: $RFP^+Pendrin^+$ cells. Scale bar: 100 μm and 25 μm for the inserts.

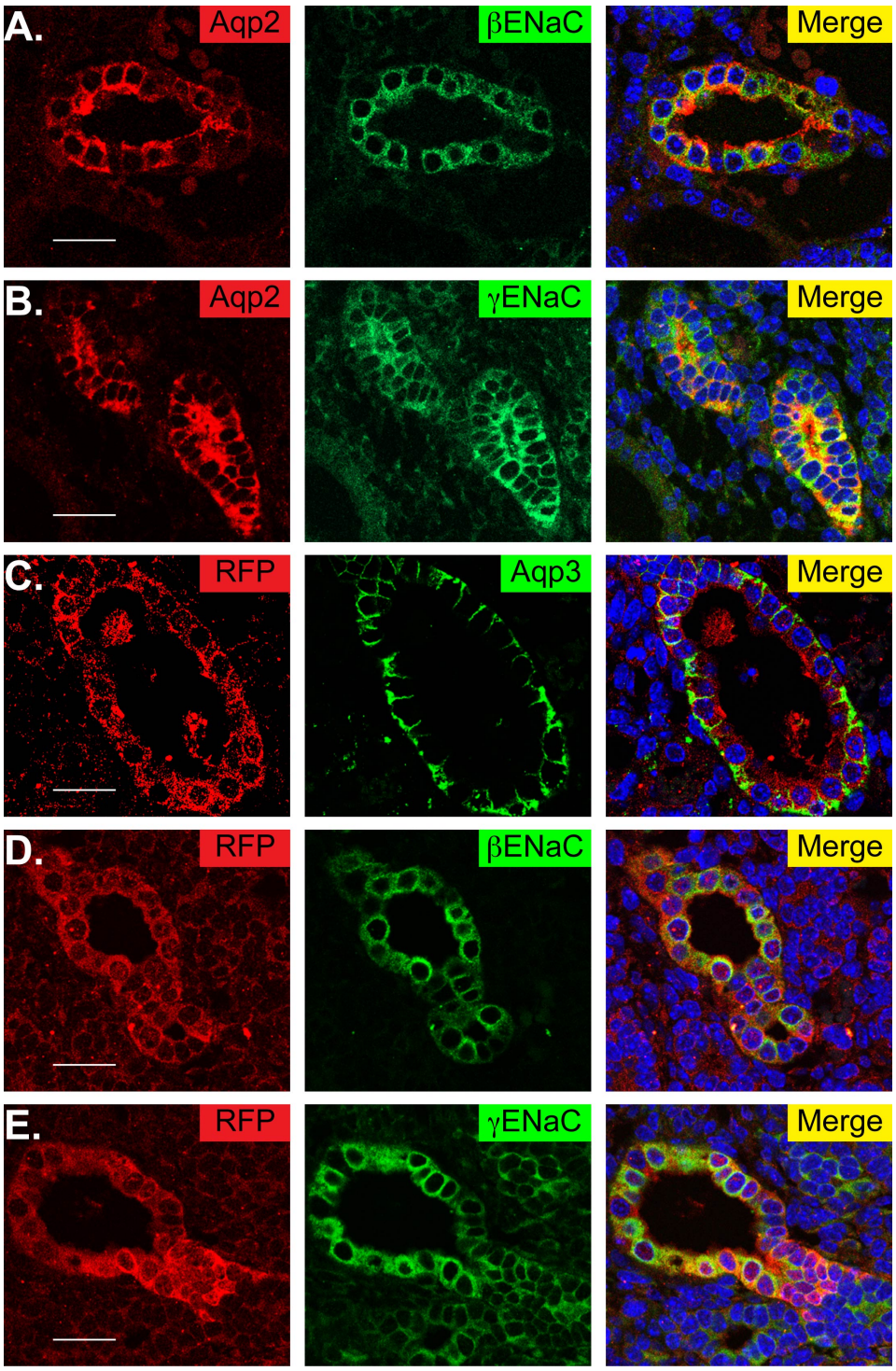

Figure 27. Aqp2^{+} cells are highly differentiated at E16.5.

Representative double IF showing coexpression of Aqp2 or RFP (red) with the other three PC markers (green): βENaC (***A & D***), γENaC (***B & E***), and Aqp3 (***C***) in E15.5 *Aqp2Cre RFP* kidney. Scale bar: 100 μm.

intercalated cells, principal cells derived from $Aqp2^+$ progenitors at E15.5 are already highly differentiated.

3.14 $Aqp2^+$ progenitors give rise to connecting tubule cells.

To determine whether the adult cortical tubules consisting of multiple RFP^+Aqp2^- or RFP^+Aqp3^- cells bear the molecular signature of distal convoluted tubule, we investigated the co-expression of RFP with Na^+-Cl^- cotransporter (NCC), a well-accepted distal convoluted tubule marker. In agreement with the published results (70), NCC^+ cells were exclusively found in the cortex, with the majority being RFP^- (Figure 28). However, the remaining NCC^+ cells have robust RFP expression. These tubules consist of multiple NCC^+RFP^+ and NCC^+RFP^- cells, indicating the possibility of the contribution of the RFP cells to the distal convoluted tubule/connecting tubule boundary (Figure 28). Indeed, tubules with a clear cut distinction between NCC^+RFP^+ and NCC^+RFP^- cells were found and the NCC^+RFP^+ and NCC^+RFP^- cells were completely separated from one another (Figure 28B). Figure 28B shows a single tubule consisting of ~17 cells. NCC and RFP labeled 14 and 11 of them, respectively. The NCC^+ cell arrangement does not indicate a connecting tubule-distal convoluted tubule junction. However, the RFP signal ends abruptly. NCC^+RFP^+ and NCC^+RFP^- cells were completely separated to show a clear junction, which, in fact, separates distal convoluted tubule from connecting tubule 3 as we defined below.

To determine whether the co-expression of NCC and RFP reflected a failure of restricting Aqp2 and NCC to connecting tubule/collecting duct and distal convoluted tubule cells, respectively, we performed Aqp2 and NCC double

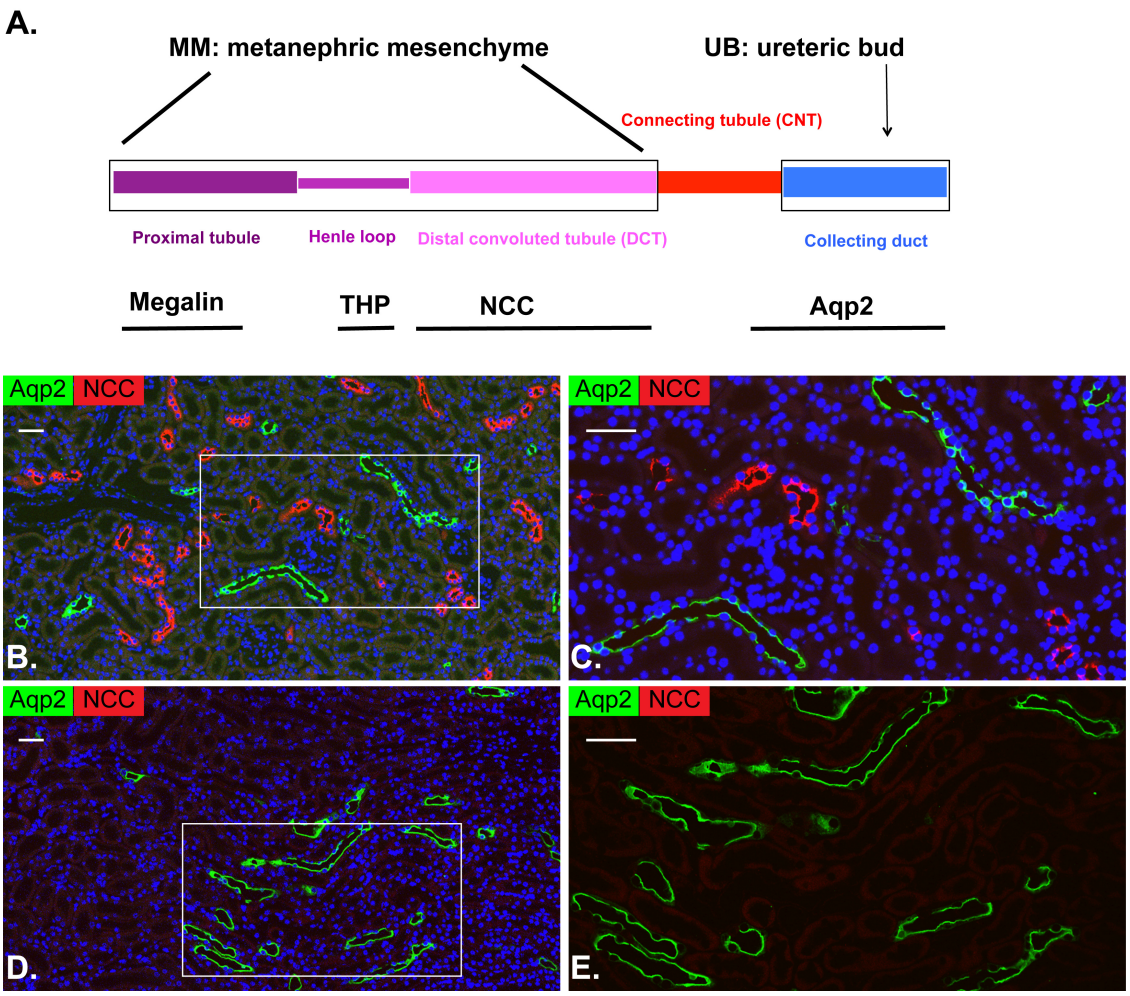

Figure 28. *Aqp2Cre* transgene does not affect the segregation of Aqp2 and NCC.

A. Diagram showing origins of nephron and collecting duct. Metanephric mesenchyme gives rise to nephron segments, from proximal to distal, including meglin^{+} proximal tubule, THP^{+} thick ascending loop, NCC^{+} distal convoluted tubule. The ureteric bud contributes to Aqp2^{+} collecting duct. ***B-E***. Representative confocal images showing staining of Aqp2 (green) and NCC (red) in the cortex (***B***-***C***) and Medulla (***D-E***) of *Aqp2Cre RFP* kidneys. Boxed areas in ***B*** and **D** were 2X magnified in ***C*** and ***E***, respectively. Scale bar: 100 μm. As expected, no co-expression of Aqp2 with NCC was found.

staining. In contrast to the RFP and NCC patterns, none of the $Aqp2^+$ cells overlap with NCC^+ cells throughout the whole *Aqp2Cre RFP* kidney (Figure 29), indicating that *Aqp2Cre* transgene does not impact the segregation of Aqp2 and NCC expression domains.

3.15 The connecting tubule contains 3 molecularly distinct segments.

Based on the partial overlapping of RFP and NCC (Figure 28 and 30), we predict that connecting tubule harbors 3 molecularly different segments (Figure 30C). From the proximal to the distal part, these segments are arranged and characterized by $RFP^+Aqp2^-Cre^-NCC^+$, $RFP^+Aqp2^-Cre^-NCC^-$, and $RFP^+Aqp2^+Cre^+NCC^-$, where + and - indicate the presence and absence of the corresponding marker alone or in combination in any cells within each segment, respectively. We named them as connecting tubule segments 3, 2, and 1 (Figure 31A). The first two are transitional and close to the distal convoluted tubule. We also predict that the classical distal convoluted tubule/connecting tubule boundary junction defined by the abrupt end of NCC expression is actually the dividing line between connecting tubule segments 2 and 3, which should have RFP^+ cells on both sides. Accordingly, we first performed a triple immunofluorescence staining to determine co-labeling of RFP, NCC, and Cre. Although both NCC and Cre were stained in green, they were restricted to the apical membrane and nuclei, respectively (Figure 31B). $RFP^+Cre^+NCC^-$ cells in a collecting duct served as a positive control for Cre staining. The adjacent connecting tubule segment 3 contained RFP^+ NCC^+ cells. However, none of

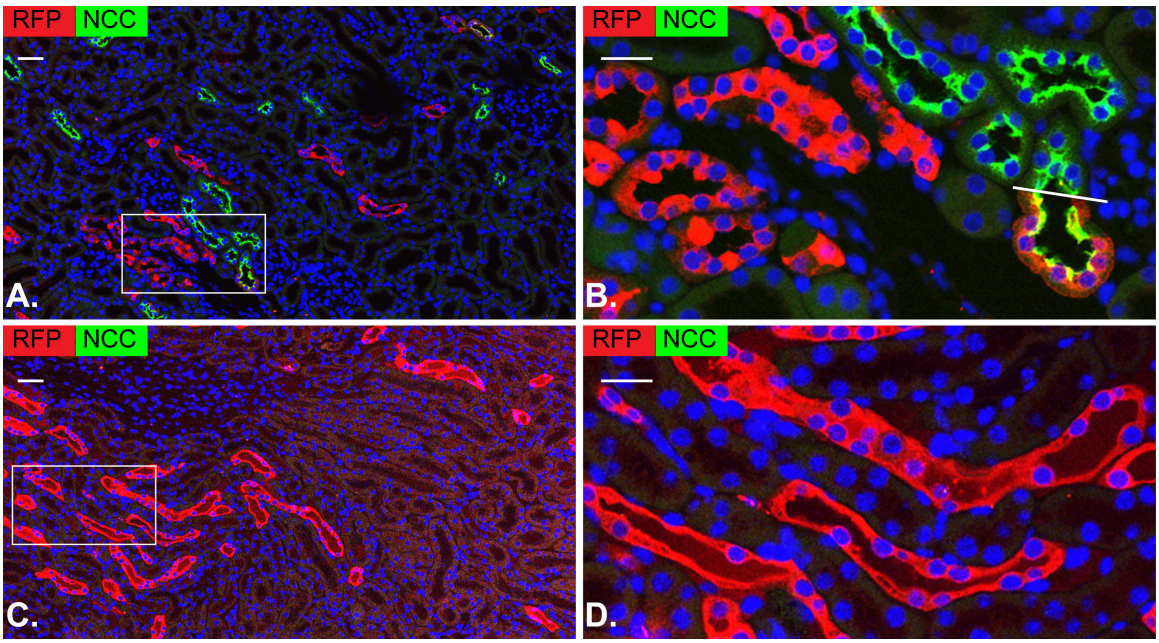

Figure 29. Partial co-expression of RFP with NCC in the cortex of *Aqp2Cre RFP* kidneys.

Representative confocal images showing staining of RFP (red) and distal convoluted tubule marker NCC (green) in the cortex (***A***-***B***) and Medulla (***C***-***D***) of *Aqp2Cre RFP* kidneys. Boxed areas in ***A*** and ***C*** were 4X magnified in ***B*** and ***D***, respectively. Scale bar: 100 μm.

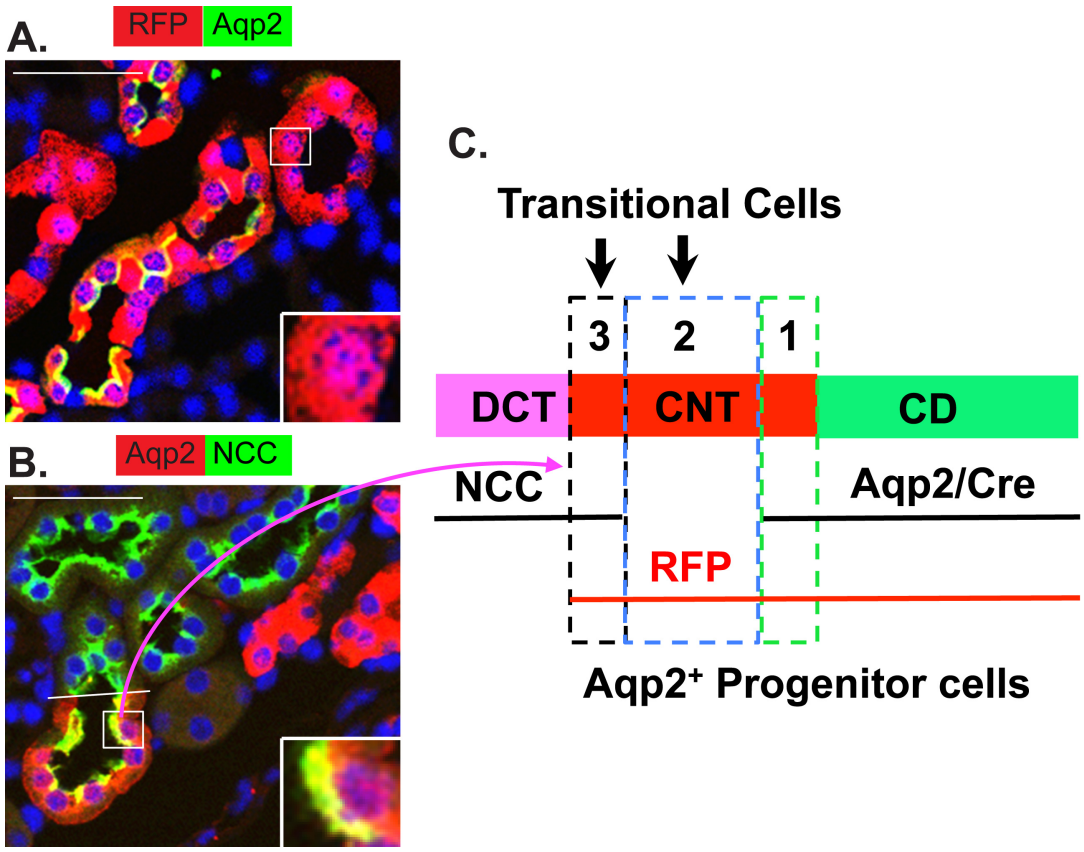

Figure 30. Aqp2$^+$ progenitor cell contribute to connecting tubule segments. Representative confocal images showing double staining of *Aqp2Cre RFP* kidneys as indicated. ***A.*** Two types of RFP$^+$ tubules were present in the *Aqp2Cre RFP* kidney. The first type is the typical collecting duct because it has both RFP$^+$Aqp2$^+$ and RFP$^+$Aqp2$^-$ cells. The second type contains RFP$^+$ cells, but no Aqp2$^+$ cells. These tubules represent the CNT2 and CNT3 transitional segments as indicated in ***C***. ***B.*** NCC$^+$RFP$^+$ cells that in CNT3 are well segregated from NCC$^+$RFP$^-$ cells in distal convoluted tubules. The clear cut distinction between NCC$^+$RFP$^+$ and NCC$^+$RFP$^-$ cells represents the boundary between distal convoluted tubule and CNT3. Accordingly, the existence of CNT2 and CNT1 are predicted (See Figure 31). ***B*** is a part of Figure 29B. Scale bar: 100 μm.

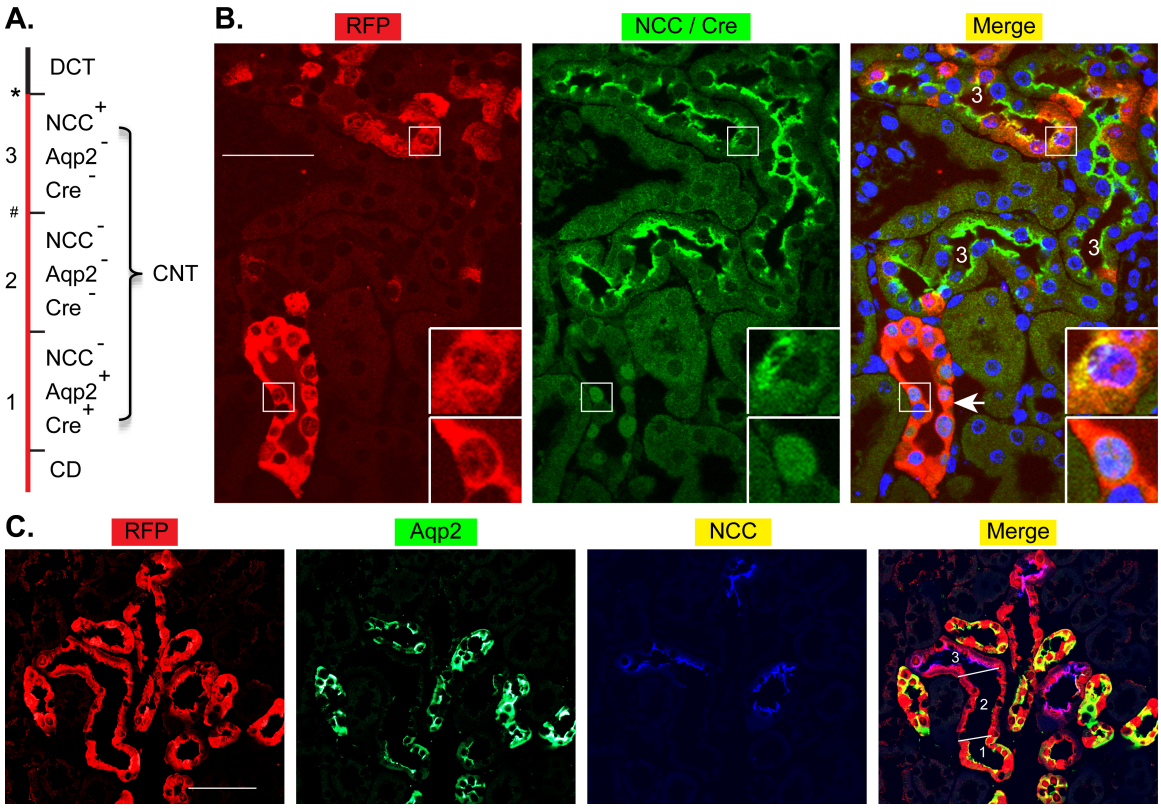

Figure 31. CNT contains 3 molecularly distinct segments and originates from Aqp2$^+$ progenitor cells.

A. Diagram showing molecularly distinct segments 1-3 in CNT. The red line indicates RFP$^+$. * and #: CNT/DCT junctions defined by abrupt end of RFP (see Figure 30B-C) and NCC (See Figure 31C), respectively. ***B.*** Representative confocal images showing triple IF with Cre and NCC in green and RFP in red. Arrow: a typical RFP-labeled CNT/CD structure with nuclear Cre signal, but without NCC membrane staining serves as a positive control of Cre staining. Tubules marked with 3 are CNT3 as in ***A***. CNT3 lacks cells with nuclear Cre signal, but has cells positive for NCC, RFP, or both. Boxed areas were 3X magnified. ***C.*** Representative confocal images showing triple IF as indicated. There were three connecting tubule segments (CNT1-3) in a single tubule. These segments were separated by RFP$^+$Aqp2$^+$NCC$^-$, RFP$^+$Aqp2$^-$NCC$^-$, and RFP$^+$Aqp2$^-$ NCC$^+$ cells, with the boundaries marked by white lines. The classical CNT/DCT junction is the one between CNT2 and CNT3.

them had nuclear Cre staining. They are presumably $Aqp2^-$ because of Cre^-. This reinforces the specificity of *Aqp2Cre* transgene and demonstrates that connecting tubule segment 3 cells, like most intercalated cells, are derived from $Aqp2^+$ progenitors. They apparently have both collecting duct and distal convoluted tubule properties: that is, the origin of $Aqp2^+$ progenitors and expression of NCC.

Next, we conducted a triple immunofluorescence stain for RFP, Aqp2, and NCC. A representative confocal image is given in Figure 31C. As predicted, a single tubule was found to have three connecting tubule segments, which were featured by $RFP^+Aqp2^+NCC^-$, $RFP^+Aqp2^-NCC^-$, and $RFP^+Aqp2^-NCC^+$ cells. Two clear junction boundary lines were clearly observed. The boundary line separating connecting tubule segment 2 from segment 3 corresponds to the classical distal convoluted tubule/connecting tubule boundary junction. RFP^+ cells on both sides of this boundary line were distinguished by the presence and absence of NCC expression. The second boundary line separates connecting tubule segment 2 from segment 1, with $Aqp2^-$ cells on the side of segment 2 and $Aqp2^+$ cells on the side of segment 1. In brief, we have detected two different junctions and 3 molecularly distinct segments in connecting tubule. Each segment harbors $Aqp2^+$ progenitor-derived, RFP-labeled cells.

To rule out the possibility of artifacts due to cutting from a particular plane, we constructed a series of 3-D structures, each of which was built with 0.5-μm confocal sections of 8-μm thickness. The 3-D structure contained 2-3 cell layers and clearly demonstrated the existence of the 3 connecting tubule segments as

we described above (movie data can not be shown). The cell layers were more clearly seen in a control slide stained for DAPI and Aqp2 (movie data can not be shown). Further increasing the thickness of the paraffin slides is impractical because samples became easily cracked, detached, and resistant to antibody penetration. While frozen slides may circumvent these limitations, the morphology of the tubules is sacrificed, complicating the data analyses.

3.16 Connecting tubule segments 2 and 3 lack a molecular signature of principal cells.

To further profile the marker expression of the connecting tubule segments, we performed 3 sets of triple immunofluorescence staining using consecutive paraffin slides 8-μm in thickness. Each slide was co-stained for RFP/Aqp2/B1B2, RFP/Aqp2/AE1, or RFP/Aqp3/AE1. Connecting tubule segments 2 and 3 were identified by lack of $Aqp2^+$ or $Aqp3^+$ cells, and possessing at least one RFP^+ cells. As shown in Figure 32, the same tubule containing connecting tubule segments 2 and 3 present on each slide contained a few RFP^+B1B2^+ and RFP^+AE1^+ cells, respectively. These results were also verified by 3-D structural analyses as in 2.15. Similarly, the RFP^+ $Aqp2^-$ tubules shown in Figures 7A, 10A and 30A should also be connecting tubule segments 2 and 3.

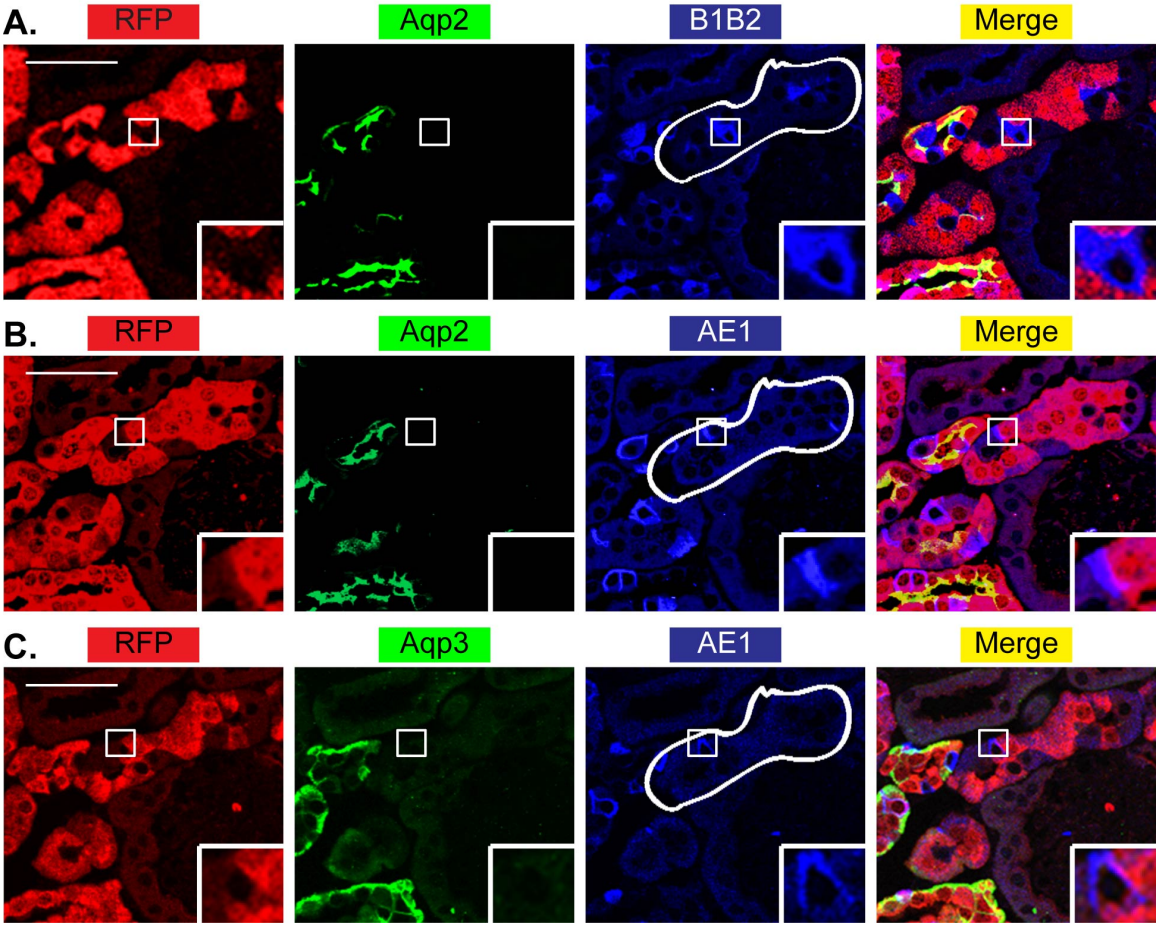

Figure 32. The CNT/DCT transitional structures lack a molecular signature of principal cells and contain intercalated cells.

Representative confocal images showing triple IF staining of three 8-μm-thick sections as indicated. The same CNT/DCT transitional structure, in which there were some cells expressing IC markers B1B2 and AE1, but no cells expressing detectable PC markers Aqp2 and Aqp3, was traced. Boxed areas were 3X magnified. Scale bar: 100 μm.

3.17 Connecting tubule segments 2 and 3 apparently exist in wild-type C57BL6 kidneys.

To address if connecting tubule segments 2 and 3 exist in non-transgenic mice, we conducted 3 sets of triple immunofluorescence staining with WT C57BL6 kidney. Each slide was co-stained with Aqp2/B1B2/NCC, Aqp2/B1B2/AE1, and Aqp3/B1B2/AE1. Confocal microscopy images displayed similar cortical tubules harboring multiple cells expressing B1B2, AE1, and NCC, but lacking detectable Aqp2 and Aqp3 (Figure 33). These data indicated that natural existence of connecting tubule segments 2 and 3 in WT C57BL6.

In brief, we propose a working model to summarize our major findings (Figure 34).

3.18 Generation of collecting duct cell lines with intact or disrupted *Dot1l*.

In addition to *Aqp2Cre RFP* mice, we crossed RFP reporter mice Ai14 with *Dot1l*$^{f/f}$ *Aqp2Cre* to generate a triple transgenic line *Dot1l*$^{f/f}$ *Aqp2Cre RFP*. To establish the collecting duct cell lines for future research, primary cells were isolated from both *Aqp2Cre RFP* and *Dot1l*$^{f/f}$ *Aqp2Cre RFP* mice. As illustrated in Figure 35A, the primary cells were transduced with a retroviral vector (LXSN-16E6E7) packaged by PA317 fibroblast line for immortalization (71). The immortalized cells were sorted on the basis of RFP into single cells to establish single-cell-derived clones. As shown in Figure 35B, immunofluorescence staining confirmed the presence and absence of H3m2K79 in the clones derived from *Aqp2Cre RFP* and *Dot1l*$^{f/f}$ *Aqp2Cre RFP* mice, respectively. Western blotting

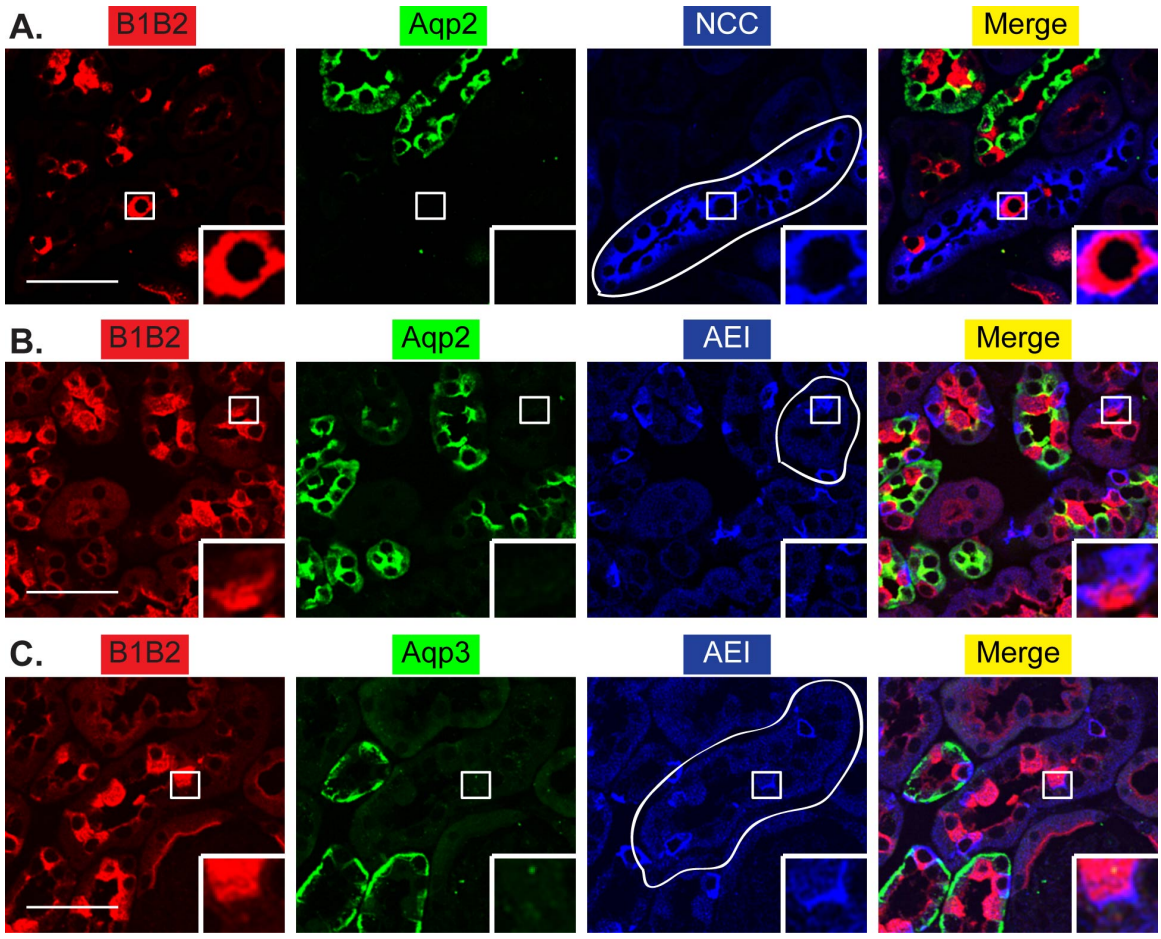

Figure 33. The CNT/DCT transitional structures exist in the wild-type C57BL6 kidney.

Representative confocal images showing the staining of the markers as indicated. The CNT/DCT transitional structures in which there are multiple cells expressing IC markers B1B2 and AE1, but no cells expressing detectable principal cell markers Aqp2 and Aqp3, were traced. Boxed areas were 2X magnified. Scale bar: 100 μm.

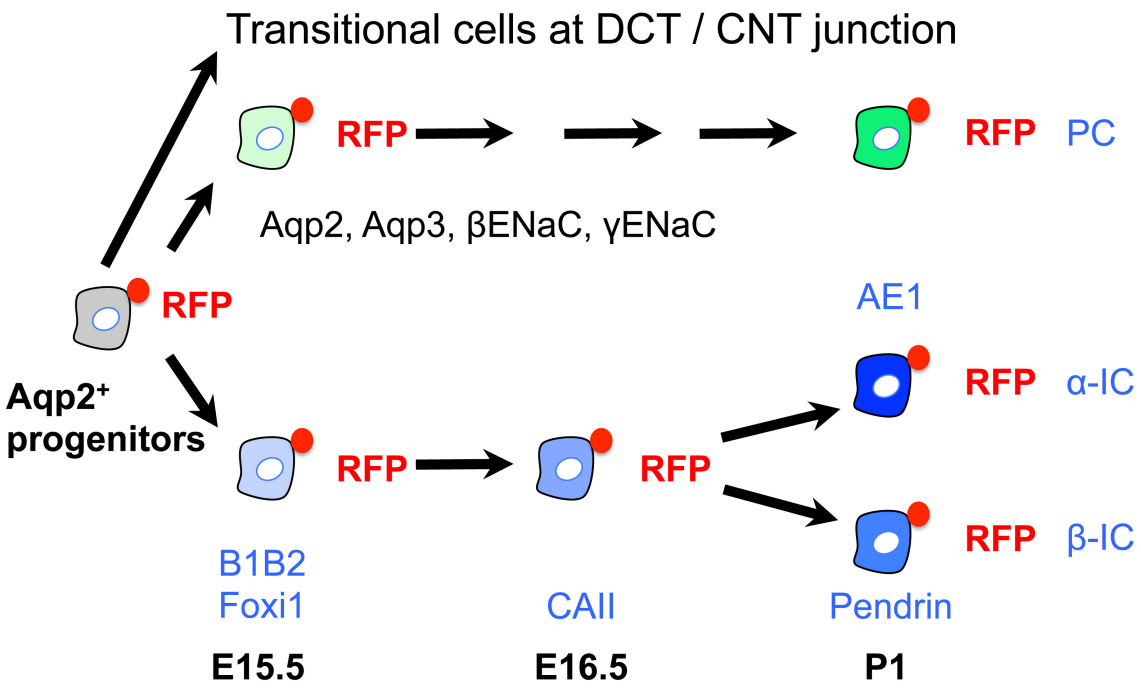

Figure 34. A step-wise differentiation model for Aqp2$^+$ progenitor cells.

Aqp2$^+$ progenitor cells are committed to a highly differentiated PC fate by maintaining/acquiring expression of Aqp2, Aqp3, βENaC, and γENaC at E15.5. Alternatively, the progenitor cells switch to IC destiny through loss of Aqp2 expression and sequential gain of Foxi1 and V-ATPase B1B2 at E15.5 and CAII at E16.5. IC further differentiates into α-IC and β-IC by obtaining either AE1 or Pendrin, respectively, at P1. For simplicity, Pendrin$^+$ non-A-non-B type of IC is not shown. Aqp2$^+$ progenitor cells can further contribute to various molecularly distinct transitional cells in the different segments of connecting tubule that connects distal convoluted tubule and collecting duct.

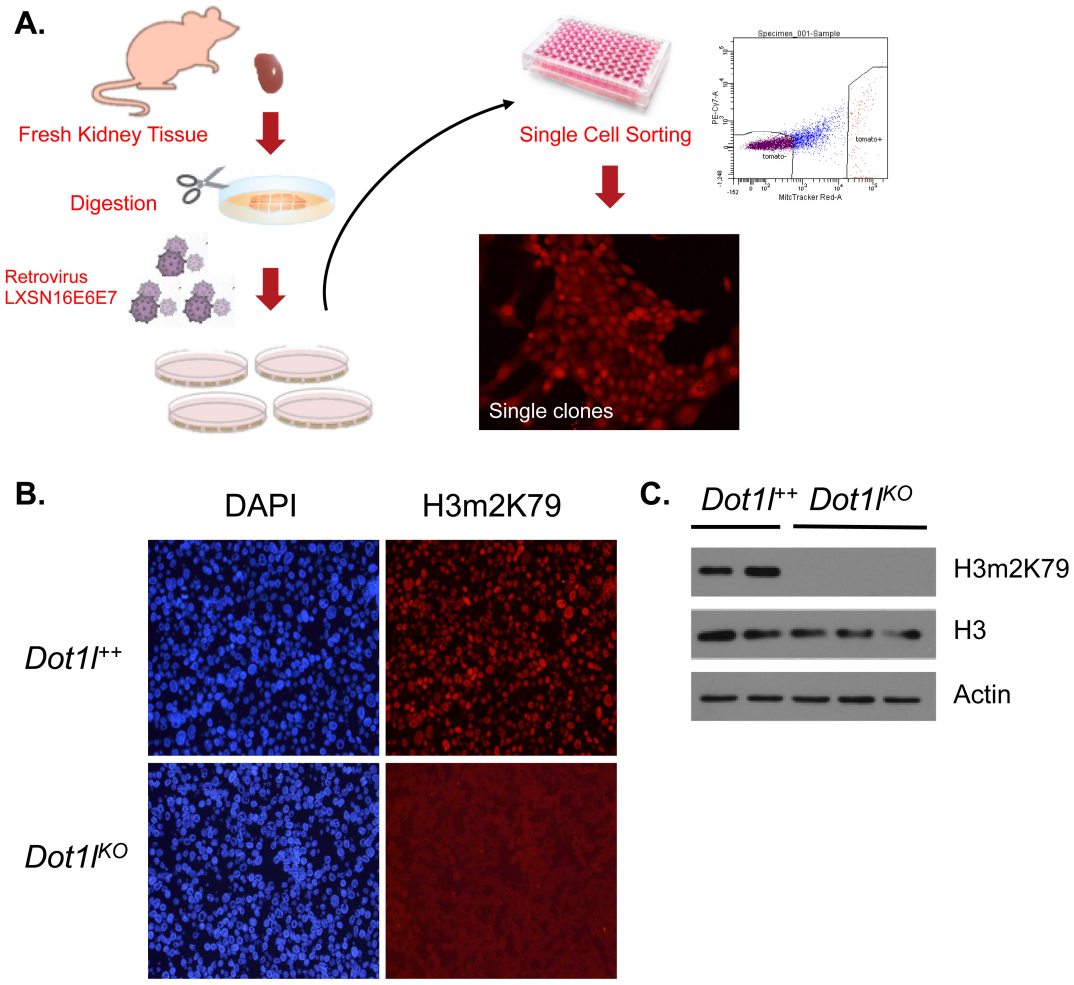

Figure 35. Generation of collecting duct cell lines with intact or disrupted *Dot1l*.

A. Diagram showing the isolation and immortalization of primary cells from *Aqp2Cre RFP* (*Dot1*$^{++}$) and *Dot1l*$^{f/f}$ *Aqp2Cre RFP* mice (*Dot1l*^{KO}). Primary kidney cells were isolated and infected by retrovirus LXSN 16E6E7 for immortalization. After selection with G418, the immortalized cells were expanded and sorted based on RFP into individual cells to form single-cell-derived clones. ***B.*** Representative immunofluorescence staining showing the presence and absence of H3m2K79 in the clones derived from *Aqp2Cre RFP* (*Dot1*$^{++}$) and *Dot1l*$^{f/f}$ *Aqp2Cre RFP* mice (*Dot1l*^{KO}). ***C.*** Western blotting showing two clones from *Aqp2Cre RFP* with high levels of H3m2K79, and three clones from *Dot1l*$^{f/f}$ *Aqp2Cre RFP* mice with undetectable H3m2K79. Identical blots were probed with antibodies for total histone H3 or actin to verify the integrity of histone H3 and equal loading across the lanes.

analyses further confirmed these results. While two clones from *Aqp2Cre RFP* had high levels of H3m2K79, three clones from *Dot1l*$^{f/f}$ *Aqp2Cre RFP* mice showed undetectable H3m2K79 (Figure 35C). Identical blots probed with antibodies for total histone H3 or actin verified the integrity of histone H3 and equal loading across the lanes (Figure 35C). To our knowledge, these cell lines are the first *Dot1l*-deficient stable cell lines and will be valuable reagents for dissecting the function and regulation of *Dot1l* in vitro.

3.19 Generation of the inducible *Aqp2ER*^{T2}*CreER*^{T2} construct.

Using *Aqp2Cre RFP* mice, we have identified and characterized the embryonic Aqp2$^+$ progenitor cells. Whether adult Aqp2$^+$ progenitor cells exist and what are their roles in the maintenance, remodeling, and injury repair of kidney as well as development of kidney disease remains virtually unknown. Since *Aqp2Cre* is constitutively and persistently activated during development, it cannot be used to trace the potential Aqp2$^+$ progenitor cells in adult kidney. Accordingly, we intend to generate an *Aqp2ER*^{T2}*CreER*^{T2} allele by inserting an *ER*^{T2}*CreER*^{T2} cassette into the *Aqp2* locus at the position of the Aqp2 initiation codon (Figure 36A). *ER*^{T2}*CreER*^{T2} expresses Cre recombinase sandwiched by a mutant estrogen receptor ligand-binding domain, which does not bind natural ligand at physiological concentrations but binds the synthetic ligand, 4-hydroxytamoxifen. Sequestered to the cytoplasm, the *ER*^{T2}*CreER*^{T2} fusion protein can only be imported into the nucleus and mediate recombination after exposure to tamoxifen (72). Therefore, *Aqp2ER*^{T2}*CreER*^{T2} mice are expected to provide temporal and

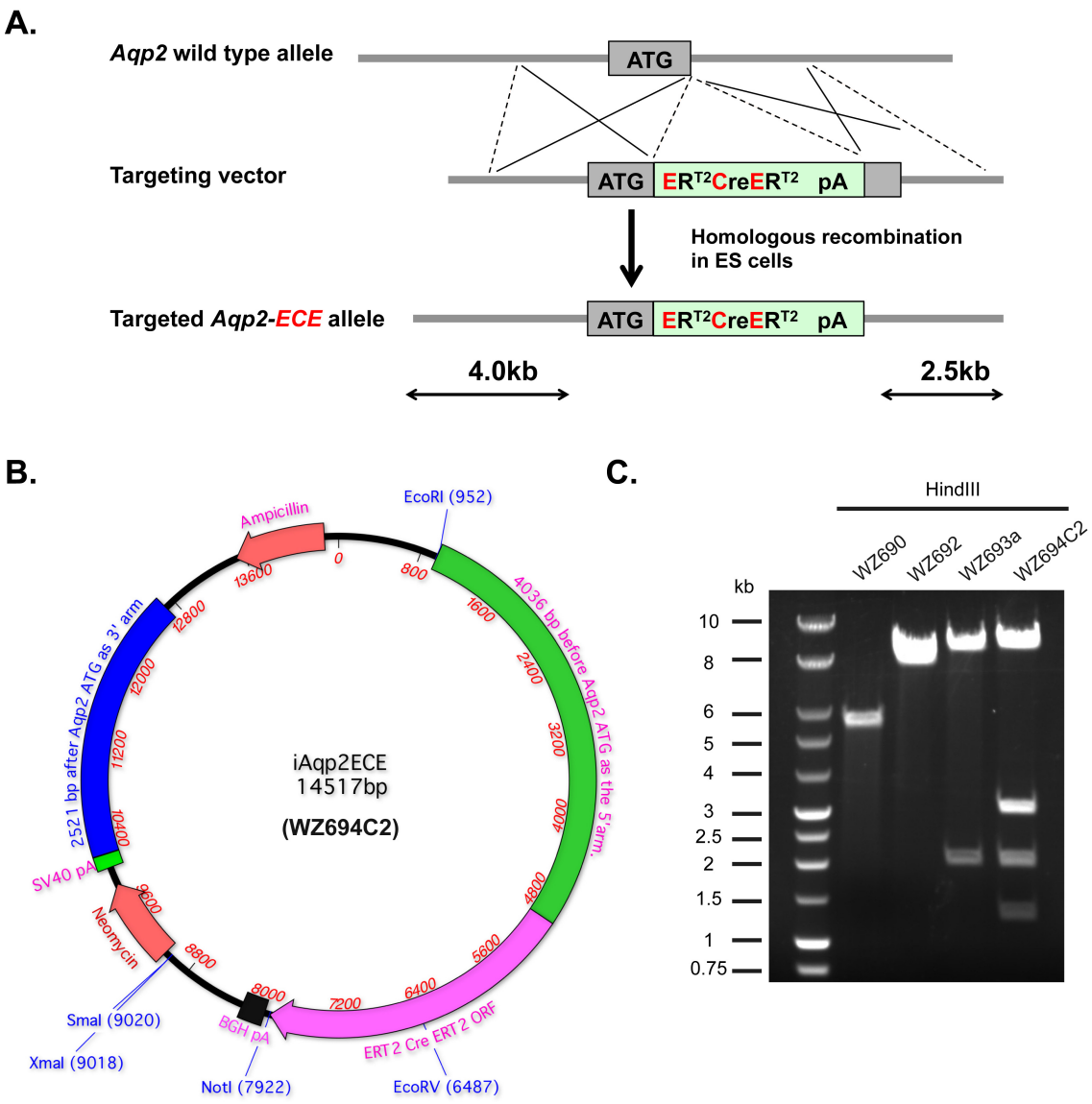

Figure 36. Generation of inducible *Aqp2ER^{T2}CreER^{T2}* construct.

A. The *Aqp2ER^{T2}CreER^{T2}* allele will be created by inserting the *ER^{T2}CreER^{T2}* cassette into the *Aqp2* locus at the position of the Aqp2 initiation codon. ***B.*** Diagram of the final target vector. ***C.*** HindIII-digestion analysis of pcDNA3.1 (+) and its derivatives including the final target vector.

spatial inactivation of floxed genes and activation of the Cre-dependent reporters. We chose *ER^{T2}CreER^{T2}* because it has been shown to have tighter regulation of Cre activity than *CreER^{T2}*. Unlike *CreER^{T2}*, which causes tamoxifen-independent recombination, *ER^{T2}CreER^{T2}* had no background recombination in the absence of drug administration (73). As the first step, we have designed and developed the final target vector (WZ 694C2) through multiple cloning steps (Figure 36B). WZ694C2 was confirmed by enzyme digestion (Figure 36C). DNA sequencing verified the authenticity of all inserts (the 5' and 3' arms and the *ER^{T2}CreER^{T2}* cassette). We are generating an *Aqp2 ER^{T2}CreER^{T2}* knock-in mouse model through a commercial service. We expect to have this model in hand in the coming months. Our future studies will be focused on the identification and characterization of adult Aqp2^{+} progenitor cells, using the *Aqp2ER^{T2}CreER^{T2}* knock-in model. With this model in hand, we will be able for the first time to directly investigate 1) if adult Aqp2^{+} progenitor cells exist; 2) if adult Aqp2^{+} progenitor cells modulate the maintenance, remodeling and injury repair of the kidney; and 3) if adult Aqp2^{+} progenitor cells contribute to development of kidney diseases such as polycystic kidney disease.

Chapter 4

Discussion and ongoing plans

In the *Dot1l*$^{f/f}$ *Aqp2Cre* mouse model, we showed that both the principal cells and intercalated cells in the collecting ducts lacked histone H3m2K79, raising the possibility that principal cells and intercalated cells are descendants of Aqp2-expressing cells (28, 74). Some intercalated cells have already lost the H3m2K79 in neonate *Dot1l*$^{f/f}$ *Aqp2Cre* mice as early as Day 3 after birth, raising the possibility of the derivation of intercalated cells from Aqp2-expressing cells during early development. Although substantial intercalated cells are still positive for H3m2K79, it may be due to the incomplete deletion of *Dot1l*. We concluded that embryonic Aqp2$^+$ progenitor cells exist and are responsible for generation of intercalated cells as well as principal cells in the absence of *Dot1l* function. We verified and extended these findings by using RFP reporter mice. In particular, we: 1) generated a new mouse model using RFP as a marker to trace Aqp2 lineage; 2) demonstrated that RFP faithfully recapitulates the spatiotemporal profile of the endogenous *Aqp2* in embryonic, neonatal, and adult mice; 3) revealed that all principal cells and most intercalated cells are differentiated from the Aqp2$^+$ progenitor cells and that such processes do not require inactivation of *Dot1l*; 4) found that some of the Aqp2$^+$ progenitor cells become highly differentiated and express all principal cell markers examined (Aqp3, βENaC, and γENaC) at E15.5. Other Aqp2$^+$ progenitor cells begin to lose the Aqp2$^+$ phenotype and progressively gain intercalated cell properties with expression of Foxi1 and B1B2 at E15.5 and CAII at E16.5; 5) showed that differentiation of Aqp2$^+$ progenitor cells into α-intercalated cells and β-intercalated cells is detectable at P1 and continues during neonatal development, with completion of

β-intercalated cell restriction in the cortex by P7; 6) found that the connecting tubule contains three molecularly distinct segments; and 7) indicated that $Aqp2^+$ progenitor cells contribute to intertubular connection by differentiating into various types of cells in the connecting tubule segments.

4.1 Previous renal lineage tracing mouse models

The use of stem/progenitor cells holds promise for development of new and powerful strategies for future regenerative medicine. As a powerful technique for identifying the stem/progenitor cell identity and origin of candidate tissue populations in their native context, lineage tracing *in vivo* absolutely depends on the faithfulness of the tracing marker to indicate the spatiotemporal pattern of the endogenous gene. Several renal cell lineage tracing mouse models have been reported, including *Six2-Cre*, *Lgr5-EGFP-ires-CreER*^{T2}, and *HoxB7-Cre* mice. The *Six2-Cre* mice include a BAC transgenic model carrying a *Tet-off-eGFPCre* (*TGC*) cassette and knock-in models with *TGC* and *eGFPCreER*^{T2} cassettes residing at the Six2 initiation codon. Restriction of GFP to most or all $Six2^+$ cells of the cap mesenchyme from the onset of nephrogenesis validated the faithfulness (9). Similarly, the faithfulness of the *Lgr5-EGFP-ires-CreER*^{T2} was established by the tight correlation between *Lgr5-EGFP* expression and endogenous *Lgr5-FISH* signals on separate kidney sections (11). *HoxB7-Cre* transgenic mice express Cre under the control of a 1.3-kb mouse *HoxB7* enhancer/promoter. Cre-mediated recombination of the *ROSA* or *Z/AP* reporter alleles was detectable in the mesonephric duct as early as E9.5, in the ureteric

bud by E10.25, and in all ureteric bud epithelial cells by E12.5. Low levels of Cre expression were also detected in the dorsal root ganglia and the spinal cord. It has been used to inactivate several genes including sonic hedgehog (*Shh*) and *αENaC* (22, 23) in the mesonephric duct and its developmental derivatives (the Wolffian duct, the collecting duct epithelium, and ureteral epithelium). Recombination apparently patterned the endogenous gene expression. However, the faithfulness of *HoxB7-Cre* remains obscure because a direct comparison of the Cre expression/activity with the endogenous *HoxB7*, to our knowledge, has not been reported.

4.2 *Dot1l*$^{f/f}$ *Aqp2Cre* as the first Aqp2-lineage tracing model

The *Aqp2Cre* model was generated by modifying a mouse genomic PAC harboring a 125-kb 5′ upstream region and a 31-kb 3′ downstream region of the *Aqp2*. A Cre-encoding fragment was inserted at the ATG of the *Aqp2* in this PAC to create the *Aqp2Cre* line. A transgenic line harboring two copies of the *Aqp2Cre* has been employed to inactivate mineralocorticoid receptor (55) and *Dot1l* (28, 38).

In this report, we first used the *Aqp2Cre* line to generate *Dot1l*$^{f/f}$ *Aqp2Cre* mice. With Cre expression driven by the Aqp2 regulatory elements and loss of Dot1l-mediated H3m2K79 as the tracing marker, we have for the first time provided strong *in vivo* evidence showing that 1) in the absence of *Dot1l* function, most of the intercalated cells are derived from Aqp2-expressing cells; and 2) derived

intercalated cells are detectable at 3 days of age, the earliest time point examined.

Both notch and Foxi1 signaling pathways have been shown to play a role in the cell fate determination of the principal cells and intercalated cells. *Mib1* is an E3 ligase that mediates the endocytosis of notch ligand. Deletion of Mib1 fails to activate the notch signaling pathway, leading to increased intercalated cells and decreased principal cells (75). Inactivation of Adam10, a S2 cleavage protease for notch receptor, also resulted in a reduction in the principal/intercalated cell ratio (76). Similarly, in our *Dot1l*$^{f/f}$ *Aqp2Cre* model, we indeed observed increased relative numbers of intercalated cells associated with a decreased principal cell population. Although no evidence exists showing that *Dot1l* participates in the notch signaling, it is worthy to investigate if there is an interaction between them.

Global deletion of *Dot1l* leads to embryonic lethality, a combinational output of cell cycle arrest, angiogenesis defects, and cardiovascular defects (30, 77). Hence, *Dot1l* may be involved in developmental programs impacted by the notch-signaling pathway. *Dot1l* has also been shown to function in embryonic stem cells (77), erythropoiesis (78), and intestinal homeostasis (79), which further provide evidence for its developmental roles.

In contrast to Notch signaling-deficient mice, mice with inactivated Foxi1 lack typical principal cells and intercalated cells, but contain only Aqp2^{+}CAII^{+} intermediate cells (68). These observations allowed the authors to draw a conclusion that both principal cells and intercalated cells are derivatives of progenitors expressing both Aqp2 and CAII. Our findings with *Dot1l*$^{f/f}$ *Aqp2Cre*

and *Aqp2Cre RFP* mouse models (discussed further below) raise the possibility that these $Aqp2^{+}CAII^{+}$ progenitor cells are derived from a more ancestral population of progenitor cells that express Aqp2, but not CAII. Considering this, we favor the notion that Aqp2 may serve as a progenitor cell marker during early development.

Although our studies with *Dot1l*$^{f/f}$ *Aqp2Cre* model argue that at least some intercalated cells are derivatives of Aqp2-expressing cells when *Dot1l* is inactivated, they do not address whether this is a general property of the population rather than just a simple result of *Dot1l* deletion, nor when restriction occurs in the collecting duct forming lineage. The intrinsic limitations of *Dot1l*$^{f/f}$ *Aqp2Cre* mice exclude the possibility to address these questions. First, since Aqp2-expressing cells are apparently able to switch from $Aqp2^{+}$ to $Aqp2^{-}$ phenotype, detection of Aqp2 protein itself as a marker may not reliably trace all of the descendents originating from Aqp2-expressing progenitor cells. Secondly, since H3m2K79 levels fluctuate and reach the lowest point in G2 (80), undetectable H3m2K79 may stem from cell cycle-dependent regulation rather than from Aqp2Cre-mediated *Dot1l* deletion. Therefore, the utility of disrupted H3m2K79 as a tracing marker for *Aqp2Cre* activity and thus Aqp2 lineage is limited, particularly in the rapidly developing *Dot1l*$^{f/f}$ *Aqp2Cre* kidneys; Thirdly, the faithfulness of *Aqp2Cre* can not be thoroughly and conclusively evaluated using loss of H3m2K79 as the tracing marker. Finally and most importantly, these experiments are dependent on the loss of *Dot1l*-mediated H3m2K79, eliminating

the possibility of lineage tracing under normal physiological conditions (i.e. *Dot1l* is not deleted).

4.3 *Aqp2Cre RFP* as a new Aqp2-lineage tracing model to overcome the limitations of *Dot1l$^{f/f}$ Aqp2Cre*

To overcome these limitations of *Dot1l$^{f/f}$ Aqp2Cre* mice, we further crossed the same *Aqp2Cre* line with the Cre-dependent RFP reporter mice to generate *Aqp2Cre RFP* mice. Through a series of double and triple immunofluorescence stains, we extensively demonstrated the spatiotemporal faithfulness of RFP as the tracing marker of Aqp2-lineage cells. RFP is expressed in most or all Aqp2$^+$ cells in the embryonic, neonatal, and adult kidneys. There is no detectable RFP in Aqp1$^+$, megalin$^+$, and uromodulin$^+$ cells and in most of calbindin$^+$ and NCC$^+$ cells. These findings indicate not only that RFP recapitulates the silencing of the endogenous *Aqp2* in most, if not all, of the tubular cells from the proximal tubules to the distal convoluted tubule, but also that *Aqp2Cre* transgene apparently has little effect on segregation of these markers, consistent with the normal renal function in *Aqp2Cre RFP* mice.

Megalin, uromodulin, calbindin, and Aqp2 are the same set of the markers used to characterize the pattern of the endogenous *Lgr5* and transgenic *Lgr5-EGFP* from the proximal tubules to the collecting duct (11). In aggregate, our data validate *Aqp2Cre RFP* model as an accurate reporter of the endogenous *Aqp2* in kidney. Moreover, although some of the potential progeny of Aqp2$^+$ cells may no

longer express Aqp2, the activated RFP reporter acts as a genetic marker, facilitating lineage tracing.

Our study not only demonstrates that some $Aqp2^+$ cells are progenitor cells responsible for production of all known cell types in the collecting duct, but also shed new light into the underlying molecular mechanism. The molecular maturation of principal cells differentiated from $Aqp2^+$ progenitor cells apparently involves maintenance of Aqp2 and concurrent acquisition of at least Aqp3, βENaC, and γENaC at E15.5. However, the possibility that $Aqp2^+$ progenitor cells are derived from more ancestral cells expressing Aqp3, βENaC, or γENaC cannot be completely ruled out. It is also unknown if the highly differentiated "principal cell" at E15.5 and mature principal cells in adult kidney can still differentiate into intercalated cells during the later developmental stages and adulthood, respectively.

Differentiation of intercalated cells obviously requires multiple steps with gradual acquisition of various intercalated cell-specific molecules. The existence of RFP^+Aqp2^+ and $Aqp2^+B1B2^+$ at E15.5 raises two alternative possibilities: potential concurrent expression of Aqp2 and B1B2 in the progenitor cells or $Aqp2^+$ cells derived from $B1B2^+$ progenitor cells. If the latter were true, most or all of the $B1B2^+$ cells should be negative for both Aqp2 and RFP. However, the majority of the $B1B2^+$ were also RFP^+ cells in embryonic, neonatal, and adult kidneys, rejecting the notion that $Aqp2^+$ cells are descendants of $B1B2^+$ progenitor cells. Because most of the cells were $Aqp2^+RFP^+B1B2^-$ and $Aqp2^-RFP^+B1B2^+$ in all stages examined, the most reasonable explanation is that the

progenitor cells express Aqp2 transiently and become either principal cells or intercalated cells very quickly. Once the intercalated cell fate is fixed, these cells sequentially acquire other intercalated cell features including CAII at E16.5, followed by either AE1 or pendrin at P1, as shown in our working model (Figure 34). Expression of CAII well before AE1 and pendrin in intercalated cells derived from $Aqp2^+$ progenitor cells is consistent with the finding that CAII may be important for intercalated cell "maturation", and that its deficiency reduces both α-intercalated cells and β-intercalated cells in the cortex (81). Our work thus more accurately defines $Aqp2^+$ rather than $Aqp2^+CAII^+$ (68) as the molecular signature of the principal cells and intercalated cell ancestral cells. Nevertheless, it remains unclear if *Dot1l* ablation favors intercalated cell differentiation (28) by de-repressing Foxi1 at E15.5.

Cells expressing intercalated cell markers (B1B2, CAII, AE1, and pendrin) but not RFP were also occasionally observed at various stages. This may stem from no or low Cre expression, low efficiency of Cre-mediated recombination, or both. Such mosaicism is frequently observed in other Cre systems (82, 83). Alternatively, $Aqp2^+$ progenitor cells are not the sole source producing these intercalated cell-marker-expressing cells. In line with this idea, some collecting duct cells may be derived from intercalation of $Wnt4^+$ interstitial cells during kidney development (84).

$AE1^+$ α-intercalated cells and $Pendrin^+$ β-intercalated cells were found at P1. Occasionally, $AE1^+$ and $Pendrin^+$ cells were found scattered in the E16.5 kidneys, and these cells were RFP^- and did not reside in the RFP-labeled tubular

structures. $AE1^+$ cells may represent the red blood cells, which express AE1 as well. A previous study suggested that $Pendrin^+$ cells may arise from undifferentiated precursor cells from separate foci, one in the connecting tubule and one in the collecting duct (65). The observed $Pendrin^+$ cells at E16.5 support the notion of separate origins of $Pendrin^+$ cells. However, Aqp2 and RFP were expressed in both connecting tubule and collecting duct and no overlapping expression of Pendrin and RFP was observed at E16.5. Whether $Pendrin^+$ cells at E16.5 are derived from $Aqp2^-$ connecting tubule/collecting duct progenitor cells or from non- connecting tubule/collecting duct progenitor cells requires further studies.

Given the tight spatiotemporal correlation of RFP with the endogenous Aqp2, we conclude that *Aqp2Cre RFP* is a reliable and faithful mouse model to trace the fate of the $Aqp2^+$ lineage. We provide strong evidence that $Aqp2^+$ progenitors not only give rise to all the principal cells and most of the intercalated cells in collecting duct during the normal development, but that they also serve as the progenitors for the connecting tubule. In the cortex region, NCC and Aqp2 were restricted to the distal convoluted tubule and connecting tubule/collecting duct, respectively. No overlap between NCC and Aqp2 was observed within the cortex. However, some RFP^+NCC^+ tubules were found throughout the cortex region, indicating that RFP tagged $Aqp2^+$ progenitor cells may contribute to the connecting region linking distal convoluted tubule to connecting tubule/collecting duct. Considering the origination of distal convoluted tubule from the metanephric mesenchyme and derivation of the collecting duct from the ureteric bud (3), the

overlap between NCC and RFP, and the restriction of Cre in collecting duct, we conclude that $Aqp2^+$ progenitors cells contribute to intertubular connection by differentiating into multiple types of cells in the connecting tubule. We further defined the connecting tubule segments 1-3, which harbor three molecularly distinct segments: $RFP^+Aqp2^+Cre^+NCC^-$, $RFP^+Aqp2^-Cre^-NCC^-$, and $RFP^+Aqp2^-Cre^-NCC^+$. Connecting tubule 1 is the classical connecting tubule and expresses Aqp2, while connecting tubule 2 and connecting tubule 3 express B1B2 and AE1 and serve as the transitional region lacking the expression of Aqp2. Connecting tubule 3 differs from connecting tubule 2 by the former expressing NCC and the latter not.

Our demonstration that most or all connecting tubule cells are offspring of $Aqp2^+$ progenitor cells is consistent with the literature. *In vivo* lineage-tracing studies have reached the same conclusion, that Cited1, Six2, and Lgr5 labeled metanephric mesenchyme progenitor cells make no contribution to the collecting duct (9, 11, 25). In the Cited1 tracing experiment, the tracing maker LacZ did not co-express with Aqp2 in the adult mouse kidneys (25). $Six2^+$ progenitors give rise to β-gal positive nephron segments but not cytokeratin positive collecting duct. No double staining of the β-gal and cytokeratin were observed, even at the nephron-collecting duct junction at E15.5 (9). The authors suggested that the connecting tubule is derived from $Six2^+$ progenitors and not from collecting duct. However, this conclusion needs to be carefully revisited. The lack of double positive cells (β-gal^+ and $cytokeratin^+$) does not necessarily mean that $Six2^+$ positive cells contribute to connecting tubule. In contrast, even though collecting

duct progenitor cells contribute to connecting tubule, which is consistent with our finding, β-gal and cytokeratin double positive cells are also not observed at E15.5. Interconnection of distal convoluted tubule and collecting duct is not likely established before late S-shaped stage (10). A careful examination of the β-gal$^+$ and cytokeratin$^+$ cells at the late S-shaped stage would be needed in that study. In addition, during the interconnecting process, the most distal part of the S shaped body cells display distinct cellular identity (10), which requires further characterization besides β-gal and cytokeratin.

In another lineage-tracing experiment, the Six2 progenitors were traced by RFP, and as expected, RFP is well segregated with Aqp2 in the adult mouse kidney (83). It is tempting to speculate that a blank region exists between RFP and Aqp2 in some connecting tubules. Lgr5$^+$ progenitor cells represent a more committed form of Six2$^+$ progenitors, which only contribute to the thick ascending region of Henle's loop and distal convoluted tubule (11). In this study, at P1 stage, only a small fraction of Lgr5 tracing marker LacZ overlapped with Aqp2, and the authors have interpreted this as evidence supporting Lgr5$^+$ progenitor contribution to connecting tubule. Based on this observation and our conclusion, Lgr5 expression may expand to connecting tubule 2 and connecting tubule 3. If this is true, a substantial overlap between LacZ and RFP would be seen. Nevertheless, the likeliness that the expression of LacZ in these Aqp2$^+$ cells is due to promiscuous Cre activity and the artificial LacZ staining is not completely eliminated. Though the conclusions reached in these studies regarding the origin

of connecting tubules are less compelling, they are complementary to our findings.

4.4 Future directions

Our studies fall short in addressing if mature principal cells in adult kidney can still function as $Aqp2^+$ progenitor cells and modulate maintenance, remodeling, and repair. Progress has been made toward the discovery of adult stem cells in intestine (85, 86), skin (87), lung (88), hair follicle (89), and other organs. In contrast to these fast turnover tissues, mammalian kidney is thought to cease generation of new nephrons after birth, and possess limited cell turnover ability during adulthood (90, 91). Recent long-term *in vivo* genetic lineage tracing and clonal analyses of individual cells show that the adult mouse kidney undergoes continuous tubulogenesis via expansions of fate-restricted clones (92). Although renal mass remains relatively constant from 12 weeks postparturition onward, the magnitude of tubulogenesis within the adult kidney is estimated to be 4.6–6 times complete renewal of the renal epithelium, as revealed by cumulative counting of cell divisions in the adult kidney, over 7 months. Kidney renewal continuously takes place despite 20%–25% of renal epithelial cells failing to proliferate. These observations suggest that only a subset of adult epithelial cells generate new tubule segments postnatally.

Kidneys recover from injury by repair through tubulogenesis (83, 93, 94). It has been reported that surviving epithelial cells are responsible for repairing the injured kidney tubular epithelia within the proximal tubule (83). Using an unbiased

DNA analog-based approach (95) to track multiple rounds of cell division in vivo, Humphreys et al found no evidence for the existence of a population of specialized progenitors that repeatedly divide in response to acute kidney injury induced by ischemia-reperfusion (96). Instead, they provided compelling evidence showing that new epithelial cells within the proximal tubule are generated from non-lethally injured cells by self-duplication and thus the proximal tubule repair apparently does not involve any specialized progenitor cell population. In contrast, long-term lineage tracing with *ActinCreER*; *R26VT2/GK3* mice, followed by ischemia-reperfusion revealed that tubulogenesis in damaged kidneys occurs through expansions of clones with segment-specific borders, indicating that fate-restricted precursors serve as unipotent progenitors and continuously maintain and self-preserve the mouse kidney throughout life (92). Consistent with this idea, the nuclear factor of activated T cells, cytoplasmic 1 (NFATc1) positive cells may act as intratubular progenitor cells and proliferate to generate tubular cells and restore the integrity of the damaged tubules (97). Similar proximal tubule progenitor cells were found in the human kidneys. These cells express CD133 and CD24, and have the capacity to differentiate into tubular cells once cultured *in vitro*. Importantly, these cells are able to ameliorate the kidney function in the acute kidney injury model (98-100).

Unlike the proximal tubule cells that are responsive to acute kidney injury, the renal collecting duct is resistant to acute kidney injury (83). Nevertheless, collecting duct has remarkable adaptivity in response to multiple metabolic stresses or administration of medicines through remodeling, a phenomenon

called plasticity (101-104). Through remodeling, the relative abundance of principal cells and intercalated cells is altered to match altered physiological conditions. However, how remodeling occurs remains incompletely understood. Several hypotheses have been proposed (101, 102), including 1) conversion of principal cells into intercalated cells; 2) increased proliferation of intercalated cells; and 3) increased cell death or detachment of principal cells, leaving intercalated cells in greater density. While there are some observations to support the last two hypotheses (101, 102), conversion of principal cells to intercalated cells has never been directly and conclusively demonstrated in kidneys of any experimental models.

The three primary limitations of the *Aqp2Cre* transgene exclude its application to address whether mature principal cells convert into intercalated cells in adult kidney during remodeling. First, since the *Aqp2Cre* transgene is active at E15.5, at which time the endogenous *Aqp2* promoter become persistently activated, the Aqp2 lineage can be marked and fate mapped permanently. This excludes the possibility to trace the fate and offspring of mature principal cell ($Aqp2^+$ cells) in adult kidney. Secondly, “Brainbow’’, a multi-color Cre-dependent reporter model, has been used to assess the self-renewal and multi-potent capacity of individual stem/progenitor cells after induction of random recombination that leads to expression of a single color-encoding gene (11, 53). However, the robust and persistent Cre expression of *Aqp2Cre* transgene causes sequential recombination, leading to lack of fluorescent reporter labeling in Aqp2-expressing cells (data not shown). Therefore, *Aqp2Cre* cannot be used to induce activation

of the Brainbow reporter to trace the output of individual Aqp2^{+} progenitor cells at embryonic, neonatal, or adult stages. The third limitation lies in its leakiness. The *Aqp2Cre* transgene was used to generate an inducible *Aqp2CreER^{T2}* construct by replacing the Cre encoding fragment with *CreER^{T2}* cassette (69). As reported, mice carrying this PAC *Aqp2CreER^{T2}* transgene display strong Cre-dependent recombination activity even without tamoxifen induction.

To overcome these limitations of the *Aqp2Cre* transgene, we have generated a new inducible *Aqp2ER^{T2}CreER^{T2}* construct. This construct has two advantages over the *Aqp2CreER^{T2}*. First, since *Aqp2CreER^{T2}* was introduced as a PAC transgene into mice, its integration site and copy number remain obscure. However, *Aqp2ER^{T2}CreER^{T2}* will be knocked-in at the endogenous Aqp2 locus, ensuring the faithful recapitulation of the endogenous Aqp2 expression and only one copy of the *Aqp2ER^{T2}CreER^{T2}* in the heterozygotic mice to minimize the high level of Cre fusion expression due to the presence of multiple copies. The second advantage is that we used *Aqp2ER^{T2}CreER^{T2}* instead of *CreER^{T2}*. It has been reported that *ER^{T2}CreER^{T2}* has tighter control of the onset of transgene expression than the *CreER^{T2}*, *ER^{T2}Cre*, or *FlpeER^{T2}* examined, leading to undetectable Cre-dependent reporter expression in the absence of tamoxifen administration (73). Therefore, *Aqp2ER^{T2}CreER^{T2}* mice may be able to provide temporal and spatial inactivation of floxed genes and activation of the RFP and Brainbow reporters. We will cross the *Aqp2ER^{T2}CreER^{T2}* mice with Ai14 or Brainbow mice to generate double transgenic *Aqp2ER^{T2}CreER^{T2} RFP* or *Aqp2ER^{T2}CreER^{T2} brainbow* models. After validation of the tight regulation of Cre

activity, we will use these new models to test if some mature principal function as adult self-renewal and multi-potent Aqp2^{+} progenitor cells in adult kidneys and if these adult Aqp2 progenitor cells modulate kidney maintenance, remodeling, and repair after various injuries. These studies will greatly advance our understanding of renal stem/progenitor cells and offer new clues toward the development of novel therapeutic strategies for kidney diseases.

References

1. Dressler, G. R. (2006) The cellular basis of kidney development. *Annual review of cell and developmental biology* **22**, 509-529

2. Davidson, A. J. (2008) Mouse kidney development. In *StemBook*, Cambridge (MA)

3. Little, M. H., and McMahon, A. P. (2012) Mammalian kidney development: principles, progress, and projections. *Cold Spring Harbor perspectives in biology* **4**

4. Little, M., Georgas, K., Pennisi, D., and Wilkinson, L. (2010) Kidney development: two tales of tubulogenesis. *Current topics in developmental biology* **90**, 193-229

5. Mugford, J. W., Sipila, P., McMahon, J. A., and McMahon, A. P. (2008) Osr1 expression demarcates a multi-potent population of intermediate mesoderm that undergoes progressive restriction to an Osr1-dependent nephron progenitor compartment within the mammalian kidney. *Developmental biology* **324**, 88-98

6. Humphreys, B. D., Lin, S. L., Kobayashi, A., Hudson, T. E., Nowlin, B. T., Bonventre, J. V., Valerius, M. T., McMahon, A. P., and Duffield, J. S. (2010) Fate tracing reveals the pericyte and not epithelial origin of myofibroblasts in kidney fibrosis. *The American journal of pathology* **176**, 85-97

7. Neiss, W. F., and Klehn, K. L. (1981) The postnatal development of the rat kidney, with special reference to the chemodifferentiation of the proximal tubule. *Histochemistry* **73**, 251-268

8. Loffing, J., Loffing-Cueni, D., Hegyi, I., Kaplan, M. R., Hebert, S. C., Le Hir, M., and Kaissling, B. (1996) Thiazide treatment of rats provokes apoptosis in distal tubule cells. *Kidney international* **50**, 1180-1190

9. Kobayashi, A., Valerius, M. T., Mugford, J. W., Carroll, T. J., Self, M., Oliver, G., and McMahon, A. P. (2008) Six2 defines and regulates a multipotent self-renewing nephron progenitor population throughout mammalian kidney development. *Cell stem cell* **3**, 169-181

10. Kao, R. M., Vasilyev, A., Miyawaki, A., Drummond, I. A., and McMahon, A. P. (2012) Invasion of distal nephron precursors associates with tubular interconnection during nephrogenesis. *Journal of the American Society of Nephrology : JASN* **23**, 1682-1690

11. Barker, N., Rookmaaker, M. B., Kujala, P., Ng, A., Leushacke, M., Snippert, H., van de Wetering, M., Tan, S., Van Es, J. H., Huch, M., Poulsom, R., Verhaar, M. C., Peters, P. J., and Clevers, H. (2012) Lgr5(+ve) stem/progenitor cells contribute to nephron formation during kidney development. *Cell reports* **2**, 540-552

12. Howie, A. J., Smithson, N., and Rollason, T. P. (1993) Reconsideration of the development of the distal tubule of the human kidney. *Journal of anatomy* **183 (Pt 1)**, 141-147

13. Hunter, R. W., Ivy, J. R., Flatman, P. W., Kenyon, C. J., Craigie, E., Mullins, L. J., Bailey, M. A., and Mullins, J. J. (2014) Hypertrophy in the Distal Convoluted Tubule of an 11beta-Hydroxysteroid Dehydrogenase Type 2 Knockout Model. *Journal of the American Society of Nephrology : JASN*

14. Schmitt, R., Ellison, D. H., Farman, N., Rossier, B. C., Reilly, R. F., Reeves, W. B., Oberbaumer, I., Tapp, R., and Bachmann, S. (1999) Developmental expression of sodium entry pathways in rat nephron. *The American journal of physiology* **276**, F367-381

15. Bagnis, C., Marshansky, V., Breton, S., and Brown, D. (2001) Remodeling the cellular profile of collecting ducts by chronic carbonic anhydrase inhibition. *American journal of physiology. Renal physiology* **280**, F437-448

16. Roy, A., Al-Bataineh, M. M., and Pastor-Soler, N. M. (2015) Collecting Duct Intercalated Cell Function and Regulation. *Clinical journal of the American Society of Nephrology : CJASN*

17. Agarwal, S. K., and Gupta, A. (2008) Aquaporins: The renal water channels. *Indian journal of nephrology* **18**, 95-100

18. Bruce, L. J., Wrong, O., Toye, A. M., Young, M. T., Ogle, G., Ismail, Z., Sinha, A. K., McMaster, P., Hwaihwanje, I., Nash, G. B., Hart, S., Lavu, E., Palmer, R., Othman, A., Unwin, R. J., and Tanner, M. J. (2000) Band 3 mutations, renal tubular acidosis and South-East Asian ovalocytosis in

Malaysia and Papua New Guinea: loss of up to 95% band 3 transport in red cells. *Biochem J* **350 Pt 1**, 41-51

19. Karet, F. E., Finberg, K. E., Nelson, R. D., Nayir, A., Mocan, H., Sanjad, S. A., Rodriguez-Soriano, J., Santos, F., Cremers, C. W., Di Pietro, A., Hoffbrand, B. I., Winiarski, J., Bakkaloglu, A., Ozen, S., Dusunsel, R., Goodyer, P., Hulton, S. A., Wu, D. K., Skvorak, A. B., Morton, C. C., Cunningham, M. J., Jha, V., and Lifton, R. P. (1999) Mutations in the gene encoding B1 subunit of H+-ATPase cause renal tubular acidosis with sensorineural deafness. *Nature genetics* **21**, 84-90

20. Smith, A. N., Skaug, J., Choate, K. A., Nayir, A., Bakkaloglu, A., Ozen, S., Hulton, S. A., Sanjad, S. A., Al-Sabban, E. A., Lifton, R. P., Scherer, S. W., and Karet, F. E. (2000) Mutations in ATP6N1B, encoding a new kidney vacuolar proton pump 116-kD subunit, cause recessive distal renal tubular acidosis with preserved hearing. *Nature genetics* **26**, 71-75

21. Rossier, B. C., and Schild, L. (2008) Epithelial sodium channel: mendelian versus essential hypertension. *Hypertension* **52**, 595-600

22. Yu, J., Carroll, T. J., and McMahon, A. P. (2002) Sonic hedgehog regulates proliferation and differentiation of mesenchymal cells in the mouse metanephric kidney. *Development* **129**, 5301-5312

23. Rubera, I., Loffing, J., Palmer, L. G., Frindt, G., Fowler-Jaeger, N., Sauter, D., Carroll, T., McMahon, A., Hummler, E., and Rossier, B. C. (2003) Collecting duct-specific gene inactivation of alphaENaC in the mouse

kidney does not impair sodium and potassium balance. *The Journal of clinical investigation* **112**, 554-565

24. Boyle, S., Shioda, T., Perantoni, A. O., and de Caestecker, M. (2007) Cited1 and Cited2 are differentially expressed in the developing kidney but are not required for nephrogenesis. *Developmental dynamics : an official publication of the American Association of Anatomists* **236**, 2321-2330

25. Boyle, S., Misfeldt, A., Chandler, K. J., Deal, K. K., Southard-Smith, E. M., Mortlock, D. P., Baldwin, H. S., and de Caestecker, M. (2008) Fate mapping using Cited1-CreERT2 mice demonstrates that the cap mesenchyme contains self-renewing progenitor cells and gives rise exclusively to nephronic epithelia. *Developmental biology* **313**, 234-245

26. van Leeuwen, F., Gafken, P. R., and Gottschling, D. E. (2002) Dot1p modulates silencing in yeast by methylation of the nucleosome core. *Cell* **109**, 745-756

27. Krogan, N. J., Dover, J., Wood, A., Schneider, J., Heidt, J., Boateng, M. A., Dean, K., Ryan, O. W., Golshani, A., Johnston, M., Greenblatt, J. F., and Shilatifard, A. (2003) The Paf1 complex is required for histone H3 methylation by COMPASS and Dot1p: linking transcriptional elongation to histone methylation. *Molecular cell* **11**, 721-729

28. Wu, H., Chen, L., Zhou, Q., Zhang, X., Berger, S., Bi, J., Lewis, D. E., Xia, Y., and Zhang, W. (2013) Aqp2-expressing cells give rise to renal intercalated cells. *Journal of the American Society of Nephrology : JASN*

24, 243-252 (Editorial in the same issue of J Am Soc Nephrol pg 163-165, Selection by Faculty of 1000)

29. Zhang, W., Hayashizaki, Y., and Kone, B. C. (2004) Structure and regulation of the mDot1 gene, a mouse histone H3 methyltransferase. *Biochem J* **377**, 641-651

30. Nguyen, A. T., and Zhang, Y. (2011) The diverse functions of Dot1 and H3K79 methylation. *Genes & development* **25**, 1345-1358

31. Okada, Y., Feng, Q., Lin, Y., Jiang, Q., Li, Y., Coffield, V. M., Su, L., Xu, G., and Zhang, Y. (2005) hDOT1L links histone methylation to leukemogenesis. *Cell* **121**, 167-178

32. Okada, Y., Jiang, Q., Lemieux, M., Jeannotte, L., Su, L., and Zhang, Y. (2006) Leukaemic transformation by CALM-AF10 involves upregulation of Hoxa5 by hDOT1L. *Nature cell biology* **8**, 1017-1024

33. Chang, M. J., Wu, H., Achille, N. J., Reisenauer, M. R., Chou, C. W., Zeleznik-Le, N. J., Hemenway, C. S., and Zhang, W. (2010) Histone H3 Lysine 79 Methyltransferase Dot1 Is Required for Immortalization by MLL Oncogenes. *Cancer Res* **70**, 10234-10242

34. Bernt, K. M., Zhu, N., Sinha, A. U., Vempati, S., Faber, J., Krivtsov, A. V., Feng, Z., Punt, N., Daigle, A., Bullinger, L., Pollock, R. M., Richon, V. M., Kung, A. L., and Armstrong, S. A. (2011) MLL-rearranged leukemia is dependent on aberrant H3K79 methylation by DOT1L. *Cancer Cell* **20**, 66-78

35. Nguyen, A. T., Taranova, O., He, J., and Zhang, Y. (2011) DOT1L, the H3K79 methyltransferase, is required for MLL-AF9-mediated leukemogenesis. *Blood* **117**, 6912-6922

36. Zhang, W., Yu, Z., Wu, H., Chen, L., Kong, Q., and Kone, B. C. (2013) An Af9 cis-element directly targets Dot1a to mediate transcriptional repression of the alphaENaC gene. *American journal of physiology. Renal physiology* **304**, F367-375

37. Zhang, X., Zhou, Q., Chen, L., Berger, S., Wu, H., Xiao, Z., Pearce, D., Zhou, X., and Zhang, W. (2013) Mineralocorticoid receptor antagonizes Dot1a-Af9 complex to increase alphaENaC transcription. *American journal of physiology. Renal physiology* **305**, F1436-1444

38. Wu, H., Chen, L., Zhang, X., Zhou, Q., Li, J. M., Berger, S., Borok, Z., Zhou, B., Xiao, Z., Yin, H., Liu, M., Wang, Y., Jin, J., Blackburn, M. R., Xia, Y., and Zhang, W. (2013) Aqp5 is a new transcriptional target of dot1a and a regulator of aqp2. *PloS one* **8**, e53342

39. Zhang, W., Xia, X., Reisenauer, M. R., Hemenway, C. S., and Kone, B. C. (2006) Dot1a-AF9 Complex Mediates Histone H3 Lys-79 Hypermethylation and Repression of ENaC{alpha} in an Aldosterone-sensitive Manner. *The Journal of biological chemistry* **281**, 18059-18068

40. Zhang, W., Xia, X., Jalal, D. I., Kuncewicz, T., Xu, W., Lesage, G. D., and Kone, B. C. (2006) Aldosterone-sensitive repression of ENaCalpha

transcription by a histone H3 lysine-79 methyltransferase. *Am J Physiol Cell Physiol* **290**, C936-946

41. Masilamani, S., Kim, G. H., Mitchell, C., Wade, J. B., and Knepper, M. A. (1999) Aldosterone-mediated regulation of ENaC alpha, beta, and gamma subunit proteins in rat kidney. *The Journal of clinical investigation* **104**, R19-23

42. Loffing, J., Zecevic, M., Feraille, E., Kaissling, B., Asher, C., Rossier, B. C., Firestone, G. L., Pearce, D., and Verrey, F. (2001) Aldosterone induces rapid apical translocation of ENaC in early portion of renal collecting system: possible role of SGK. *American journal of physiology. Renal physiology* **280**, F675-682

43. Kleyman, T. R., Carattino, M. D., and Hughey, R. P. (2009) ENaC at the cutting edge: regulation of epithelial sodium channels by proteases. *The Journal of biological chemistry* **284**, 20447-20451

44. Kim, Y. H., Pech, V., Spencer, K. B., Beierwaltes, W. H., Everett, L. A., Green, E. D., Shin, W., Verlander, J. W., Sutliff, R. L., and Wall, S. M. (2007) Reduced ENaC protein abundance contributes to the lower blood pressure observed in pendrin-null mice. *American journal of physiology. Renal physiology* **293**, F1314-1324

45. Hamm, L. L., Feng, Z., and Hering-Smith, K. S. (2010) Regulation of sodium transport by ENaC in the kidney. *Curr Opin Nephrol Hypertens* **19**, 98-105

46. Bhalla, V., and Hallows, K. R. (2008) Mechanisms of ENaC regulation and clinical implications. *Journal of the American Society of Nephrology : JASN* **19**, 1845-1854

47. Reisenauer, M. R., Anderson, M., Huang, L., Zhang, Z., Zhou, Q., Kone, B. C., Morris, A. P., Lesage, G. D., Dryer, S. E., and Zhang, W. (2009) AF17 competes with AF9 for binding to Dot1a to up-regulate transcription of epithelial Na+ channel alpha. *The Journal of biological chemistry* **284**, 35659-35669

48. Zhang, W., Xia, X., Reisenauer, M. R., Rieg, T., Lang, F., Kuhl, D., Vallon, V., and Kone, B. C. (2007) Aldosterone-induced Sgk1 relieves Dot1a-Af9-mediated transcriptional repression of epithelial Na+ channel alpha. *The Journal of clinical investigation* **117**, 773-783 (Comment in the same issue of J Clin Invest pg 592–595, Selection by Faculty of 1000)

49. Wu, H., Chen, L., Zhou, Q., and Zhang, W. (2011) AF17 facilitates Dot1a nuclear export and upregulates ENaC-mediated Na+ transport in renal collecting duct cells. *PloS one* **6**, e27429

50. Chen, L., Wu, H., Pochynyuk, O. M., Reisenauer, M. R., Zhang, Z., Huang, L., Zaika, O. L., Mamenko, M., Zhang, W., Zhou, Q., Liu, M., Xia, Y., and Zhang, W. (2011) Af17 deficiency increases sodium excretion and decreases blood pressure. *Journal of the American Society of Nephrology : JASN* **22**, 1076-1086 (Selected by Faculty of 1000. Invited author interview by Hemodialysis.com)

51. Nagy, A. (2000) Cre recombinase: the universal reagent for genome tailoring. *Genesis* **26**, 99-109

52. Humphreys, B. D., and DiRocco, D. P. (2014) Lineage-tracing methods and the kidney. *Kidney international* **86**, 481-488

53. Kretzschmar, K., and Watt, F. M. (2012) Lineage tracing. *Cell* **148**, 33-45

54. Madisen, L., Zwingman, T. A., Sunkin, S. M., Oh, S. W., Zariwala, H. A., Gu, H., Ng, L. L., Palmiter, R. D., Hawrylycz, M. J., Jones, A. R., Lein, E. S., and Zeng, H. (2010) A robust and high-throughput Cre reporting and characterization system for the whole mouse brain. *Nature neuroscience* **13**, 133-140

55. Ronzaud, C., Loffing, J., Bleich, M., Gretz, N., Grone, H. J., Schutz, G., and Berger, S. (2007) Impairment of sodium balance in mice deficient in renal principal cell mineralocorticoid receptor. *Journal of the American Society of Nephrology : JASN* **18**, 1679-1687

56. Breggia, A. C., and Himmelfarb, J. (2008) Primary mouse renal tubular epithelial cells have variable injury tolerance to ischemic and chemical mediators of oxidative stress. *Oxidative medicine and cellular longevity* **1**, 33-38

57. Halbert, C. L., Demers, G. W., and Galloway, D. A. (1991) The E7 gene of human papillomavirus type 16 is sufficient for immortalization of human epithelial cells. *Journal of virology* **65**, 473-478

58. Wagner, C. A., Finberg, K. E., Breton, S., Marshansky, V., Brown, D., and Geibel, J. P. (2004) Renal vacuolar H+-ATPase. *Physiol Rev* **84**, 1263-1314

59. Verkman, A. S. (1999) Lessons on renal physiology from transgenic mice lacking aquaporin water channels. *Journal of the American Society of Nephrology : JASN* **10**, 1126-1135

60. Yang, B., Ma, T., Dong, J. Y., and Verkman, A. S. (2000) Partial correction of the urinary concentrating defect in aquaporin-1 null mice by adenovirus-mediated gene delivery. *Hum Gene Ther* **11**, 567-575

61. Miller, R. L., Zhang, P., Smith, M., Beaulieu, V., Paunescu, T. G., Brown, D., Breton, S., and Nelson, R. D. (2005) V-ATPase B1-subunit promoter drives expression of EGFP in intercalated cells of kidney, clear cells of epididymis and airway cells of lung in transgenic mice. *Am J Physiol Cell Physiol* **288**, C1134-1144

62. Hemmingsen, C. (2000) Regulation of renal calbindin-D28K. *Pharmacol Toxicol* **87 Suppl 3**, 5-30

63. Sabolic, I., Brown, D., Gluck, S. L., and Alper, S. L. (1997) Regulation of AE1 anion exchanger and H(+)-ATPase in rat cortex by acute metabolic acidosis and alkalosis. *Kidney international* **51**, 125-137

64. Soleimani, M., Greeley, T., Petrovic, S., Wang, Z., Amlal, H., Kopp, P., and Burnham, C. E. (2001) Pendrin: an apical Cl-/OH-/HCO3- exchanger

in the kidney cortex. *American journal of physiology. Renal physiology* **280**, F356-364

65. Song, H. K., Kim, W. Y., Lee, H. W., Park, E. Y., Han, K. H., Nielsen, S., Madsen, K. M., and Kim, J. (2007) Origin and fate of pendrin-positive intercalated cells in developing mouse kidney. *Journal of the American Society of Nephrology : JASN* **18**, 2672-2682

66. Parreira, K. S., Debaix, H., Cnops, Y., Geffers, L., and Devuyst, O. (2009) Expression patterns of the aquaporin gene family during renal development: influence of genetic variability. *Pflugers Arch* **458**, 745-759

67. Romagnani, P., Lasagni, L., and Remuzzi, G. (2013) Renal progenitors: an evolutionary conserved strategy for kidney regeneration. *Nature reviews. Nephrology*

68. Blomqvist, S. R., Vidarsson, H., Fitzgerald, S., Johansson, B. R., Ollerstam, A., Brown, R., Persson, A. E., Bergstrom, G. G., and Enerback, S. (2004) Distal renal tubular acidosis in mice that lack the forkhead transcription factor Foxi1. *The Journal of clinical investigation* **113**, 1560-1570

69. Ronzaud, C., Loffing, J., Gretz, N., Schutz, G., and Berger, S. (2011) Inducible renal principal cell-specific mineralocorticoid receptor gene inactivation in mice. *American journal of physiology. Renal physiology* **300**, F756-760

70. Loffing, J., Vallon, V., Loffing-Cueni, D., Aregger, F., Richter, K., Pietri, L., Bloch-Faure, M., Hoenderop, J. G., Shull, G. E., Meneton, P., and Kaissling, B. (2004) Altered renal distal tubule structure and renal Na(+) and Ca(2+) handling in a mouse model for Gitelman's syndrome. *Journal of the American Society of Nephrology : JASN* **15**, 2276-2288

71. Fichorova, R. N., Rheinwald, J. G., and Anderson, D. J. (1997) Generation of papillomavirus-immortalized cell lines from normal human ectocervical, endocervical, and vaginal epithelium that maintain expression of tissue-specific differentiation proteins. *Biol Reprod* **57**, 847-855

72. Hayashi, S., and McMahon, A. P. (2002) Efficient recombination in diverse tissues by a tamoxifen-inducible form of Cre: a tool for temporally regulated gene activation/inactivation in the mouse. *Developmental biology* **244**, 305-318

73. Matsuda, T., and Cepko, C. L. (2007) Controlled expression of transgenes introduced by in vivo electroporation. *Proceedings of the National Academy of Sciences of the United States of America* **104**, 1027-1032

74. Sampogna, R. V., and Al-Awqati, Q. (2013) Salt and pepper distribution of cell types in the collecting duct. *Journal of the American Society of Nephrology : JASN* **24**, 163-165

75. Jeong, H. W., Jeon, U. S., Koo, B. K., Kim, W. Y., Im, S. K., Shin, J., Cho, Y., Kim, J., and Kong, Y. Y. (2009) Inactivation of Notch signaling in the

renal collecting duct causes nephrogenic diabetes insipidus in mice. *The Journal of clinical investigation* **119**, 3290-3300

76. Guo, Q., Wang, Y., Tripathi, P., Manda, K. R., Mukherjee, M., Chaklader, M., Austin, P. F., Surendran, K., and Chen, F. (2015) Adam10 Mediates the Choice between Principal Cells and Intercalated Cells in the Kidney. *Journal of the American Society of Nephrology : JASN* **26**, 149-159

77. Jones, B., Su, H., Bhat, A., Lei, H., Bajko, J., Hevi, S., Baltus, G. A., Kadam, S., Zhai, H., Valdez, R., Gonzalo, S., Zhang, Y., Li, E., and Chen, T. (2008) The histone H3K79 methyltransferase Dot1L is essential for mammalian development and heterochromatin structure. *PLoS genetics* **4**, 1-11

78. Feng, Y., Yang, Y., Ortega, M. M., Copeland, J. N., Zhang, M., Jacob, J. B., Fields, T. A., Vivian, J. L., and Fields, P. E. (2010) Early mammalian erythropoiesis requires the Dot1L methyltransferase. *Blood* **116**, 4483-4491

79. Mahmoudi, T., Boj, S. F., Hatzis, P., Li, V. S., Taouatas, N., Vries, R. G., Teunissen, H., Begthel, H., Korving, J., Mohammed, S., Heck, A. J., and Clevers, H. (2010) The leukemia-associated Mllt10/Af10-Dot1l are Tcf4/beta-catenin coactivators essential for intestinal homeostasis. *PLoS biology* **8**, e1000539

80. Feng, Q., Wang, H., Ng, H. H., Erdjument-Bromage, H., Tempst, P., Struhl, K., and Zhang, Y. (2002) Methylation of H3-lysine 79 is mediated by a new family of HMTases without a SET domain. *Curr Biol* **12**, 1052-1058

81. Breton, S., Alper, S. L., Gluck, S. L., Sly, W. S., Barker, J. E., and Brown, D. (1995) Depletion of intercalated cells from collecting ducts of carbonic anhydrase II-deficient (CAR2 null) mice. *The American journal of physiology* **269**, F761-774

82. Grouls, S., Iglesias, D. M., Wentzensen, N., Moeller, M. J., Bouchard, M., Kemler, R., Goodyer, P., Niggli, F., Grone, H. J., Kriz, W., and Koesters, R. (2012) Lineage specification of parietal epithelial cells requires beta-catenin/Wnt signaling. *Journal of the American Society of Nephrology : JASN* **23**, 63-72

83. Humphreys, B. D., Valerius, M. T., Kobayashi, A., Mugford, J. W., Soeung, S., Duffield, J. S., McMahon, A. P., and Bonventre, J. V. (2008) Intrinsic epithelial cells repair the kidney after injury. *Cell stem cell* **2**, 284-291

84. Li, J., Ariunbold, U., Suhaimi, N., Sunn, N., Guo, J., McMahon, J. A., McMahon, A. P., and Little, M. (2015) Collecting duct-derived cells display mesenchymal stem cell properties and retain selective in vitro and in vivo epithelial capacity. *Journal of the American Society of Nephrology : JASN* **26**, 81-94

85. Crosnier, C., Stamataki, D., and Lewis, J. (2006) Organizing cell renewal in the intestine: stem cells, signals and combinatorial control. *Nature reviews. Genetics* **7**, 349-359

86. Barker, N., Bartfeld, S., and Clevers, H. (2010) Tissue-resident adult stem cell populations of rapidly self-renewing organs. *Cell stem cell* **7**, 656-670

87. Lavker, R. M., and Sun, T. T. (2000) Epidermal stem cells: properties, markers, and location. *Proceedings of the National Academy of Sciences of the United States of America* **97**, 13473-13475

88. Treutlein, B., Brownfield, D. G., Wu, A. R., Neff, N. F., Mantalas, G. L., Espinoza, F. H., Desai, T. J., Krasnow, M. A., and Quake, S. R. (2014) Reconstructing lineage hierarchies of the distal lung epithelium using single-cell RNA-seq. *Nature* **509**, 371-375

89. Taylor, G., Lehrer, M. S., Jensen, P. J., Sun, T. T., and Lavker, R. M. (2000) Involvement of follicular stem cells in forming not only the follicle but also the epidermis. *Cell* **102**, 451-461

90. Guo, J. K., and Cantley, L. G. (2010) Cellular maintenance and repair of the kidney. *Annual review of physiology* **72**, 357-376

91. Hartman, H. A., Lai, H. L., and Patterson, L. T. (2007) Cessation of renal morphogenesis in mice. *Developmental biology* **310**, 379-387

92. Rinkevich, Y., Montoro, D. T., Contreras-Trujillo, H., Harari-Steinberg, O., Newman, A. M., Tsai, J. M., Lim, X., Van-Amerongen, R., Bowman, A., Januszyk, M., Pleniceanu, O., Nusse, R., Longaker, M. T., Weissman, I. L.,

and Dekel, B. (2014) In vivo clonal analysis reveals lineage-restricted progenitor characteristics in mammalian kidney development, maintenance, and regeneration. *Cell reports* **7**, 1270-1283

93. Oliver, J. A., Maarouf, O., Cheema, F. H., Martens, T. P., and Al-Awqati, Q. (2004) The renal papilla is a niche for adult kidney stem cells. *The Journal of clinical investigation* **114**, 795-804

94. Oliver, J. A., Klinakis, A., Cheema, F. H., Friedlander, J., Sampogna, R. V., Martens, T. P., Liu, C., Efstratiadis, A., and Al-Awqati, Q. (2009) Proliferation and migration of label-retaining cells of the kidney papilla. *Journal of the American Society of Nephrology : JASN* **20**, 2315-2327

95. Humphreys, B. D. (2015) Cutting to the chase: taking the pulse of label-retaining cells in kidney. *American journal of physiology. Renal physiology* **308**, F29-30

96. Humphreys, B. D., Czerniak, S., DiRocco, D. P., Hasnain, W., Cheema, R., and Bonventre, J. V. (2011) Repair of injured proximal tubule does not involve specialized progenitors. *Proceedings of the National Academy of Sciences of the United States of America* **108**, 9226-9231

97. Langworthy, M., Zhou, B., de Caestecker, M., Moeckel, G., and Baldwin, H. S. (2009) NFATc1 identifies a population of proximal tubule cell progenitors. *Journal of the American Society of Nephrology : JASN* **20**, 311-321

98. Angelotti, M. L., Ronconi, E., Ballerini, L., Peired, A., Mazzinghi, B., Sagrinati, C., Parente, E., Gacci, M., Carini, M., Rotondi, M., Fogo, A. B., Lazzeri, E., Lasagni, L., and Romagnani, P. (2012) Characterization of renal progenitors committed toward tubular lineage and their regenerative potential in renal tubular injury. *Stem cells* **30**, 1714-1725

99. Kim, K., Park, B. H., Ihm, H., Kim, K. M., Jeong, J., Chang, J. W., and Cho, Y. M. (2011) Expression of stem cell marker CD133 in fetal and adult human kidneys and pauci-immune crescentic glomerulonephritis. *Histology and histopathology* **26**, 223-232

100. Lindgren, D., Bostrom, A. K., Nilsson, K., Hansson, J., Sjolund, J., Moller, C., Jirstrom, K., Nilsson, E., Landberg, G., Axelson, H., and Johansson, M. E. (2011) Isolation and characterization of progenitor-like cells from human renal proximal tubules. *The American journal of pathology* **178**, 828-837

101. de Groot, T., Alsady, M., Jaklofsky, M., Otte-Holler, I., Baumgarten, R., Giles, R. H., and Deen, P. M. (2014) Lithium causes G2 arrest of renal principal cells. *Journal of the American Society of Nephrology : JASN* **25**, 501-510

102. Christensen, B. M., Kim, Y. H., Kwon, T. H., and Nielsen, S. (2006) Lithium treatment induces a marked proliferation of primarily principal cells in rat kidney inner medullary collecting duct. *American journal of physiology. Renal physiology* **291**, F39-48

103. Al-Awqati, Q. (1996) Plasticity in epithelial polarity of renal intercalated cells: targeting of the H(+)-ATPase and band 3. *The American journal of physiology* **270**, C1571-1580

104. Schwartz, G. J., Barasch, J., and Al-Awqati, Q. (1985) Plasticity of functional epithelial polarity. *Nature* **318**, 368-371

Vita

Lihe Chen was born on December 4, 1987 in Changsha, Hunan Province, PR China. He attended Wuhan University in China from 2006 to 2010. From there, he received his B.S with a major in Biology. During that time, He was awarded an Annual Outstanding Student Scholarship for 4 years running (2006-2010). Then, he was admitted to The Graduate School of Biomedical Sciences at the University of Texas Health Science Center at Houston in 2010 to pursue his PhD under the supervision of Dr. Wenzheng Zhang. In 2013, He was awarded the Dean's Research Scholarship Award. He focused on the identification and characterization of a novel kidney progenitor cell population, as well as the function and regulation of the histone H3 K79 methyltransferase Dot1l signaling pathway in renal physiology and renal pathology.

Current address: 1885 El Paseo #548, Houston, Texas, 77054